Constraining the Cosmological Parameters and the Underlying Theoretical Models with CMB Anisotropy and Polarization Measurements

Dissertation
submitted for the award of the degree of
Master of Philosophy
in
Physics
by

Shaja Rasool Wani

Under the Supervision of

Dr. Manzoor A. Malik

Department of Physics,
Faculty of Physical and Material Science,
University of Kashmir, Srinagar - 190 006

March, 2012

Acknowledgments

I would like to take this occasion to thank all those people who directly or indirectly helped me during the course of this study. Firstly I am very grateful to my supervisor, Dr. Manzoor A. Malik, for his guidance, cooperation and continuous support throughout the course that enabled me to complete this dissertation. His help, both at the academic as well as at the personal level, was an inspiration and motivation for me. I am also thankful to all the faculty members and the non-teaching staff of the physics department, University of Kashmir for their kind help right from the M.Sc years.

I thank my seniors Raja Nisar, Waheed and Gowher for their valuable advices. I am also thankful to my M.Phil batch mates Asif, Bilal, Shabir and other scholars Asloob, Feroz, Bilal Malik, Sajad, Mubashir for helping me in every possible way. I can not forget the batch mates of my M.Sc especially Ilyas, Gulzar and Riyaz to whom I am very grateful.

I am thankful to the officials of Inter University Centre for Astronomy and Astrophysics (IUCAA) for their hospitality during my stay there. Special thanks to Professor Tarun Souradeep and his scholar Santanu Das for their valuable suggestions.

Last but not the least, I am highly grateful to all my family members, especially my sister Shaheen, for their continuous support and guidance right from the birth. Besides these I am thankful to all my friends, teachers and good wishers.

Shaja Rasool Wani

Post Graduate Department of Physics, University of Kashmir, Srinagar.

Certificate

This is to certify that the dissertation entitled "***Constraining the Cosmological Parameters and the Underlying Theoretical Models with CMB Anisotropy and Polarization Measurements***" submitted by ***Shaja Rasool Wani***, in partial fulfillment for the award of the degree of ***Master of Philosophy*** in ***Physics***, is the original research work carried out by him under my supervision. It is further certified that the dissertation has not been submitted for the award of M. Phil. or any other degree to this University or any other University. The scholar has attended the department for statutory period as required under rules.

Dr. Manzoor A. Malik
(*Supervisor*)

Dr. Manzoor A. Malik
(*Head of the department*)

Contents

List of Figures

Chapter 1

General Introduction

Cosmic Microwave Background (CMB) provides a snapshot of the universe when it was barely 0.3 million years old. Measurement of the temperature fluctuations (anisotropies), at the level of 1 part in 10^5, by COBE (Cosmic Background Explorer) and vastly improved by the WMAP (Wilkinson Microwave Anisotropy Probe) and other ground and balloon based experiments have addressed some of the key questions in cosmology like age of the Universe, its expansion rate, its shape, size and composition, formation of structures that we see in the Universe today etc. Since the COBE detection [1], followed by a number of small angular scale measurements and the remarkable results from WMAP [2 - 6], anisotropies have dominated the CMB studies. These data are broadly consistent with cold dark matter (CDM) model in which the Universe is spatially flat and is composed of radiation, baryons, neutrinos and the exotic CDM and dark energy. The main impact of CMB anisotropy measurement has been the reduction in the number of cosmological models under active discussion. The early baryon dominated models and the hot dark matter dominated models [7] have been nearly ruled out.

Rapid advances in observational cosmology are leading to the establishment of the first precision cosmological model, with many of the key cosmological parameters like the matter density, Hubble constant, spatial curvature etc., determined to one or two significant figure accuracy. However, the most accurate model of the Universe requires consideration of a wide range of different types of observations, with complimentary probes providing consistency checks. It has now been established that the structure of the CMB power spectrum when combined with others cosmological probes, such as SDSS (Sloan Digital Sky Survey) [8], 2df Galaxy red shift survey [9] allow extremely precise measure-

ment of the cosmological parameters of the ΛCDM model. While most of the fluctuations seen by WMAP and other CMB experiments were started off at the last surface of scattering, structure formed at low red shift also leave imprints on the CMB. These anisotropies contribute only slightly to the CMB power spectrum on scales measured by WMAP, but they can be detected by cross correlating CMB with suitable tracers of the large scale structure [10]. Future developments are expected to clarify whether the existing set of cosmological parameters subjected to more stringent constraints will continue to prove sufficient or it may become necessary to deploy new parameters.

Besides being consistent with previous results, the new 7-year WMAP data [11 - 14] has improved due to reduced noise from the additional integration time, improved knowledge of the instrument performance, and improved data analysis. The seven year data set is well fit by a minimal six-parameter flat Lambda-CDM model. Finally, Planck is expected to perform the ultimate measurement of primary CMB temperature anisotropies.

The focus has now shifted to CMB polarization measurements as it promises to be an even cleaner probe and is destined to compliment the CMB temperature anisotropy measurements. Ever since the first detection of CMB polarization by DASI (Degree Angular Scale Interferometer) team [15], the field is rapidly growing with several noteworthy results [16 - 22], including the WMAP cross power spectrum TT and polarization EE spectrum [23]. A measurement of B-mode polarization on large scales can show the way to directly determine the energy scale of inflation. CMB polarization data is likely to test alternative theories of gravitation, wherein vector and tensor polarization modes may leave a characteristic signature which could, in principle, be probed by measurements on the CMB E- and B- modes [24, 25]. In fact, at present the highest bid in CMB polarization analysis is the detection of the B-modes. Future polarization measurements may throw light on the possible presence of nontrivial gravitational wave signatures in the CMB polarization spectrum.

1.1 Cosmology from WMAP

We already have a wealth of new and improved data from ground, balloon and satellite based experiments. Among these experiments, WMAP witnessed a phenomenal success and therefore deserves a special mention.

WMAP has mapped the CMB radiation and produced the first fine-resolution (0.2

degree) full-sky map of the microwave sky. The remarkable findings of the WMAP team includes the first direct detection of pre-stellar helium which provided an important test of the big bang prediction, detection of a key signature of inflation, and exploration of the possibilities of what transpired in the first trillionth of a trillionth of a second, ruling out well-known textbook models for the first time. Besides this, WMAP now places 50% tighter limits on the standard model of cosmology, strongly constrains dark energy and geometry of the universe, definitively determined the age of the universe to be 13.73 billion years old to within 1% (0.12 billion years) and nailed down the curvature of space to within 1% of "flat" Euclidean, improving on the precision of previous award-winning measurements by over an order of magnitude. The CMB became the "premier baryometer" of the universe with WMAP's precision determination that ordinary atoms (also called baryons) make up only 4.6% of the universe (to within 0.1%), dark matter (not made up of atoms) make up 23.3% (to within 1.3%) and dark energy makes up 72.1% of the universe (to within 1.5%), causing the expansion rate of the universe to speed up [11]. WMAP also places new constraints on the number of neutrino-like species in the early universe, has detected temperature shifts induced by hot gas in galaxy clusters, mapped the polarization of the microwave radiation over the full sky, discovered that the universe was reionized earlier than previously believed and produced a visual demonstration of the polarization pattern around hot and cold spots. The statistical properties of the CMB fluctuations measured by WMAP appear random; however, there are several hints of possible deviations from simple randomness that are still being assessed. Significant deviations would be a very important signature of new physics in the early universe.

1.2 Cosmology from PLANCK

Since WMAP has already been extremely successful, it is natural to ask whether anything remains to be done. As explained below, WMAP can measure less than 10% of the information contained in the CMB temperature anisotropies, and only a tiny fraction of the information contained in the polarization anisotropies. Planck will measure essentially all of the temperature information in the CMB, and a substantial fraction of the polarization information. This translates into huge gains in our knowledge of the early Universe, the epoch of recombination and structure formation at late times.

Some of the main advantages of Planck mission include much improved angular resolution (3 times that of WMAP), an order of magnitude lower noise at the optimal

frequency bands around 100 GHz, and wider frequency coverage from 30-857 GHz [151]. The improved angular resolution and sensitivity will permit much more accurate estimates of the CMB power spectra. For the C_l^T power spectrum alone, Planck is expected to be cosmic-variance limited to at least a factor of four higher in l leading to a gain of at least a factor of 16 in the sheer number of modes measured with signal-to-noise ratio ~ 1. The wider frequency coverage ensures that Planck will be able to measure and separate the CMB from confusing foregrounds with the accuracy required by its low noise level. This will be especially important in the case of polarization. All of this results in a dramatic improvement in constraints on cosmological parameters and more importantly, in Planck's unique new capabilities for constraining cosmology.

Owing to its improved sensitivity and polarization measurement capability, Planck promises to improve the tests of inflationary models of the early universe, help precisely measure the higher peaks in the CMB power spectrum thus allowing a more accurate estimation of the cosmological parameters. Besides, Planck is expected to give an estimate of the polarization power spectra which WMAP because of its poor sensitivity could not establish. Further, though most inflationary models [26, 27] suggest that the fluctuations are Gaussian, there are evidences of non-Gaussianity. Planck may help resolve the issue by providing greater sensitivity to any non-Gaussianity signatures that may exist.

A host of new higher-order effects can be measured because of the sensitivity, angular resolution, and frequency coverage of Planck. Examples include the thermal and kinetic Sunyaev-Zel'dovich effects from rich clusters of galaxies, lensing of the CMB to measure the matter power spectrum and potentially the neutrino mass, the integrated Sachs-Wolfe effect as a probe of low-z physics (perhaps constraining fluctuations in the dark energy), and a range of related cross-correlation studies which could further constrain the properties of the dark sector of the Universe.

Ever since the COBE detection of CMB anisotropies, there have been remarkable advances in our cosmological understanding. Fundamental questions relating to the geometry of the Universe, its composition, and its age can now be answered in fairly precise terms, using several complementary astrophysical techniques together with observations of the CMB.

Despite this spectacular recent progress in measuring the geometry and contents of the Universe, we are far from understanding why it is the way it is, and precisely how structure formed within it. Empirical progress on these questions requires much more

precise measurements, which is precisely what Planck was designed to do. In particular, unresolved questions connected with the early Universe include:

- What is the dark energy that appears to be causing the Universe to accelerate at late times? What is its physical origin? Why do we exist at the epoch when the dark energy is just becoming dominant?
- What is the nature of the dark matter that dominates the present matter density? Is it made up of relic super-symmetric particles? Does it have properties which affect structure formation?
- Do we have a full inventory of the matter content of the Universe? What is the net contribution of massive neutrinos? Are we missing other components, for example, singlet neutrinos?
- When and how were the baryons created? Why is $\Omega_b \simeq \Omega_c/10$? And a host of unresolved questions.

Possible answers to many of these questions are still highly speculative. The essential point is that whatever turns out to be the correct theoretical framework, high precision CMB anisotropy measurements are the most promising empirical probe of the fundamental physics of the early Universe.

While the ongoing Planck space mission will further improve the CMB anisotropy and polarization measurements, there are already proposals for the next generation dedicated satellite missions in 2015 - 2020 for CMB polarization measurements at unprecedented sensitivities. We hope to have a general consensus on the origin and evolution of universe in near future.

1.3 Structure of the Dissertation

This dissertation is about general properties of the CMB, its temperature and polarization anisotropies and what information they contain to constrain the cosmological parameters and the models.The dissertation is organized as under:

In chapter 2, a brief introduction to CMB and its history is given. Then we discuss its origin giving a brief account of the thermal history of the universe.We also discuss

how the spectrum of the CMB closely resembles a perfect black body spectrum and the isotropic nature of the radiation with very small fluctuations of the order of 10^{-5} which could explain the large scale structure of the universe, discussed briefly at the end of the chapter.

Chapter 3 discusses the CMB temperature anisotropies including both primary as well as secondary. The primary anisotropies are discussed in some detail where we use statistics to calculate multipole coefficients C_l and discuss the power spectrum of the CMB to know what information can be drawn from it about the universe. The power spectrum can be studied for different angular scales (or mutipole moments l) which include Sachs-Wolfe plateau, acoustic peaks and the damping tail.Then we give a brief account of secondary anisotropies which include, the Integrated Sachs Wolfe effect, Ress-Sciama effect, Gravitational lensing of the CMB, Ostriker-Vishniac effect, and the Sunyaev-Zel'dovich effect. At the end of the chapter, we discuss briefly the foreground contamination which affects the CMB measurements, the Gaussianity of the CMB anisotropies and searches for non-Gaussianity in it.

Chapter 4 describes CMB polarization where firstly we discuss it's origin, then give a brief introduction of Stokes parameters to understand the polarization properties of CMB. We also discuss Thomson scattering, statistics, power spectrum and how information contained in CMB polarization can be used as a tool in cosmology. At the end of the chapter, CMB polarization detection and the challenges posed by B-mode measurements are discussed.

Constraining the cosmological parameters and the theoretical models is discussed in chapter 5. In this chapter, we first study the statistical tools for cosmological parameter estimation which includes the Frequentist approach and the Bayesian approach of parameter estimation. Then we give an account of the standard cosmological model and constrains on cosmological parameters.

Conclusion of the dissertation, future extensions and prospective problems for the Ph.D programme are given in chapter 6.

Chapter 2

Cosmic Microwave Background Radiation

2.1 Introduction

The Universe started from a very hot, dense phase about 15 billion years ago in the Big Bang. The very early Universe was opaque due to the constant interchange of energy between matter and radiation. The baryons were in a plasma form until 300,000 years after the Big Bang ($Z \sim 1100$). At this point, the universe had cooled sufficiently for protons to capture free-electrons and form neutral hydrogen. Prior to this, due to the high temperature, matter was completely ionized. Compton scattering couples the photons to the electrons and the electron are coupled to baryons by electromagnetic interactions. As the protons recombine with electrons, at 3,000 K, the universe becomes transparent. The radiation is said to decouple, and freely propagates through the universe until reaching us. Before decoupling, the radiation and matter were in thermal equilibrium and the lack of interactions thereafter resulted in the radiation having a blackbody spectrum. The temperature of the radiation drops according to $T = (1 + Z)T_0$ due to the expansion of the universe. Consequently, the present day temperature of this radiation is roughly 2.7 K and is observable in the microwave region of the sky. The radiation is uniform in all directions of the sky and originate from the last-scattering-surface. This radiation was emitted before any astronomical objects such as stars, galaxies or quasars existed.

CMB, the relic radiation, was first predicted to exist by Gamow in 1948 [28]. The CMB's discovery by Penzias & Wilson (1965) [29] was one of the successes of hot big

bang models. The temperature of the CMB was measured by the COBE-FIRAS instrument as 2.728 ± 0.004 K [30] and found to have a perfect blackbody spectrum. Equally importantly, in 1992 the first primordial temperature fluctuations were detected by the COBE-DMR instrument [1]. These fluctuations have been sought since the discovery of the CMB. The temperature anisotropies are translations of the primordial matter fluctuations. Crucially, the temperature anisotropies are small of the order of 10^{-5} due to radiation pressure and have evolved linearly. Therefore, we can easily trace the temperature anisotropies back to their primordial form unlike the case for the matter distribution. The anisotropies can be categorized according to their source. Primary anisotropies are generated at, or prior, to decoupling. Secondary anisotropies are imprinted on the CMB photons as they traverse from the last-scattering-surface to our observatories. All the anisotropies are characterized by the power they induce at particular scales which is usually illustrated by the angular power spectrum.

The dominant observed anisotropy is the kinetic dipole arising from the Doppler shift of the photon due to the motion of the emitter and observer. This dipole is much larger than the other CMB anisotropies and was first measured by Smoot, Gorenstein $\&$ Muller (1977) [31]. The dipole principally reflects the motion of the Local Group of galaxies.

The primary anisotropies that dominate at large scales (super-horizon sizes) are caused by the Sachs-Wolfe effect [32].This effect represents the gravitational redshift of the photon due to the difference in gravitational potential between the location of emission and observation. At these scales, the initial perturbations cannot be effected by causal process and thus these anisotropies are directly related to the initial matter power spectrum. These large scales were first probed by the COBE-DMR instrument.

On intermediate scale ($0.1^o < \theta < 2^o$) the anisotropies are dominated by the acoustic peaks. These peaks in power are the result of acoustic oscillations of the photon-baryon fluid within the sound horizon. The first acoustic peak corresponds to the scale where the primordial density inhomogeneities are just reaching a maximum amplitude at the surface of last scattering. Further acoustic peaks correspond to scales that are reaching antinodes of oscillation. These peaks encode a wealth of information about the geometry, contents and evolution of the universe both before and after recombination. For example, the positions of these peaks are determined by the geometry of the universe. A physical scale subtends a smaller angle in an open universes ($k = -1$) compared to the Euclidean case ($k = 0$). The peaks are consequently observed at smaller scales for the open case than

in the flat case. The amplitude of these acoustic peaks depends on a combination of the baryon fraction, matter density and Hubble parameter. Clearly, accurate measurements of these peaks will help constrain a number of cosmological models. The first peak has been measured by a number of ground based and balloon-borne instruments and instruments on board the WMAP satellite measured the first and second peaks [6].

At small scales, the inhomogeneities in the photons are damped due to mechanisms that decrease either the matter or radiation inhomogeneities. Photons defusing out of over dense regions drag baryons and thus lead to damping [33]. Free-streaming of collision less particles (such as neutrinos) from high to low density regions will also cause damping. On top of this, small scales are damped because decoupling is not instantaneous and therefore the last-scattering-surface has a finite thickness. Nevertheless, these processes are again sensitive to cosmological parameters making measurements of these scales worthwhile.

Secondary anisotropies reveal details of the evolution of the universe after decoupling. They can be categorized into gravitational or rescattering effects. In the former case we have examples such as the Integrated Sachs Wolf Effect (ISW). If a photon falls into a potential well which varies temporally, then the photon's energy will be shifted when it climbs out of the well. On the other hand, gravity can deflect the path of the photon without adjusting its energy (i.e. gravitational lensing). The second category relates to the reionization of the universe. When the universe reionizes, free-electrons are produced that will scatter the photons and potentially wash out the primary anisotropies. An important example of this is the thermal Sunyaev-Zel'dovich (SZ) effect [34]. Photons are scattered by hot electrons in the intracluster gas of clusters of galaxies, producing distortions in the black-body spectrum of the CMB.

CMB is polarized and the (vector) polarization field potentially harbors more information than the (scalar) temperature field. In CMB measurements, two scalar fields E and B are used to describe the polarization field. The polarization field directly probes the time of last-scattering. At last-scattering, if the radiation field has a local quadrupole then the scattering of photons off electrons will result in linearly polarized radiation. The polarization fraction is small because only those photons that last-scatter in an optically thin region possess a local quadrupole. The standard assumption is that the polarization signal is 10% of the level of the temperature anisotropies i.e. of the order of 10^{-6} . Consequently, it is a significant experimental challenge to measure this signal, nevertheless, measurements were achieved by the DASI experiment [15]. The power spectrum of the polarization anisotropies and cross-correlation between the temperature field will lead to

a sharpening of cosmological constraints. The most dramatic results lie on the largest angular scales where the field probes primordial gravitational waves and the reionization epoch [35].

CMB is an impressive tool for exploring models of our universe. It is our most distant and cleanest probe of the early universe. Yet it also yields information on the nearby universe. Through CMB observations, cosmological parameters can be determined and models ruled out. Equally, the very foundations of these models can be scrutinized. Evidence of peculiar features in the CMB may require a reassessment of these building blocks. More likely, peculiar features may be artifacts of some non-cosmological signal. Nevertheless, whether the origin of these strange attributes is primordial or local, their discovery would be instructive [36].

Cosmology has become a precision science due to a wealth of new precise data from various astronomical observations. It is therefore important, from a methodological point of view, to develop new statistical and numerical tools to study the CMB radiation and Large Scale Structure (LSS), in order to test different models of the Universe.

2.2 Brief History

After the prediction of the CMB in the Gamow, Alpher and Herman model for element formation, the difficulties this model had in creating elements heavier than lithium led to a general neglect of the prediction, even though the development of radar during World War II and the invention of the Dicke radiometer provided the tools necessary for the direct detection of the CMB. The first indirect evidence for the CMB was the rotational excitation of the interstellar cyanogen (CN) radical seen in 1939 by McKellar, but this observation was not connected to Gamow's prediction. The effective discovery of the CMB, by Penzias and Wilson in 1965, was made when they systematically tried to identify all the sources of noise in a very sensitive antenna used by Bell Labs for early communication satellite experiments. In every direction of sky they saw a constant level of excess noise, and neither instrumental noise nor atmospheric emission could account for this emission. Ironically, a group led by Dicke himself was building a radiometer to look for the CMB when they heard of the Penzias and Wilson discovery. Many groups made measurements of the intensity of the CMB at different wavelengths and quickly showed that the spectrum was close to a blackbody. However, these ground-based measurements of the CMB

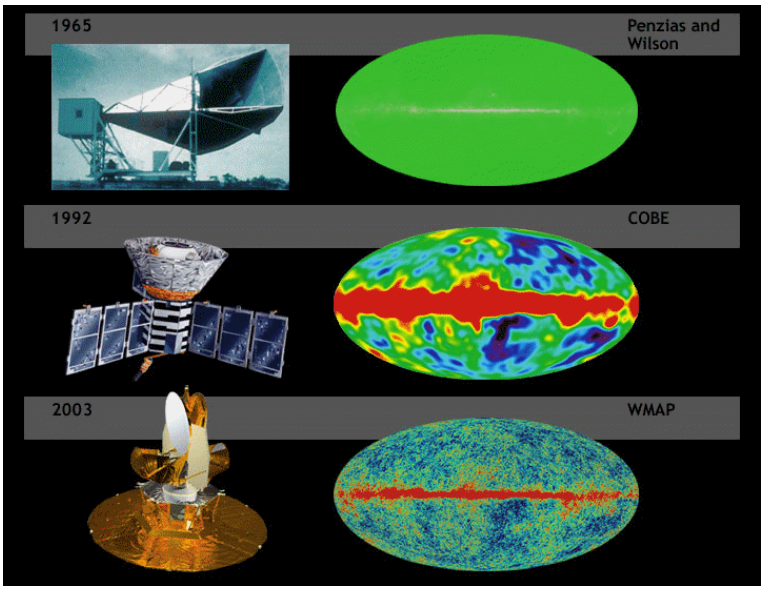

Figure 2.1: Landmark CMB Experiments: Top panel shows the Horn antenna used by Penzias and Wilson that detected the CMB. Notice the isotropy of CMB in the map. Middle panel shows the COBE satellite and the temperature anisotropies detected by COBE. Lower panel shows WMAP satellite and the anisotropies as detected by WMAP. Notice the improved resolution. Source- http://lambda. gsfc.nasa.gov/product/

spectrum still allowed for possible deviations of 10% or more from a blackbody spectrum at millimeter wavelengths.

Searches for the anisotropy of the CMB led to a tentative detection of a dipole pattern by Conklin in 1969 which was confirmed by Henry in 1971, Corey and Wilkinson in 1976 and Smoot et al. in 1977 [37, 31]. A dipole pattern has two poles, with one side of the sky hotter than average, peaking at a hot pole, and the other side cooler than average, giving a cold pole. This dipole pattern is a measure of the motion of our solar system at 370 kms^{-1} relative to the observable universe. After the dipole pattern was subtracted out of the observed temperature map, any anisotropy was less than the sensitivity of these early experiments, which was a few 100 parts per million.

Since the formation of clusters of galaxies by gravitational collapse requires the existence of density contrasts of 1 part per thousand when the universe became transparent, a concerted search for anisotropy beyond the dipole pattern was needed. An alternative model for the formation of large-scale structure assumed that giant explosions would push the matter in the universe into giant shells, but these explosions would add

energy to the CMB at late times in a way that would make the spectrum deviate from a simple blackbody law. The Cosmic Background Explorer (COBE) project, proposed in 1974 but launched in 1989, carried an instrument to search for spectral distortions, the Far-InfraRed Absolute Spectrophotometer (FIRAS), and an instrument to search for anisotropy, the Differential Microwave Radiometers (DMR). The announcement in 1990 that the CMB spectrum measured by COBE showed no deviations from a blackbody led to a standing ovation at an American Astronomical Society meeting. The detection of non-dipole anisotropy by COBE was described as the discovery of the century, if not of all time by Stephen Hawking in 1992.

Based on the absence of distortions in the spectrum and the presence of non-dipole anisotropy, the large-scale structure of the universe appears to have been generated by gravitational forces acting on Dark Matter. The extremely small initial density perturbations that produced the gravitational forces were created during the first picosecond after the big bang. Thus the properties of the CMB have provided a wealth of information about Cosmology.

Inspired by the COBE results, a series of ground and balloon-based experiments measured cosmic microwave background anisotropies on smaller angular scales. The primary goal of these experiments was to measure the scale of the first acoustic peak, which COBE did not have sufficient resolution to resolve. This peak corresponds to large scale density variations in the early universe that are created by gravitational instabilities, resulting in acoustical oscillations in the plasma. The first peak in the anisotropy was tentatively detected by the Toco experiment and the result was confirmed by the BOOMERanG and MAXIMA experiments. These measurements demonstrated that the geometry of the Universe is approximately flat, rather than curved.

The second peak was tentatively detected by several experiments before being definitively detected by WMAP, which has also tentatively detected the third peak. As of 2012, several experiments to improve measurements of the polarization and the microwave background on small angular scales are ongoing, such as the Planck Surveyor, launched in May, 2009.

2.3 Origin of the CMB Radiation

The Hot Big Bang theory successfully explaining the beginning of the universe believes that our universe began as a minute fraction of its present size (formally an infinitesimal singularity). If inflation occurred in the first fraction of a second, the universe became matter dominated while expanding exponentially and then returned to radiation domination by the reheating caused by the decay of the inflation. Baryonic matter formed within the first second, and the nucleosynthesis of the lightest elements took only a few minutes as the universe expanded and cooled. The baryons were in the form of plasma until about 300,000 years after the Big Bang, when the universe had cooled to a temperature near 3000 K, sufficiently cool for protons to capture free electrons and form atomic hydrogen; this process is referred to as recombination. The recombination epoch occurred at a redshift of 1100, meaning that the universe has grown over a thousand times larger since then [38]. The ionization energy of a hydrogen atom is 13.6 eV, but recombination did not occur until the universe had cooled to a characteristic temperature (kT) of 0.3 eV [39]. This delay had several causes. The high entropy of the universe made the rate of electron capture only marginally faster than the rate of photo-dissociation. Moreover, each electron captured directly into the ground state emits a photon capable of ionizing another newly formed atom, so it was through recombination into excited states and the cooling of the universe to temperatures below the ionization energy of hydrogen that neutral matter finally condensed out of the plasma. Until recombination, the universe was opaque to electromagnetic radiation due to scattering of the photons by free electrons. As recombination occurred, the density of free electrons diminished greatly, leading to the decoupling of matter and radiation as the universe became transparent to light.

Cosmic microwave background radiation (CMBR) released during this era of decoupling has a mean free path long enough to travel almost unperturbed until the present day, where we observe it peaked in the microwave region of the spectrum. We see this radiation today coming from the surface of last scattering (which is really a spherical shell of finite thickness) at a distance of nearly 15 billion light years.

The number density of photons in the universe at a redshift z is given by [40]

$$n_\gamma = 420(1+z)^3 cm^{-3} \tag{2.1}$$

where $(1+z)$ is the factor by which the linear scale of the universe has expanded since

then. The radiation temperature of the universe is given by $T = T_0(1 + z)$ so it is easy to

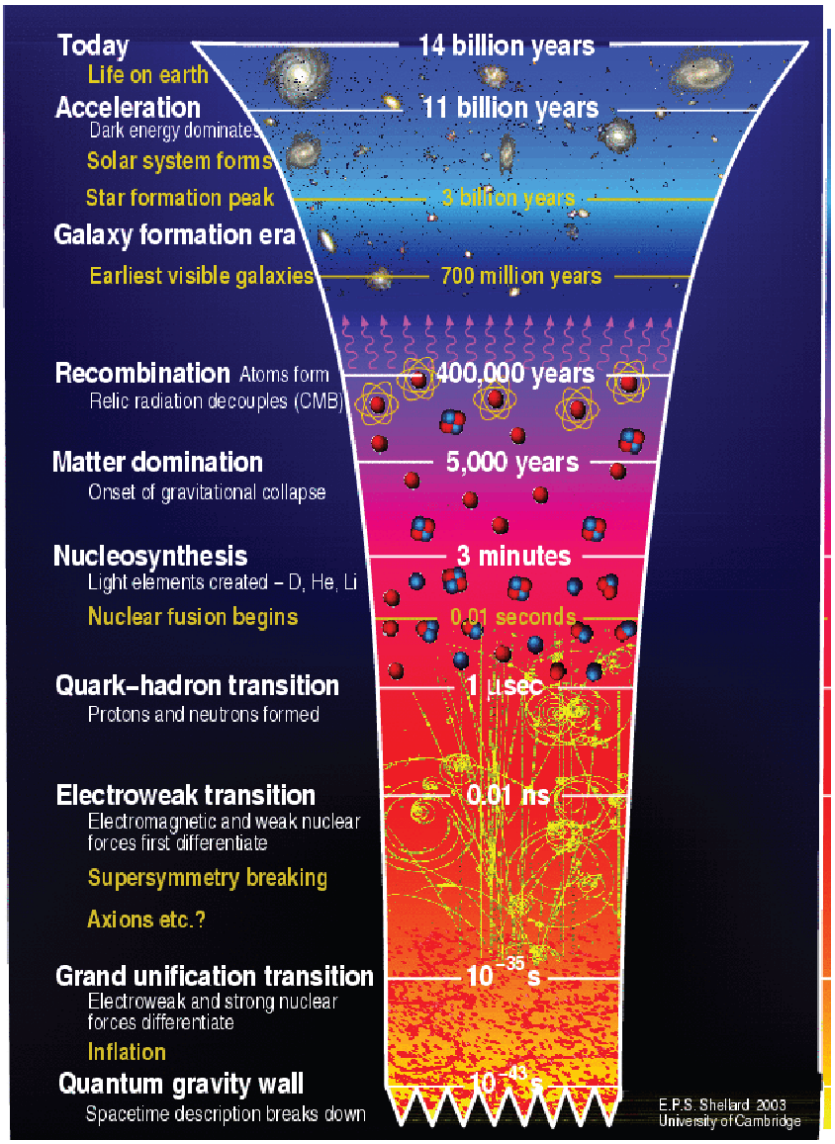

Figure 2.2: Schematic diagram of the history of the Universe from the Planck time to the present. Source- E.P.S. Shellard, 2003, University of Cambridge

see how the conditions in the early universe at high redshifts were hot and dense.

CMBR is our best probe into the conditions of the early universe. Theories of the formation of large-scale structure predict the existence of slight inhomogeneities in the distribution of matter in the early universe which underwent gravitational collapse to form galaxies, galaxy clusters, and superclusters. These density inhomogeneities lead

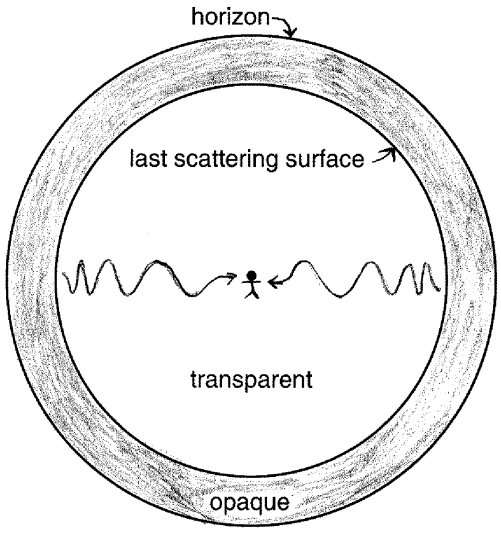

Figure 2.3: An observer is surrounded by a spherical last scattering surface. The photons of the CMB travel straight to us from the last scattering surface, being continuously redshifted.[60]

to temperature anisotropies in the CMBR due to a combination of intrinsic temperature fluctuations and gravitational blue/redshifting of the photons leaving under/overdense regions. The DMR (Differential Microwave Radiometer) instrument of the COBE satellite discovered primordial temperature fluctuations on angular scales larger than 7^0 of order $\triangle T/T = 10^{-5}$ [1].Subsequent observations of the CMB have revealed temperature anisotropies on smaller angular scales which correspond to the physical scale of observed structures such as galaxies and clusters of galaxies.

2.3.1 Thermalization

There were three main processes by which this radiation interacted with matter in the first few hundred thousand years: Compton scattering, double Compton scattering, and thermal bremsstrahlung. The simplest interaction of matter and radiation is Compton scattering of a single photon off a free electron, $\gamma + e^- \rightarrow \gamma + e^-$. The photon will transfer momentum and energy to the electron if it has significant energy in the electron's rest frame. However, the scattering will be well approximated by Thomson scattering if the photon's energy in the rest frame of the electron is significantly less than the rest mass, $h\nu \ll m_e c^2$. When the electron is relativistic, the photon is blueshifted by roughly

a factor γ in energy when viewed from the electron rest frame, is then emitted at almost the same energy in the electron rest frame, and is blueshifted by another factor of γ when re-transformed to the observer's frame. Thus, energetic electrons can efficiently transfer energy to the photon background of the universe. This process is referred to as Inverse Compton scattering. The combination of cases where the photon gives energy to the electron and vice versa allows Compton scattering to generate thermal equilibrium (which is impossible in the Thomson limit of elastic scattering). Compton scattering conserves the number of photons. There exists a similar process, double Compton scattering, which produces (or absorbs) photons, $e^- + \gamma \leftrightarrow e^- + \gamma + \gamma$.

Another electromagnetic interaction which occurs in the plasma of the early universe is Coulomb scattering. Coulomb scattering establishes and maintains thermal equilibrium among the baryons of the photon-baryon fluid without affecting the photons. However, when electrons encounter ions they experience an acceleration and therefore emit electromagnetic radiation. This is called thermal bremsstrahlung or free-free emission. For an ion X, we have $e^- + X \leftrightarrow e^- + X + \gamma$. The interaction can occur in reverse because of the ability of the charged particles to absorb incoming photons; this is called freefree absorption. Each charged particle emits radiation, but the acceleration is proportional to the mass, so we can usually view the electron as being accelerated in the fixed Coulomb field of the much heavier ion. Bremsstrahlung is dominated by electric-dipole radiation [41] and can also produce and absorb photons.

The net effect is that Compton scattering is dominant for temperatures above 90 eV whereas bremsstrahlung is the primary process between 90 eV and 1 eV. At temperatures above 1 keV, double Compton is more efficient than bremsstrahlung. All three processes occur faster than the expansion of the universe and therefore have an impact until decoupling. A static solution for Compton scattering is the Bose-Einstein distribution,

$$f_{BE} = \frac{1}{e^{x+\mu} - 1} \tag{2.2}$$

where μ is a dimensionless chemical potential [42]. At high optical depths, Compton scattering can exchange enough energy to bring the photons to this Bose-Einstein equilibrium distribution. A Planckian spectrum corresponds to zero chemical potential, which will occur only when the number of photons and total energy are in the same proportion as they would be for a blackbody. Thus, unless the photon number starts out exactly right in comparison to the total energy in radiation in the universe, Compton scattering will

only produce a Bose-Einstein distribution and not a blackbody spectrum. It is important to note, however, that Compton scattering will preserve a Planck distribution,

$$f_p = \frac{1}{e^x - 1} \tag{2.3}$$

All three interactions will preserve a thermal spectrum if one is achieved at any point. It has long been known that the expansion of the universe serves to decrease the temperature of a blackbody spectrum,

$$B_\nu = \frac{2h\nu^3/c^2}{e^{h\nu/kT} - 1}, \tag{2.4}$$

but keeps it thermal [43]. This occurs because both the frequency and temperature decrease as $(1+z)$ leaving $h\nu/kT$ unchanged during expansion. Although Compton scattering alone cannot produce a Planck distribution, such a distribution will remain unaffected by electromagnetic interactions or the universal expansion once it is achieved. A non-zero chemical potential will be reduced to zero by double Compton scattering and, later, bremsstrahlung which will create and absorb photons until the number density matches the energy and a thermal distribution of zero chemical potential is achieved. This results in the thermalization of the CMBR at redshifts much greater than that of recombination.

Thermalization, of course, should only be able to create an equilibrium temperature over regions that are in causal contact. The causal horizon at the time of last scattering was relatively small, corresponding to a scale today of about 200 Mpc, or a region of angular extent of one degree on the sky. However, observations of the CMB show that it has an isotropic temperature on the sky to the level of one part in one hundred thousand! This is the origin of the Horizon Problem, which is that there is no physical mechanism expected in the early universe which can produce thermodynamic equilibrium on super horizon scales. The inflationary universe paradigm [44 - 46] solves the Horizon Problem by postulating that the universe underwent a brief phase of exponential expansion during the first second after the Big Bang, during which our entire visible Universe expanded out of a region small enough to have already achieved thermal equilibrium.

2.4 CMB Spectrum

CMBR is the most perfect blackbody ever seen, according to the FIRAS instrument of COBE, which measured a temperature of $T_0 = 2.726 \pm 0.010$ K [47]. The theoretical

prediction that the CMB will have a blackbody spectrum appears to be confirmed by the FIRAS observation (Figure 2.4). But this is not the end of the story. FIRAS only observed the peak of the blackbody. Other experiments have mapped out the Rayleigh-Jeans part of the spectrum at low frequency. Most are consistent with a 2.73 K blackbody, but some are not. It is in the low-frequency limit that the greatest spectral distortions might occur because a Bose-Einstein distribution differs from a Planck distribution there. However, double Compton and bremsstrahlung are most effective at low frequencies so strong deviations from a blackbody spectrum are not generally expected.

Spectral distortions in the Wien tail of the spectrum are quite difficult to detect due to the foreground signal from interstellar dust at those high frequencies. For example, broad emission lines from electron capture at recombination are predicted in the Wien tail but cannot be distinguished due to foreground contamination [48]. However, because the energy generated by star formation and active galactic nuclei is absorbed by interstellar dust in all galaxies and then re-radiated in the far-infrared, we expect to see an isotropic Far-Infrared Background (FIRB) which dominates the CMB at frequencies above a few hundred GHz. This FIRB has now been detected in FIRAS data [49 - 51] and in data from the COBE DIRBE instrument [52, 53].

Although Compton, double Compton, and bremsstrahlung interactions occur frequently until decoupling, the complex interplay between them required to thermalize the CMB spectrum is ineffective at redshifts below 10^7. This means that any process after that time which adds a significant portion of energy to the universe will lead to a spectral distortion today. Neutrino decays during this epoch should lead to a Bose-Einstein rather than a Planck distribution, and this allows the FIRAS observations to set constraints on the decay of neutrinos and other particles in the early universe [54]. The apparent impossibility of thermalizing radiation at low redshift makes the blackbody nature of the CMB strong evidence that it did originate in the early universe and as a result serves to support the Big Bang theory.

The process of Compton scattering can cause spectral distortions if it is too late for double Compton and bremsstrahlung to be effective. In general, low frequency photons will be shifted to higher frequencies, thereby decreasing the number of photons in the Rayleigh-Jeans region and enhancing the Wien tail. This is referred to as a Compton-y distortion and it is described by the parameter

$$y = \int \frac{T_e(t)}{m_e} \sigma n_e(t) dt. \tag{2.5}$$

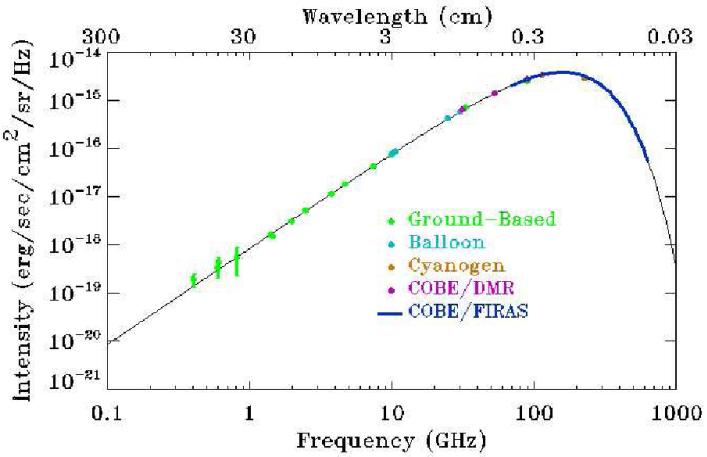

Figure 2.4: The figure shows a selected compilation of the best measurements of the energy spectrum of the CMB photons as a function of frequency. The distribution is extremely well fit by a black-body spectrum at a temperature of $T_0 = 2.726(\pm 0.002)$ making the CMB the most perfect Black-body known in nature. The blue measurement points around the peak (from 60-600 GHz.) are from the FIRAS instrument on board the COBE satellite that won the Nobel prize in Physics in 2006. The figure has been obtained from the website of the ARCADE experiment that has made accurate measurements of the temperature at a lower frequency of 10 GHz.

The apparent temperature drop in the long-wavelength limit is

$$\frac{\delta T}{T} = -2y \tag{2.6}$$

The most important example of this is Compton scattering of photons off hot electrons in galaxy clusters, called the Sunyaev-Zel'dovich (SZ) effect. The electrons transfer energy to the photons, and the spectral distortion results from the sum of all of the scatterings off electrons in thermal motion, each of which has a Doppler shift. The SZ effect from clusters can yield a distortion of $y \simeq 10^{-5}$ - 10^{-3} and these distortions have been observed in several rich clusters of galaxies. The FIRAS observations place a constraint on any fullsky Comptonization by limiting the average y-distortion to $y < 2.5 \times 10^{-5}$ [42]. The integrated y-distortion predicted from the SZ effect of galaxy clusters and large-scale structure is over a factor of ten lower than this observational constraint [55] but that from "cocoons" of radio galaxies [56] is predicted to be of the same order. A kinematic SZ

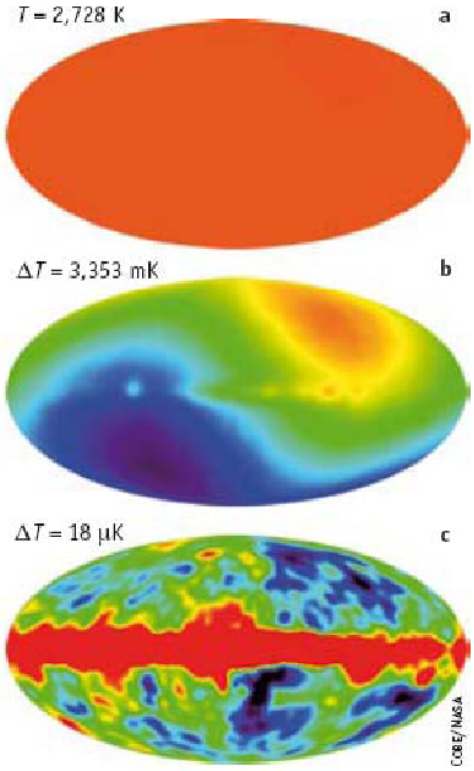

Figure 2.5: (a) The measurements made by the COBE satellite have shown us that the omnipresent cosmic background radiation is distributed extremely evenly (isotropically) across the sky. (b) Only after amplifying the contrast one thousand times can the dipole components that reflect the movement of the observer (of the Sun) through the cosmic radiation field be recognized. (c) Further amplifying the contrast allows tiny but significant deviations in homogeneity to be recognized. Source-http://lambda.gsfc.nasa.gov/product/ cobe/ monopole-top, dipole-middle, and multipole-bottom

effect is caused by the bulk velocity of the cluster; this is a small effect which is very difficult to detect for individual clusters but will likely be measured statistically by the Planck satellite.

2.5 Isotropy of the CMB

The CMB is completely isotropic to about one part per thousand, and, except for the velocity of the solar system, would be isotropic to better than 40 parts per million. Figure

(2.5) shows the temperature of the sky without any contrast enhancement, and no structure can be seen. This is quite a remarkable property and would normally require that many messages be passed back and forth between different regions seen in different directions on the sky. However, in the space-time geometry of the simplest standard big bang model, the distance that light can travel between the big bang and a time t after the big bang is given by $3ct$. It is larger than ct because the distances traveled at early times have grown with the expansion of the universe. The universe appears to be about 13 Gyr old, so the radius of the sky (actually the circumference of the sky divided by 2π) as seen now is about 39 billion light years. At the time the universe became transparent, about 300,000 years after the big bang, light would have traveled 900,000 light years since the big bang. However, this distance would grow by a factor of 1100 during the expansion of the universe from then until now, so the apparent angle subtended by the distance light could have traveled between the big bang and recombination is given by $\tan\theta = 1/39$ or $\theta = 1.5^0$. Thus while many messages back and forth across the whole sky would be needed to establish the observed isotropy, in the standard big bang model one message could only travel 1% of the way around the sky in the time available. This is the horizon problem in the standard big bang model, and thus the observed isotropy of the CMB is evidence in favor of the inflationary scenario which can solve the horizon problem.

2.6 The CMB and large-scale structure

CMB anisotropy measurement determine the gravitational potential at the time of recombination, and thus the gravitational forces that act on the initial smooth distribution of matter are known. In order to produce the clustered pattern seen today, these forces have to act freely on most of the matter in the universe over the whole time interval from 10,000 years after the big bang until the present. Since ordinary baryonic matter cannot move freely until recombination, the CMB anisotropy data already show that most of the matter of the universe is dark.

The accurate determination of the CMB angular power spectrum by WMAP and PLANCK will establish the initial conditions that existed at recombination. Before recombination, ordinary matter was strongly tied to the photons, and large-scale structures such as clusters of galaxies were not able to grow. After recombination, these structures could start to grow, and the CMB data will specify the properties of both the gravitational potential and the density fluctuations at recombination. With these initial conditions, de-

tailed calculations of the behavior of matter between the time of recombination and now can be performed. These calculations often involve following the motions of tens of millions of particles using N-body computer codes. With the CMB data providing the initial conditions, and large scale surveys of galaxies like the Sloan Digital Sky Survey providing the final result, the significant physical effects that produce the observed large-scale structure can be identified.

2.7 Summary

In this chapter, we discussed how the properties of the CMB can give information about the early universe. We also discussed the history,origin and the spectrum of this relic radiation. It provides an image of the universe at an early time when the relevant physical processes were all very simple. Observations of the CMB have already provided a wealth of information about the universe. Its thermodynamic spectrum is a robust prediction of the Hot Big Bang cosmology and has been confirmed observationally. The CMB spectrum gives data from a month or two after the big bang. The anisotropy of the CMB shows the state of the universe at recombination, but that state was established during the inflation epoch less than 1 ps after the big bang. Thus study of the CMB provides data from the earliest evolution of the universe.

Chapter 3

Anisotropies in the Cosmic Microwave Background

3.1 Introduction

We have already mentioned that the cosmic microwave background is not completely isotropic. Instead slightly different temperatures are measured in different directions. These differences are all with respect to the mean value, which can be considered as the monopole term.

Calculations of cosmological perturbation theory predict temperature fluctuations in the smooth background of CMB. With the discovery of the microwave background, efforts were taken to detect these temperature fluctuations. The temperature fluctuations in the CMB were proposed to have signatures of initial density perturbations in the early universe which ultimately lead to the growth of structures. The COBE satellite made a full-sky map of the temperature fluctuations in the CMB with an angular precision of 7 degrees [1]. The WMAP satellite measured these temperature fluctuations and the corresponding power spectrum with an angular resolution of 30 arcminutes [6].

Before the epoch of last scattering (i.e. redshift of $z \simeq 1100$), the universe was fully ionized. The photons were strongly coupled with the baryons by Compton scattering. The fluctuations in the density of matter, CDM and the neutrinos were initiated during an early phase of rapid expansion of the early universe called inflation. As there are anisotropies in density, gravity tries to make the denser regions more dense, whereas the pressure of

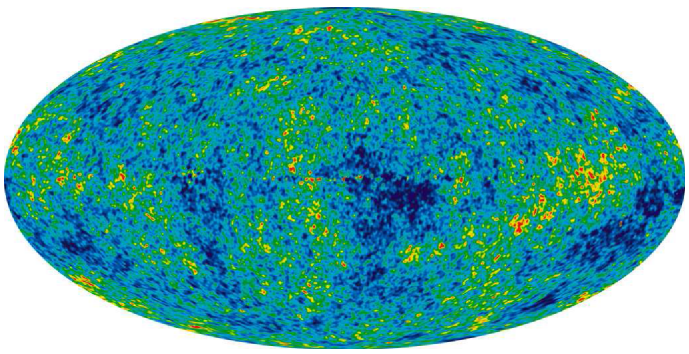

Figure 3.1: The Cosmic Microwave Background temperature fluctuations from the 7-year Wilkinson Microwave Anisotropy Probe data seen over the full sky. The image is a mollweide projection of the temperature variations over the celestial sphere. The average temperature is 2.725 Kelvin, and the colors represent the tiny temperature fluctuations, as in a weather map. Red regions are warmer and blue regions are colder by about 0.0002 degrees. Source- http://wmap.gsfc.nasa.gov/media/101080,NASA.

the radiation tries to resist this compression. Therefore the sound waves flow through the primordial plasma, i.e. the density regions oscillate and the plasma remains in equilibrium. But after $z \simeq 1100$, the energy of the photons were not high enough to keep the H atoms ionized. Therefore the protons and the electrons combine to form neutral hydrogen atom and the universe becomes neutral and thus the photons decoupled. The fluctuations in the matter density therefore quickly grow and form the present structures of the universe. Now as the photons travel freely after the decoupling therefore the anisotropies of the last scattering surface are retained in the phase space distribution of the CMBR which we observe as the CMBR anisotropies. These anisotropies are often known as the primary anisotropy. However there are several other factors which cause the anisotropy in the CMB power spectrum after the last scattering surface, such as the reionization of the universe, gravitational lensing from the clusters etc. These types of anisotropies are known as the secondary anisotropies.

The study of the cosmic microwave background (CMB) temperature anisotropies has long been recognized as one of the most powerful tools to answer the basic questions about the nature of the universe: what is its geometry, its matter and energy content, what are the initial conditions which seeded the formation of structure, etc. These fluctuations are the signatures of different physical mechanisms at different epochs of the evolutionary history of the universe, and they serve as tools to study the entire thermal history of the universe. It is a firm theoretical conclusion that the angular distribution of the CMB

anisotropies must encode a vast amount of information on the cosmological parameters. The majority of this information is thought to be concentrated at angular scales smaller than about 1 degree on the sky, corresponding to regions of the universe that were in casual contact when the background photons decoupled from the matter. On this scales, physical processes in the early universe were able to leave an imprint on the CMB.

3.2 Primary Anisotropies in the CMB

Anisotropies found in the cosmic microwave background result from small perturbations in the energy density of the very early universe. Hence the detection of these anisotropies has provided evidence for the existence of the density perturbations in the early universe and by studying the anisotropies in the CMB information about these perturbations can be found. In order to do this it is convenient to expand the temperature difference $\triangle T(\hat{n})$ between the temperature measured in the direction of the unit vector $\hat{n}$ and the mean value of the temperature T_0 in terms of spherical harmonics $Y_l^m(\hat{n})$

$$\triangle T(\hat{n}) \equiv T(\hat{n}) - T_0 = \sum_{lm} a_{lm} Y_l^m(\hat{n}), \quad T_0 \equiv \frac{1}{4\pi} \int d^2\hat{n} T(\hat{n}). \tag{3.1}$$

The sum over l runs over all positive integers and m runs from $-l$ to l. The choice for an expansion in terms of spherical harmonics is logical since we expect the last scattering surface to be spherical. The temperature difference $\triangle T(\hat{n})$ is real and therefore there is the reality condition

$$a_{lm}^* = a_{l-m}. \tag{3.2}$$

The quantities of interest are averages. These averages are either averages over all positions in space or ensemble averages. The ergodic theorem states that under reasonable assumptions these two types of averages are the same. The average of a quantity A will be denoted by $< A >$, where this can now either mean an average over position or an ensemble average. Furthermore it is assumed that the universe is rotationally invariant on the average, i.e. $< T(\hat{n_1})T(\hat{n_2})T(\hat{n_3}).... >$ is an invariant function of $\hat{n_1}$ etc.

Looking at the temperature fluctuations, the simplest non-trivial quantity to look at is the average of two $\triangle T$s. This quantity has to be rotational invariant and therefore we

have the following restriction for the product of two $a_{lm}s$

$$\langle a_{lm} a^*_{l'm'} \rangle = \delta_{l,l'} \delta_{m,-m'} C_l. \tag{3.3}$$

The average of the product of two temperature differences gives

$$\langle T(\hat{n}) T(\hat{n'}) \rangle = \sum_{lm} C_l Y_l^m(\hat{n}) Y_l^{-m}(\hat{n}') \tag{3.4}$$

$$= \sum_l C_l \Big(\frac{2l+1}{4\pi} \Big) P_l(\hat{n} \cdot \hat{n}'), \tag{3.5}$$

where the sum over m is performed in the second line and yields a Legendre polynomial P_l. This relation can be inverted to obtain an expression for the multipole coefficients C_l

$$C_l = \frac{1}{4\pi} \int d^2\hat{n} d^2\hat{n'} P_l(\hat{n} \cdot \hat{n'}) \langle T(\hat{n}) T(\hat{n'}) \rangle. \tag{3.6}$$

The multipole coefficients C_l are real and positive. The l is related to the angle θ between different directions $\hat{n}$ by $l \sim 1/\theta$. Thus large ls correspond to small angles θ and vice versa.

The average in Eq.(3.6) can be computed in two ways. One way would be to average over all positions in the universe, but this is impossible for observers on earth. The other way would be to prepare a large number of universes and measure $\triangle T(\hat{n})$ in each of these universes and average over these measurements. But this is also impossible. The best we can do is compute

$$C_l^{obs} \equiv \frac{1}{4\pi} \int d^2\hat{n} d^2\hat{n'} P_l(\hat{n} \cdot \hat{n'}) T(\hat{n}) T(\hat{n'}). \tag{3.7}$$

Then the question is how good is this approximation for C_l. Therefore, one would like to know the fractional difference between these two quantities. This fractional difference is called the cosmic variance and is given by

$$\Big\langle \Big(\frac{C_l - C_l^{obs}}{C_l} \Big) \Big(\frac{C_{l'} - C_{l'}^{obs}}{C_{l'}} \Big) \Big\rangle = \delta_{l,l'} \frac{2}{2l+1} \tag{3.8}$$

This expression goes to zero for large l. Thus for large l (small angles), C_l^{obs} hardly differs from C_l. For small l the difference is larger implying a large uncertainty in C_l (see Figure 3.2).

Thus, for $l < 5$ the cosmic variance is too big for C_l^{obs} to be of any cosmological

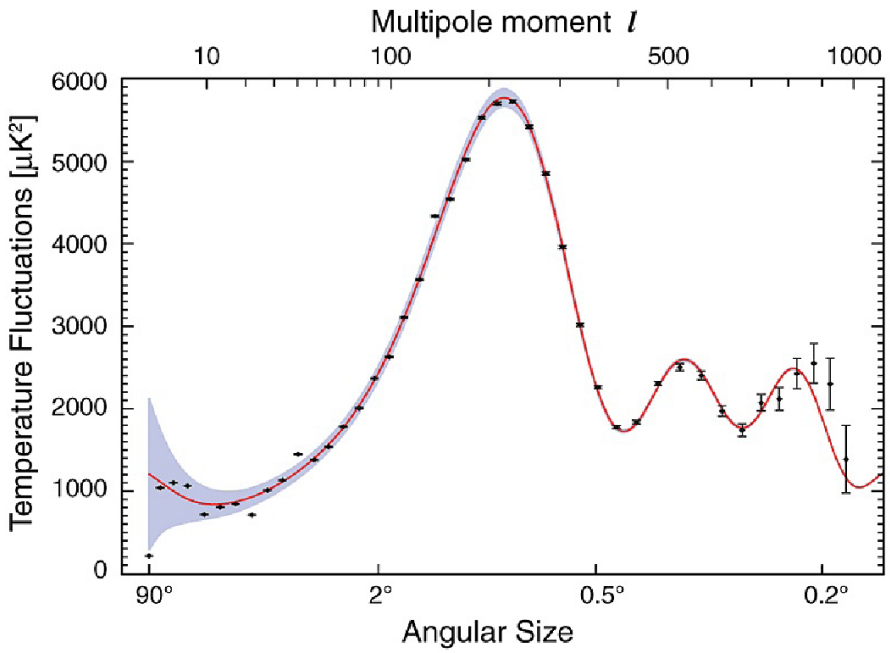

Figure 3.2: The power spectrum of the cosmic microwave background. The blue region denotes the cosmic variance. It is large for small l and it disappears at large l. Source-Figure taken from WMAP homepage

interest. And for $l > 2000$ the uncertainty in C_l^{obs} becomes too large (due to foreground effects) to be of any interest. To obtain information about the universe we are restricted to the region between 5 and 2000, still a rather large region.

The temperature fluctuations in the CMB at higher multipoles ($l \geq 2$) are interpreted as being mostly the result of perturbations in the density of the very early universe and then especially at the surface of last scattering. Though all higher multipoles result from perturbations in the density, they do not all have exactly the same origin. Different regions in l have different physical origins [57]. There are roughly 4 main regions as shown in Figure (3.3), namely the ISW rise, the Sachs-Wolfe plateau, the acoustic peaks and the damping tail. A brief description of all these regions is given below:

3.2.1 The ISW rise, $l \lesssim 10$, and Sachs-Wolfe plateau, $10 \lesssim l \lesssim 100$

The large angle effect (small l) result from perturbations in the gravitational potential at the time of last scattering. This is called the Sachs-Wolfe effect, because Sachs and Wolfe were the first to calculate this effect in 1967 [32]. The region where this effect is

important is for $10 \leq l \leq 100$. Small potential wells in the early universe plasma would attract matter and the wells would get even deeper. Photons emitted from such a potential well have a shifted frequency and thus a temperature shifted from the average temperature by an amount

$$\Big(\frac{\triangle T(\hat{n})}{T_0}\Big) = \delta\phi(\hat{n}r_L), \tag{3.9}$$

where r_L is the radial coordinate of the surface of last scattering, given by

$$r_L = \frac{1}{\Omega_k^{1/2} H_0 a(t_0)} \sinh\Big[\Omega_K^{1/2} \int_{1/(1+z_L)}^{1} \frac{dx}{\sqrt{\Omega_\Lambda x^4 + \Omega_K x^2 + \Omega_M x + \Omega_R}}\Big], \tag{3.10}$$

where $\Omega_K = 1 - \Omega_\Lambda - \Omega_M - \Omega_R$; z_L is the redshift of last scattering, $z_L \approx 1089$; and t_0 is today. The perturbation to the gravitational has also an effect on the expansion rate, it shifts the expansion rate by an amount of $\delta\phi(x)$. And since the temperature in a matter-dominated universe scales as a^{-1} this shifts the redshift at which the universe reaches the surface of last scattering in a certain direction $\hat{n}$ by a fractional amount

$$\Big(\frac{\delta z}{1+z}\Big)_{T=3000K} = -\Big(\frac{\delta a(t)}{a(t)}\Big)_{T=3000K} = \Big(\frac{\dot{a}}{a}\Big)_{T=3000K} \tag{3.11}$$

$$\delta\phi(r_L\hat{n})t_L = \frac{2}{3}\delta\phi(r_L\hat{n}). \tag{3.12}$$

This effect will shift the observed temperature in the direction $\hat{n}$ by a fractional amount

$$\Big(\frac{\triangle T(\hat{n})}{T_0}\Big) = -\frac{2}{3}\delta\phi(\hat{n}r_L). \tag{3.13}$$

Thus, the Sachs-Wolfe effect consists actually of two effects, namely a shift in the temperature due to a perturbation in the gravitational potential and a shift in the temperature due to the fact that the expansion rate is effected by a perturbation in the gravitational potential. The sum of these to effect gives the total Sachs-Wolfe effect. This is the sum of Eq.(3.9) and Eq.(3.13) and yields

$$\Big(\frac{\triangle T(\hat{n})}{T_0}\Big)_{SW} = \frac{1}{3}\delta\phi(\hat{n}, r_L) \tag{3.14}$$

To further study this effect a closer look to the gravitational potential is needed. It is

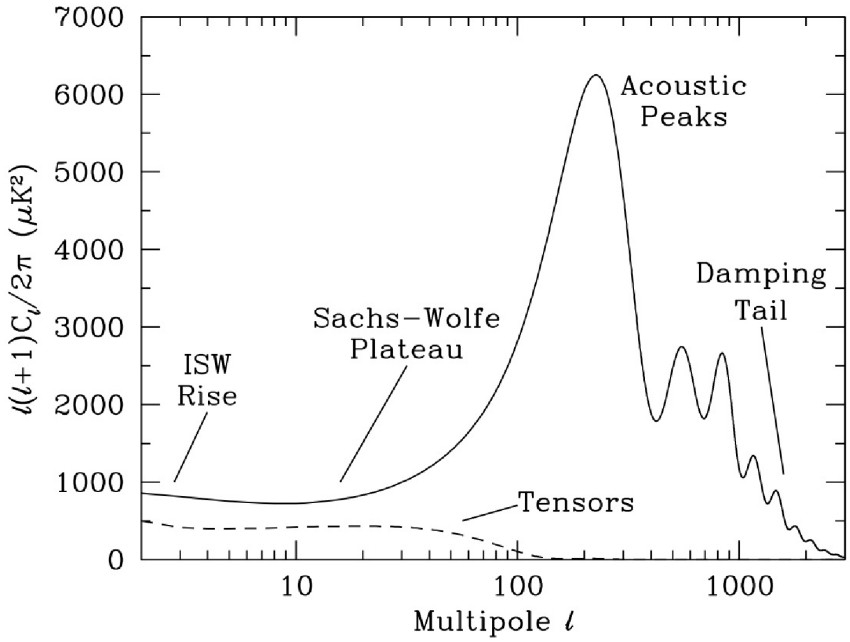

Figure 3.3: The theoretical CMB power spectrum. Used is a standard ΛCDM model from CMBFAST. The different regions are labeled: the ISW rise; Sachs-Wolfe plateau; acoustic and damping tail, [57].

convenient to write $\delta\phi(x)$ as a Fourier transform

$$\delta\phi(X) = \int d^3q e^{iq\cdot X}\delta\phi_q. \tag{3.15}$$

The exponential can be written in terms of Legendre polynomials in the following way

$$e^{iq\cdot X} = \sum_l (2l+1) i^l P_l(\hat{q}\cdot\hat{n}) j_l(qr), \tag{3.16}$$

where j_l is the spherical Bessel function. The total Sachs-Wolfe effect, Eq.(3.14), then becomes

$$\left(\frac{\triangle T(\hat{n})}{T_0}\right)_{SW} = \frac{1}{3}\sum_{l=0}^{\infty}(2l+1)i^l \int d^3q \delta\phi_q j_l(qr_L) P_l(\hat{q}\cdot\hat{n}) \tag{3.17}$$

Again, we want to calculate the average of a product of two fractional temperature shifts in two different directions. Although the gravitational potential depends on the position, the probability distribution of $\delta\phi(X)$ is invariant under spatial rotations and translations.

This implies that

$$\langle \delta\phi_q \delta\phi_{q'} \rangle = P_\phi(q)\delta^3(q+q'), \tag{3.18}$$

where $P_\phi(q)$ depends only on the magnitude of the momentum. And because the gravitational potential is real it follows that $P_\phi(q)$ is real and positive.

Now using the above properties together with Eq.(3.17) and the orthogonality of the Legendre polynomials results in

$$\langle \triangle T(\hat{n}) \triangle T(\hat{n'}) \rangle_{SW} = \frac{4\pi T_0^2}{9} \sum_l (2l+1) P_l(\hat{n} \cdot \hat{n}') \int_0^\infty q^2 dq P_\phi(q) j_l^2(q r_L). \tag{3.19}$$

This result can, as before, be rewritten into an expression for the multipole coefficients

$$(C_l)_{SW} = \frac{16\pi^2 T_0}{9} \int_0^\infty q^2 dq P_\phi(q) j_l^2(q r_L) \tag{3.20}$$

An educated guess for the form of $P_\phi(q)$, when the gravitational potential is produced by cold dark matter, is a rather simple form, such as a power of q. This is often written as

$$P_\phi(q) = N_\phi^2 q^{n-4}, \tag{3.21}$$

where N_ϕ^2 is a positive constant and n is called the scalar spectral index. To compute $\langle \triangle T(\hat{n}) \triangle T(\hat{n}') \rangle_{SW}$ we can use the standard formula for the spherical Bessel function

$$\int_0^\infty j_l^2(s) s^{n-2} ds = \frac{2^{n-4}\pi \Gamma(3-n)\Gamma(l+\frac{n-1}{2})}{\Gamma^2(\frac{4-n}{2})\Gamma(l+2-\frac{n-1}{2}))}. \tag{3.22}$$

For $l < 100$ we then find for the multipole coefficients

$$(C_l)_{SW} \to \frac{16\pi^3 2^{n-4}\Gamma(3-n) r_L^{1-n} N_\phi^2 T_0^2}{9\Gamma^2(\frac{4-n}{2})} \frac{\Gamma(l+\frac{n-1}{2})}{\Gamma(l+2-\frac{n-1}{2})}. \tag{3.23}$$

For n = 1 this reduces to

$$(C_l)_{SW} \to \frac{8\pi^2 N_\phi^2 T_0^2}{9l(l+1)}. \tag{3.24}$$

The value for n can be found by studying the cosmic microwave background and it turns out that it is close to 1, but it is not exactly 1. Eq.(3.24) shows that in this region for $l, l(l+1)C_l$ is constant. This can also be seen in Figure (3.3) where $l(l+1)C_l$ is plotted instead of l for exactly this reason. And this also explains the name plateau.

This calculation was only for small perturbations in the gravitational potential during time of last scattering. But there can also be small perturbations on the way between the last scattering and us which the photons have to pass. These perturbations will also effect the frequency of the photon, but only if the perturbations are time-dependent. If the perturbation was time-independent, the blueshift caused by the photon falling into the potential well would be exactly canceled by the redshift caused when the photon climbs out of the well.

To calculate this effect one has to perform a line integral along the path of the photon. This effect is therefore called the integrated Sachs-Wolfe effect. It is the most important effect for the multipole coefficients with $l \lesssim 10$. For larger l the Sachs-Wolfe effect becomes larger and dominates.

3.2.2 The acoustic peaks, $100 \lesssim l \lesssim 1000$

In the early Universe before decoupling, rapid scattering couples photons and baryons into a plasma which behaves as perfect fluid. Initial quantum overdensities create potential (gravitational) wells - inflationary seeds of the Universe's structure. Infall of the fluid into the potential wells is resisted by its pressure, thus forming acoustic oscillations: periodic compression (overdensities in the fluid; hot spots) and rarefactions (underdensities; cold spots). These acoustic oscillations of the early Universe are frozen at recombination and give the CMB spectrum a unique signature.

The CMB data reveals that the initial inhomogeneities in the Universe were small. An overdense regions would grow by gravitationally attracting more mass, but only after the entire region is in causal contact. This means that only regions which are smaller than the horizon at decoupling had time to compress before then. Regions which are sufficiently smaller than the horizon had enough time to compress gravitationally until the outward-acting pressure halted the compression via Thomson scattering, and possibly even go through a number of such acoustic oscillations. Therefore, perturbations of particular sizes may have gone through: (i) one compression (fundamental wave); (ii) one compression and one rarefaction (first overtone); (iii) one compression, one ramification and one compression again (second overtone); etc... (Fig. 3.4).

The most pronounced temperature variation in the CMB radiation will be due to the fundamental sound wave. This is because the portions of the sky separated by the scale equal to the horizon at decoupling - corresponding to the fundamental sound wave - will

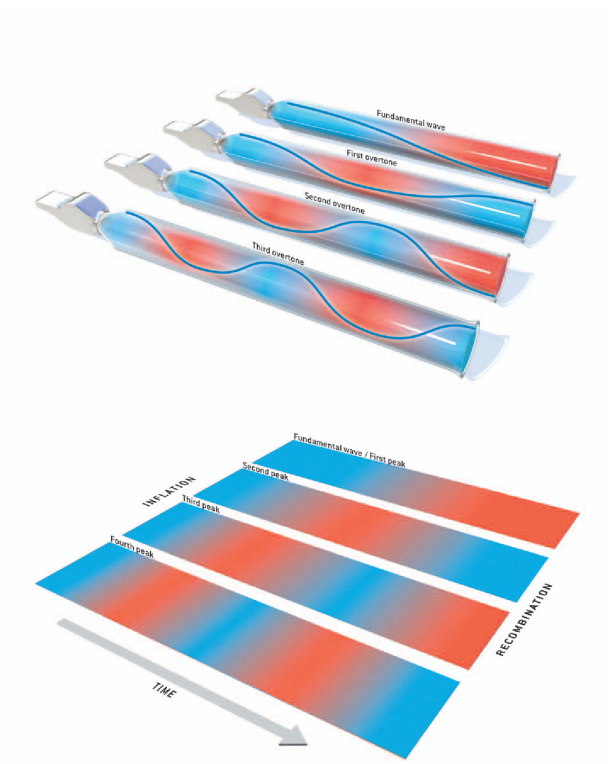

Figure 3.4: Sound waves in a pipe (top) and acoustic waves in the early Universe. Source- Hu & White, Scientific American, February 2004.

be completely out of phase.

Consider a standing wave $A_k(x,t) \propto sin(kx)cos(\omega t)$, going through space at the speed of sound (in plasma $v_s \approx c/\sqrt{3}$), with the frequency ω and wave number k, related by $\omega = kv_s$. The displacement - and hence the correlation in temperature - will be maximal at the decoupling time t_{dec} for $\omega t_{dec} = kv_s t_{dec} = \pi, 2\pi, 3\pi....$ The subsequent peaks in the power spectrum represent the temperature variations caused by overtones. The series of peaks strongly supports the theory that inflation all of the sound waves at the same time. If the perturbations had been continuously generated over time, the power spectrum would not be so harmoniously ordered.

3.2.3 The damping tail, $l \gtrsim 1000$

At the smallest scales, the acoustic oscillations are progressively suppressed by different phenomena, causing an exponential damping in the power spectrum. The two main effects responsible for damping are both due to the fact that the recombination is not an instantaneous process. In fact, the ionization fraction decreases progressively, thus increasing the mean free path of the electrons. In other words, the Last Scattering Surface has a finite thickness, which is around 100 in redshift. This dimension provides the characteristic scale for the considered effects ($l \sim 2500$) and is sensitive to the baryon content and the thermal history of the Universe.

The first effect is called photon diffusion or Silk damping [33] : while random walking through the baryons, the photons destroy the perturbations having size smaller than their mean free path. The second effect is due to the fact that along any given line of sight we see a time average of the fluctuations through the recombination process. Thus, on scales smaller than the thickness of the LSS we have many hot and cold perturbations, which statistically tend to cancel once averaged.

There is a final effect concurring to damping, which is related to the amount and nature of the Hot Dark Matter (HDM) in the Universe. It is now established that dark matter, the principal matter constituent of the Universe, is mainly non-baryonic and cold (the hot/cold classification depending on the velocity dispersion of the particle being close to relativistic or not at the epoch of equal densities of matter and radiation). Nevertheless, HDM, whose candidate particle is massive neutrino, could be present in a sub-dominant fraction. The presence of such component can be probed through its damping effect on the CMB anisotropies. In fact, free streaming associated with a non-zero neutrino mass suppresses the amplitude of the matter fluctuations at wave number greater than $k \sim 0.03(m_v/eV)\Omega_m^{1/2} hMpc^{-1}$ [58, 59].

3.3 Secondary Anisotropies

In the last section the generation of primary anisotropies is discussed briefly. However there are several secondary effects which distort the power spectrum. These types of effects are known as the secondary anisotropies.

After recombination, photons and the matter were decoupled leaving the photons

to move freely. However the photons can interact with the gravitational potential wells or the ionized electrons which are there in their trajectories. If the universe was not re-ionized then the photons can show the secondary anisotropies only due to the gravitational variation in their line of sight, because significant Compton scattering can not occur from the atoms or molecules. But if the universe is re-ionized homogeneously then we must get a significant Compton scattering from these free electrons. So in this case also Compton scattering will become a part of the secondary anisotropy generation.

The secondary fluctuations include all the temperature anisotropies that are generated after the epoch of recombination and decoupling (z = 1100) in the CMB. The secondary anisotropies in the CMB are

1. The integrated Sachs Wolfe (ISW) effect,
2. Ress-Sciama (RS) effect,
3. Gravitational lensing of the CMB,
4. Ostriker-Vishniac (OV) effect,
5. The kinetic Sunyaev-Zel'dovich (KSZ) effect, and
6. The thermal Sunyaev-Zel'dovich (TSZ) effect.

The first three are termed as gravitational secondaries and the last three are called scattering secondaries. The ISW, RS, and lensing effects are achromatic in nature, and the OV, KSZ, and TSZ effects have frequency variation.

3.3.1 The integrated Sachs Wolfe (ISW) effect

After decoupling the universe expands, and the seeds of small anisotropies that are generated in the gravitational potential continue to grow as large scale structures in the universe. The ISW effect arises from the time varying component of the gravitational potential. When the universe is matter dominated as it is at the time of recombination and decoupling, the gravitational potential stays static. However at the epoch of radiation domination ($z \geq 10000$), and dark energy domination (z below 0.8) the gravitational potential becomes time varying. This can be shown from the Poisson equation. The growth of CDM perturbations in a at universe is given by the following equation, [60]

$$\frac{d^2\delta_k}{dt^2} + 2H\frac{d\delta_k}{dt} - \frac{3}{2}\Omega_m H^2 \delta_k = 0, \tag{3.25}$$

where terms being usual. The Poisson equation can be written as,

$$\bigtriangledown^2(\delta\phi) = 4\pi G\delta\bar{\rho}\delta, \tag{3.26}$$

where δ is the density perturbation, and ϕ is the gravitational potential. For matter domination we can solve the perturbation equation using a power law solution. This will give an indicial equation of $3n(n-1)+4n-2=0$, where n is the power law index. This gives us a growing mode solution $\delta \propto t^{2/3}$. From Poisson equation we can write the potential at matter domination as $\phi \propto R^2\rho\delta \propto a^2a^{-3}t^{2/3}$. At matter domination $a \propto t^{2/3}$. This makes the potential to be time-independent. When the energy content of the universe is dominated by both matter and radiation (early universe), or dark energy and matter (as it is now), one can do a numerical calculation to show that the gravitational potential varies with time [61]. The ISW effect becomes important at these two epochs. The photon undergoes redshift, and blueshift respectively while climbing up, and down, the potential well. For a time varying potential this could induce a net blueshift or a redshift to the photon which manifests as temperature anisotropy in the CMB. At the time of radiation domination this effect is termed as early ISW effect whereas at the onset of dark energy domination, we call it the late ISW effect.

The amplitude of the early ISW effect is very small and it occurs at lower angular scales. This is in marked difference with the late ISW effect which is dominant at larger angular scales. In the late ISW effect the potential decays over a longer amount of time (of the order of a Hubble time), and thus small scale anisotropies are washed out due to the traveling of photons through multiple peaks and troughs of the gravitational potential [62]. The ISW effect can be probed by observations of large scale structure. The ISW effect has been detected by several groups through cross-correlation of the CMB sky with galaxy survey data sets from SDSS, National Radio Astronomy Observatory (NRAO)-Very Large Array (VLA) Sky Survey (NVSS), 2- Micron All Sky Survey (2MASS) [63 - 68, 10].

3.3.2 Ress-Sciama (RS) effect

The Ress-Scaima (RS) effect is the non-linear ISW effect, where the perturbation in the gravitational potential is considered beyond first order. If the photon crossing time through the gravitational well is comparable to the evolution time of the gravitational po-

tential there will be a non-zero contribution to the temperature anisotropy at small angular scales [69]. This can also be true for an isolated collapsed structure along the line of sight of the CMB [70], where there could be a change in the gravitational potential of the collapsed structure due to its bulk motion [62]. This is known as the moving halo effect. Analytic, and numerical calculations show that the RS effect peaks at l between 100, and 300. The temperature fluctuation $\triangle T/T$ is between $10^{-6} - 10^{-7}$ [71 - 73].

3.3.3 CMB Lensing

As the CMB photons propagate from the surface of last scattering to $z = 0$, the primary fluctuations in the CMB get lensed by the intervening matter distribution [74]. This effect is called the lensing of the CMB. With the effect of lensing, certain patches of the sky are magnified and demagnified. The effect would not have been present if the CMB would have been perfectly isotropic. For CMB lensing the important factor is not the absolute value of the light deflection, but the relative deflection compared to close by light rays [62]. The deflection of an anisotropic temperature field results in transfer of power from higher angular scales to lower ones [72]. Weak lensing of the CMB does not correspond to any characteristic scale and its effect is seen at scales below an arcminute, where there is a modification in the CMB power spectrum due to transfer of power.

To understand the full significance of lensing, higher order correlations are also important [75 - 78]. The lensing effect in the CMB can couple the E and B modes of polarization in the CMB [62]. The induced B mode polarization signal from CMB lensing would be an important source of confusion for detection of primordial gravity waves through B-mode polarization measurements [79]. There is evidence of detection of the lensing effect from cross-correlation with large scale structure data sets [80, 10]. Detection of CMB lensing is possible with arcminute scale microwave experiments like ACT through cross-correlation with large scale structure tracers and cross-correlation cosmography [81].

3.3.4 Ostriker-Vishniac (OV) effect

The Lyman-alpha resonance line of hydrogen at a wavelength of 1216 $\mathring{A}$ has been used to trace the source of neutral hydrogen through its absorption in quasar spectra [82]. The absence of the Gunn-Peterson effect in quasar spectra was the strongest suggestion for

reionization of the universe after recombination. It is now believed that reionization occurred between a redshift of $7.0 \leq z \leq 20.0$ [62]. Plausible sources for reionizing the universe are radiation from first generation stars [83]. The CMB photons are scattered by the ionized electrons that generates scattering secondaries in the CMB. The velocity field of the scattering electrons induces Doppler shifts in the CMB photon distribution. The modulation of the velocity field occurs due to density contrast of the baryon distributions, and the spatial variations of ionization fractions. The OV effect occurs when the ionization fraction is homogeneous, and the anisotropies are generated by the fluctuations in the density field of the baryons [84, 85]. The OV effect arises from the linear perturbation in the density field of the underlying baryon (electron) distribution. The effect is proportional to the square of the density contrast ($\propto \delta^2$) since the linear perturbation in the velocity field introduces the extra term in density [86]. The effect peaks at a scale of an arcminute with a characteristic amplitude of a μK [87].

3.3.5 The kinetic Sunyaev-Zel'dovich (KSZ) effect

The KSZ effect [88, 89] is essentially the non-linear extension of the OV effect where the Doppler shift of the CMB photon arises due to the line of sight component of the bulk motion of collapsed structures such as clusters of galaxies. The KSZ effect can be used to measure cluster peculiar velocities from SZ experiments like ACT. Measurements of peculiar velocities can be useful in constraining dark energy parameters [90]. They can also be used to measure the large scale velocity fields of the universe. A combined measurement of velocity and density fields can be used to put constraint on theories of modified gravity through the Poisson equation.

3.3.6 The thermal Sunyaev-Zel'dovich (TSZ) effect

The TSZ effect [91] is the inverse Compton scattering of the CMB photons from hot electrons present in galaxy clusters along the line of sight, and is the most prominent secondary fluctuation in the CMB. The change in intensity is proportional to the integrated electron pressure along the line of sight. In the non-relativistic limit the TSZ signal appears as a decrement in CMB intensity below 220 GHz and an increase at higher frequencies. The equivalent intensity difference manifests as a temperature difference in the CMB. A typical cluster of mass $10^{14} M_{\odot}$ induces a temperature distortion of about

$\sim 100\mu K$. The TSZ effect is independent of redshift and hence is an important observational tool in cosmology [92].

3.4 Gaussianity of the CMB anisotropies

The processes turning density inhomogeneities into CMB anisotropies are linear, so cosmological models that predict Gaussian primordial density inhomogeneities also predict a Gaussian distribution of CMB temperature fluctuations. Several techniques have been developed to test COBE and future datasets for deviations from Gaussianity [93 - 95]. Most tests have proven negative, but a few claims of non-Gaussianity have been made. Gaztanaga et al. [96] found a very marginal indication of non-Gaussianity in the spread of results for degree-scale CMB anisotropy observations being greater than the expected sample variances. Ferreira et al. [97] have claimed a detection of non-Gaussianity at multipole $l = 16$ using a bispectrum statistic, and Pando et al. [98] find a non-Gaussian wavelet coefficient correlation on roughly 15° scales in the North Galactic hemisphere. Both of these methods produce results consistent with Gaussianity, however, if a particular area of several pixels is eliminated from the dataset [99]. A true sky signal should be larger than several pixels so instrument noise is the most likely source of the non-Gaussianity. A different area appears to cause each detection, giving evidence that the COBE dataset had non-Gaussian instrument noise in at least two areas of the sky.

3.5 Foregrounds

CMB measurements can be contaminated by other astrophysical emissions arising from our neighborhood [100]. Some examples are as follows.

- *Synchrotron emission*. Relativistic electrons accelerated by a magnetic field produce synchrotron radiation, with a spectrum depending on both the intensity of the magnetic field and energy and flux of the electrons. The Galactic magnetic field of order of a few nG is strong enough to produce this effect. The energy spectrum of the electrons is usually modeled as a power law, $\nu^{-\beta}$, with $\beta \simeq 3$ [101]. Synchrotron is the dominant foreground for lower CMB frequency observations.

- *Bremsstrahlung (or free-free) radiation*. In a hot gas, ions decelerate free electrons,

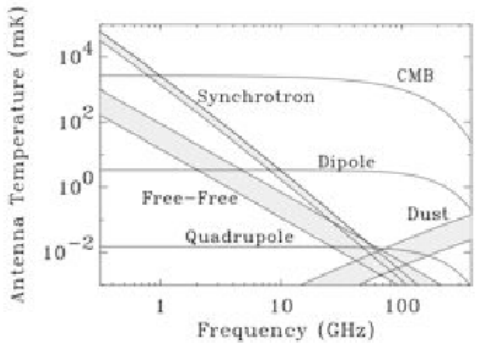

Figure 3.5: Graph showing frequency dependence and approximate relative strength of Galactic synchrotron, free-free, and dust emission as well as that of the cosmic microwave background and its main features. Source- http://science. doe.gov/hep/TFCRreport.pdf

thereby producing thermal radiation. Once again, the free-free spectrum can often be modeled as a power law with spectral index $\beta \simeq 2.1$ [101]. As with synchrotron, free-free emission is most evident at lower CMB frequencies.

- *Galactic dust emission*. Cold dust within our own Galaxy can emit via thermal radiation (vibrational dust) or by excitation of their electrical dipolar moment (rotational dust). Thermal radiation is modeled as a grey body at $T \sim 17K$, with an emission maximum in the far-infrared. In the radio-millimetric domain, the dust emissivity can be modeled as ν^2 [52]. Vibrational dust emission has been claimed to have been seen between 10 and 100 GHz and with a maximum around 20 GHz [102], though it is still a matter of debate.

- *Extragalactic point sources*. Some point sources can emit in the radio-millimetric domain. To avoid contamination by these, they are masked before the CMB power spectrum is estimated. For the background of undetected sources, their effect on the CMB spectrum is evaluated with Monte-Carlos.

Figure (3.5) shows representative foreground spectra, though they may vary depending on location on the sky. CMB experiments usually measure the CMB in the window between $\sim$ 20 and 300 GHz, while measurements at higher and lower frequencies help estimate and limit the level of foreground contaminants within the CMB band.

While some experiments have measured polarized foregrounds, notably Parkes [103] and WMAP [104] for synchrotron and free-free and ARCHEOPS for diffuse dust emis-

sion on large angular scales [105, 106], foreground polarization over the full sky is still not well known. Thus foreground residuals have become one of the largest (if not the largest) source of systematic errors in CMB analysis.

As mentioned, foreground emission can be a major contaminant to CMB measurements. Thus, all CMB experiments take care to either avoid observing regions with excessive foreground emission or to reject these regions when the data are analyzed.

To this point, all satellite-based CMB experiments have used scanning strategies which covered the entire sky, motivated by a combination of technical simplicity and the fact that it is one of the few ways to consistently measure the largest scale anisotropies in the CMB. However, this means that some regions, such as the Galactic plane, are not usable and must be excised from the data. Balloon experiments such as the 19 GHz Experiment [107], FIRS [108] and Archeops [109] have been used to cover large fractions of the sky. In these experiments, the Galactic plane is treated in much the same way as for satellites, with data in high-foreground regions simply avoided in the analysis.

A number of balloon-borne experiments, however, have been used to make maps of localized regions of a few per cent of the sky. In such cases, the observation fields are chosen to coincide with low emission from our Galaxy. In addition, almost all ground-based experiments map only a few per cent of the sky at most and use the same foreground avoidance technique. An example of this is shown in figure (3.6).

3.6 Beyond the power spectrum: non-Gaussianity

Non-Gaussianity in the CMB is a very active field of investigation. The search for primordial non-Gaussianity is mainly related to testing the inflationary models. Moreover, non-Gaussianity is due to secondary anisotropies as well as to foreground emissions and instrument systematics.

The primary challenge in studies of non-Gaussianity is choosing the statistics that quantifies it: non-Gaussianity tells us what the distribution is not, not what it is. The secondary challenge is to optimize the statistics against the Gaussian noise of primary anisotropies and the non-Gaussian noise of foregrounds and systematics.

One of the non-Gaussian tests is the bispectrum, the harmonic analogue of the three-point correlation function. Theoretical work on the bispectrum showed that the inflation-

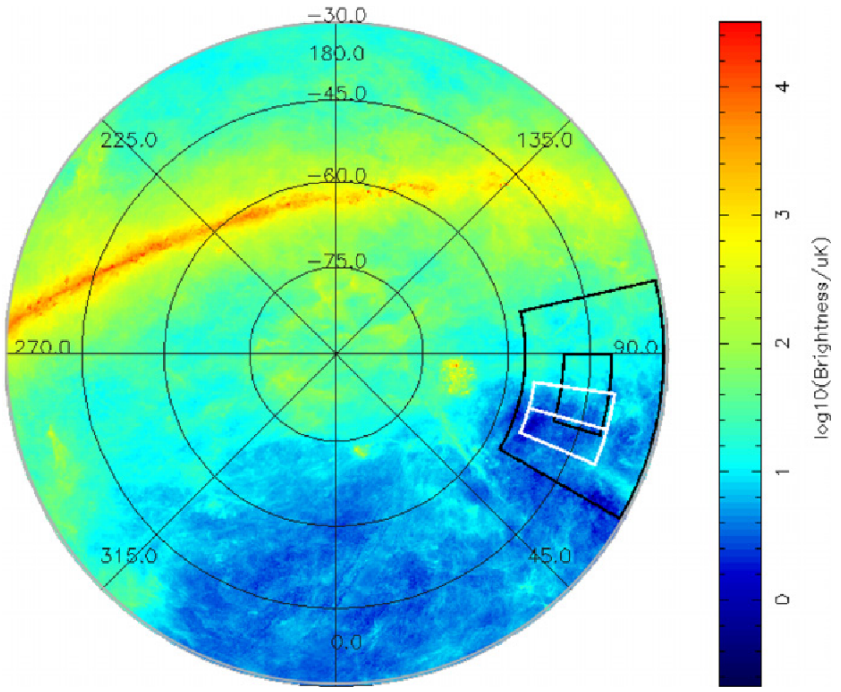

Figure 3.6: Graphic showing an estimate of the emission from dust which would be seen by polarization-sensitive experiments at 150 GHz. The centre of the plot is the zenith at the South Pole-that is declination -90^o. The edge of the plot is -30^o (that is it shows the bottom of the celestial sphere). Zero right ascension is down in the plot, increasing in the counterclockwise direction. The brightness estimates come from application of a model by [110]. The boxes to the right represent the sky coverage for QUaD and BOOMERanG, two CMB anisotropy experiments. The larger and smaller black boxes are the BOOMERanG so-called shallow and deep fields, respectively. The two white boxes are the two fields QUaD observed in their first season of observations.[111]

ary contribution is not expected to be detectable in most models [112 - 114]. Conversely, signatures of secondary anisotropies turned out to be detectable.

The trispectrum, the harmonic analogue of the four-point function, also has advantages for the study of secondary anisotropies. It is also intimately related to the power spectra of quadratic combinations of the temperature field and has been applied to study gravitational lensing effects [75, 76, 115].

Tests for non-Gaussianity localized in angular space include the Minkowsky functionals [116], the statistic of temperature extrema [117], and wavelet coefficients [118]. These may be more useful for examining foreground contamination and trace amounts of topological defects.

3.7 Recent searches for non-Gaussianity

Searches of non-Gaussianity in CMB data have been performed on the whole-sky data sets presently available: the COBE and the WMAP data. Both have been found compatible with the Gaussian hypothesis by the majority of the statistical tests applied. Monte Carlo simulations, taking into account the instrumental and observational constraints of the data under analysis, are usually performed to estimate distributions of the testing statistic as well as confidence levels.

In the case of WMAP, Komatsu et al. (2003) [119] analyzed the temperature maps with angular bispectrum and Minkowsky functional techniques. They found that the WMAP data are consistent with Gaussian primordial fluctuations, and established the most stringent limits on f_{NL} obtained so far, $58 < f_{NL} < 134$, at the 95% confidence level. Both COBE and WMAP CMB maps show some weak evidence for non-Gaussianity, however all these effects resulted to be of systematic origin.

Also ground- and balloon-based experiments could shed more light on the Gaussian hypothesis, however these experiments will suffer from their ability to cover only a small fraction of the sky over a restricted range of frequencies, and are therefore unlikely to make significant impact.

Thanks to the full sky coverage and the improved sensitivity compared to WMAP, Planck should give better constraints on non-Gaussianity. Of course, this will be possible only when non-Gaussian signals due to foreground emissions will be removed from the data, so component separation will be a crucial step.

3.8 Summary

Shortly after the discovery of CMBR, it was predicted that CMBR should show angular variation in its temperatures. this was necessary to explain, in particular, the large scale structure of the universe that we see today. These anisotropies in the CMBR took a long time to discover but once discovered it not only earned a Noble for the discoverers [1] but also revolutionized cosmology leading it to a precision science. In this chapter we have tried to emphasize the physics behind the generation of CMBR anisotropies. We have given details of the computation of the primary temperature anisotropies, and also discussed briefly secondary anisotropies. The observation of the CMB anisotropies an-

gular power spectrum with its plateau, acoustic peaks, and high frequency damping tail have established a standard cosmological model consisting of a flat (critical density) geometry, with contents being mainly dark energy and dark matter and a small amount of ordinary matter. In this successful model the dark and ordinary matter formed its structure through gravitational instability acting on the quantum fluctuations generated during the very early inflationary epoch. Current and future observations will test this model and determine its key cosmological parameters with spectacular precision and confidence. We have already learned a great deal from the detailed observations of the degree and subdegree scale temperature anisotropies, particularly the acoustic peaks. The exploration of small angular scale anisotropies holds the promise of revealing a wealth of information, on the gastrophysics of structure formation. Already WMAP results have revealed a surprisingly large redshift for the reionization of the universe. We can expect in the years to come much more information on cosmology from missions like PLANCK and other CMB experiments, with the possibility of more surprises.

Chapter 4

Polarization of the Cosmic Microwave Background

4.1 Introduction

Studies of the temperature anisotropies in the CMB have provided strong constraints on many of the cosmological parameters. However, for precision cosmology we still need to consider the polarization information of the CMB to break some of the degeneracies that exist between some combinations of parameters. Furthermore, the additional information from CMB polarization is very helpful for studies of cosmological physics on super-horizon scales, where our ability of extracting cosmological information is limited by cosmic variance [98]. Moreover, polarization data can help to distinguish the ingredients which go to make up the temperature power spectrum and therefore the cosmological model. We know that different modes of temperature anisotropies (scalar, vector and tensor) give distinguishable polarization patterns. On the other hand, polarization provides us with a direct probe of the last scattering surface, as opposed to the temperature anisotropies that are affected by various physical effects that occur between the last scattering surface and present. Therefore polarization can help distinguish the sources of anisotropy [120]. However, the CMB polarization is extremely difficult to measure, because it is small and because the polarized foregrounds are poorly known. Nevertheless, there are a number of upcoming experiments designed to make such measurements.

4.2 Theory of CMB polarization

The CMB polarization originates from re-scattering of the primordial photons on the hot electron gas on their way to us. Imagine an electron at rest in the origin. This electron is accelerated by an incoming plane wave of radiation with wave vector $\vec{k_i}$ and re-radiates an outgoing wave along $\vec{k_s}$. Compton scattering allows all the radiation transverse to the outgoing direction to pass through unimpeded, while stopping any radiation parallel to the outgoing direction. Such a process in which the photon energy remain unchanged is called Thomson scattering. The plane spanned by $\vec{k_i}$ and $\vec{k_s}$is the scattering plane, and the cross-section for outgoing photons is proportional to $|\vec{k_i}.\vec{k_s}|^2$. Thus the scattered radiation intensity peaks in the direction normal to the incident polarization [121].

Now imagine the incoming plane wave is traveling along the x axis towards the origin, with its corresponding electric and magnetic fields oscillating in the $y-z$ plane. If the intensity along the two transverse directions y and z is equal, then the light is unpolarized. This ray then scatters off an electron at the origin and gets deflected into all directions with varying probability. The Thomson scattering can then guarantee that the outgoing radiation observed in the $+\hat{z}$ direction has a linear polarization pattern. This is due to the fact that none of the incoming intensity along the outgoing direction (z-axis) gets transmitted. The intensity along the y-axis is the only component of the polarization that passes through unimpeded in the $+\hat{z}$ direction. Hence the outgoing radiation is polarized in the y-direction if observed along the z axis. Obviously, this result is for one single incoming ray and if we generalize to radiation incident from all directions we realize that producing polarization will not be as easy.

Imagine an unpolarized incoming isotropic radiation (monopole) incident from all directions on an electron. Figure (4.1) is a simple representation of such a case where incoming rays from only two directions, the $+\hat{x}$ and $+\hat{y}$ directions, have been depicted. We are still interested in the polarization of outgoing photons in the $\hat{z}$ direction. The intensity of the outgoing ray along the x-axis comes from the radiation incident from the $\hat{y}$ direction, while the outgoing y-intensity comes from the radiation from the x-axis. Since the incoming amplitudes from both directions have equal intensity for an isotropic radiation, the outgoing radiation along the x and y axes will turn out to have equal intensities, leading to an unpolarized outgoing radiation along the $\hat{z}$ direction. Hence, isotropic radiation does not produce polarization.

Incoming dipole radiation also produces no polarization. The simplest example of

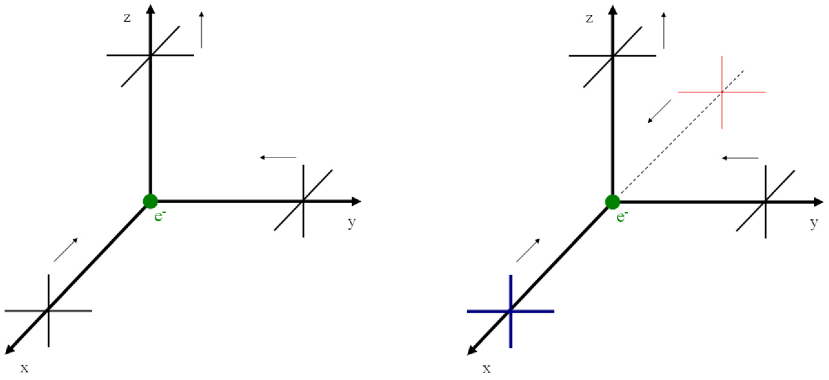

Figure 4.1: Thomson scattering of incoming isotropic (left) and dipole (right) radiation. Here black lines denote radiation with average intensity.Blue (thick) lines show incoming radiation that is hotter than average intensity and red (thin) lines represent radiation that is colder that average. The net result for both isotropic and dipole radiation is outgoing unpolarized light.[122]

a dipole is the case when the incoming radiation is hotter (colder) that average from the $+\hat{x}(+\hat{y})$ direction and colder than average from $-\hat{x}(-\hat{y})$ direction. Figure (4.1) represent such a case. Here the outgoing intensity along the $x-axis$ comes from the $\pm\hat{y}$ incident radiations which have the average temperature. The two rays from the $\pm\hat{x}$ directions also produce an outgoing intensity that is neither hot nor cold along the $y-axis$ because it is just equal to the average intensity of the incoming rays along the $\pm\hat{x}$ direction. Since these have the same average intensity, the intensity of the outgoing wave along x and y axes are equal. Hence the net result is outgoing unpolarized radiation.

To produce polarized radiation, the incident radiation field should actually possess a quadrupole variation in intensity or temperature. This happens when the average incoming radiation from the $\hat{y}$ direction is hotter (colder) than it is along the $\hat{x}$ direction. Figure (4.2) illustrates such a case where the incident radiation along the x-axis is hotter than it is in the y direction. Therefore, the intensity of the outgoing radiation is greater along the y-axis than along the x-axis. Thus, the outgoing radiation is polarized for a quadrupole radiation. Furthermore, since the scattering cross-section of the Thomson scattering is quadratic, we do not proceed to study the effect of larger multipoles.

In reality, a quadrupole anisotropy of the photon flux at one point on the last scattering surface, when the universe is still ionized, can generate polarization in the cosmic background radiation. Before recombination, the high electron density means that the

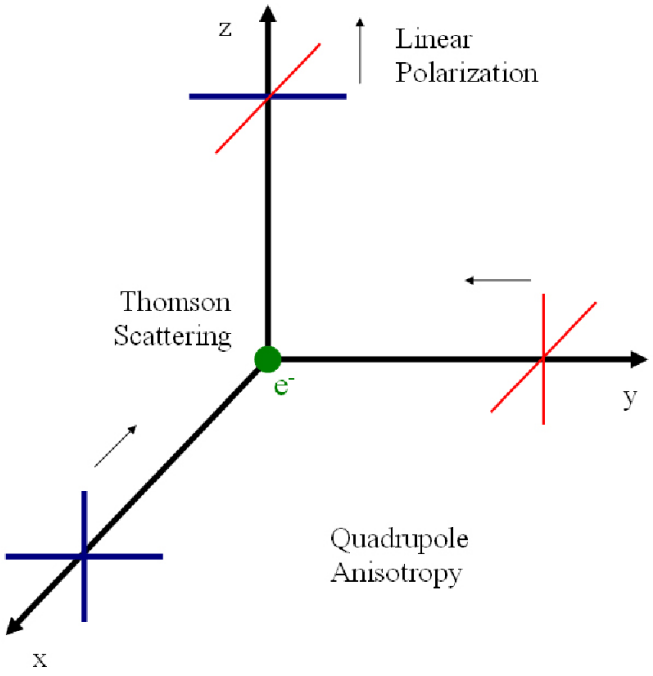

Figure 4.2: Thomson scattering of radiation with a quadrupole anisotropy generates linear polarization. Blue colors (thick lines) represent hot and red colors (thin lines) cold radiation. Source- Wayne Hu, background.uchicago.edu /whu

mean free path of the photons is too small to produce a quadrupole; however after the recombination the electron density is too low for significant Thomson scattering to occur. The polarization can only be produced during a short period around recombination, so we expect the amplitude of the polarization to be smaller than the temperature anisotropies. Also, although late re-ionization, which is due to the process of early star formation, enhances the polarization at large scales, it does not modify the quantitative conclusion that the polarization signal is expected to be small [122].

The quadrupole anisotropy of the photon flux in the last scattering epoch can arise from the velocity gradients of the density fluctuations. In the photon-baryon fluid rest frame, the fluid is accelerated towards the cold spot, or decelerated towards a hot spot. In the former case, the velocity of neighboring particles tends to diverge radially from and converge transversely to the scattering point. In the later case, the velocity of neighboring particles tends to converge radially to and diverge transversely from the scattering point. We see the patterns produced by these processes in figure (4.3). Then the Doppler shift induces a quadrupole flux anisotropy around the last scattering point, leading to ra-

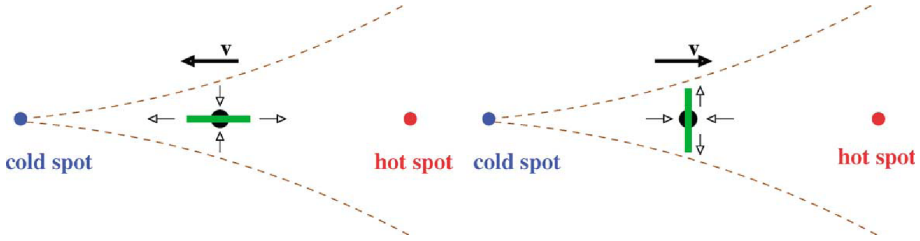

Figure 4.3: Generation of the local quadrupole anisotropies in the photon flux on the last scattering surface from velocity gradients.[163]

dial polarization in the first case and to transverse polarization in the second case. This mechanism does not produce any circular polarization, so from now we set the circular components of the polarization equal to zero.

The polarization properties of the CMB can be best understood using the formalism of Stokes parameters [123]. Consider a nearly monochromatic electromagnetic wave propagating in the z direction, with x and y components of the electric field given by:

$$E_x = a_x(t)\cos[\omega_0 t - \theta_x(t)],$$

$$E_y = a_y(t)\cos[\omega_0 t - \theta_y(t)], \tag{4.1}$$

Then, the Stokes parameters are defined by:

$$I \equiv \langle a_x^2 \rangle + \langle a_y^2 \rangle,$$

$$Q \equiv \langle a_x^2 \rangle - \langle a_y^2 \rangle,$$

$$U \equiv \langle 2a_x a_y \cos(\theta_x - \theta_y) \rangle,$$

$$V \equiv \langle 2a_x a_y \sin(\theta_x - \theta_y) \rangle. \tag{4.2}$$

where the brackets $\langle\ \rangle$ represent the average over a time much longer than the period of the wave. The physical interpretation of the Stokes parameters is straightforward. The parameter I is simply the average intensity of the radiation. The polarization properties of the wave are described by the remaining parameters: Q and U describe linear polarization, while V describes circular polarization. Unpolarized radiation (or natural light) is characterized by having $Q = U = V = 0$. CMB polarization is produced through Thomson scattering (see below) which, by symmetry, cannot generate circular polariza-

tion. Then, $V = 0$ always for CMB polarization. The amount of linear polarization along the x or y directions is measured by the Stokes parameter Q. When $U = 0$, a positive Q describes a wave with polarization oriented along the x axis, while a negative Q describes a wave with polarization oriented along the y axis. Similarly, the Stokes parameter U measures the amount of linear polarization along the two directions forming an angle of 45^o with the x and y axis.This implies that the Stokes parameters Q and U are not scalar quantities. It is straightforward to show that when the reference frame rotates of an angle ϕ around the direction of observation, Q and U transform as:

$$\begin{pmatrix} Q' \\ U' \end{pmatrix} = \begin{pmatrix} \cos 2\phi & \sin 2\phi \\ -\sin 2\phi & \cos 2\phi \end{pmatrix} \begin{pmatrix} Q \\ U \end{pmatrix} \tag{4.3}$$

This means that Q and U are not the components of a vector. Mathematically, Q and U are the components of a second-rank symmetric trace-free tensor:

$$P_{ab} = \begin{pmatrix} Q & U \\ U & -Q \end{pmatrix}, \tag{4.4}$$

which represents a spin-2 field. For visualization purposes only, one can define a polarization vector with amplitude $P = (Q^2 + U^2)^{1/2}$ and orientation $\alpha = 1/2tan^{-1}(U/Q)$: this is not properly a vector, since it remains identical after a rotation of π around z, thus defining an orientation but not a direction.

4.2.1 Thomson scattering

Having introduced the proper formalism, we can focus on the physical mechanism that generates the polarized component of CMB radiation. Before the formation of neutral hydrogen atoms in the primordial universe (a process termed recombination which takes place a few hundred thousand years after the big bang, at redshift ≈ 1100), the CMB photons closely interact with the free electrons of the primeval plasma through Thomson scattering. The angular dependence of the scattering cross-section is given by:

$$\frac{d\sigma}{d\Omega} = \frac{3\sigma_T}{8\pi} |\hat{\varepsilon}.\hat{\varepsilon}'|^2, \tag{4.5}$$

where $\hat{\varepsilon}$ and $\hat{\varepsilon}'$ are the polarization directions of incident and scattered waves. After scattering, initially unpolarized light has:

$$I = \frac{3\sigma_T}{16\pi} I'(1+\cos^2\theta),$$

$$Q = \frac{3\sigma_T}{16\pi} I'(\sin^2\theta),$$

$$U = 0. \tag{4.6}$$

Decomposing the incident radiation in spherical harmonics and integrating over all incoming directions gives:

$$I = \frac{3\sigma_T}{16\pi}\Big[\frac{8}{3}\sqrt{\pi}a_{00} + \frac{4}{3}\sqrt{\frac{\pi}{5}}a_{20}\Big],$$

$$Q - iU = \frac{3\sigma_T}{4\pi}\sqrt{\frac{2\pi}{15}}a_{22}. \tag{4.7}$$

Then, polarization is only generated when a quadrupolar anisotropy in the incident light at last scattering is present. This has two important consequences. Because it is generated by a causal process, CMB polarization peaks at scales smaller than the horizon at last scattering. Moreover, the degree of polarization depends on the thickness of last scattering surface. As a result, the polarized signal for standard models at angular scales of tens of arcminutes is about 10% of the total intensity (even less at larger scales). Typically, this means a polarized signal of a few μK.

4.2.2 Statistics

In order to connect the observed polarized signal to theoretical prediction, it is convenient to expand the polarization tensor in terms of two scalar fields: a so-called electric (or gradient) field, E, and a magnetic (or curl) field, B. This is analogous to the decomposition of a vector into a gradient and divergence-free vector. These fields can then be expanded into spherical harmonics just as it is done with the temperature field, as:

$$P_{ab} = T_0 \sum_{l=2}^{\infty} \sum_{m=-l}^{l} \Big[a^E_{lm} Y^E_{(lm)ab} + a^B_{lm} Y^B_{(lm)ab}\Big] \tag{4.8}$$

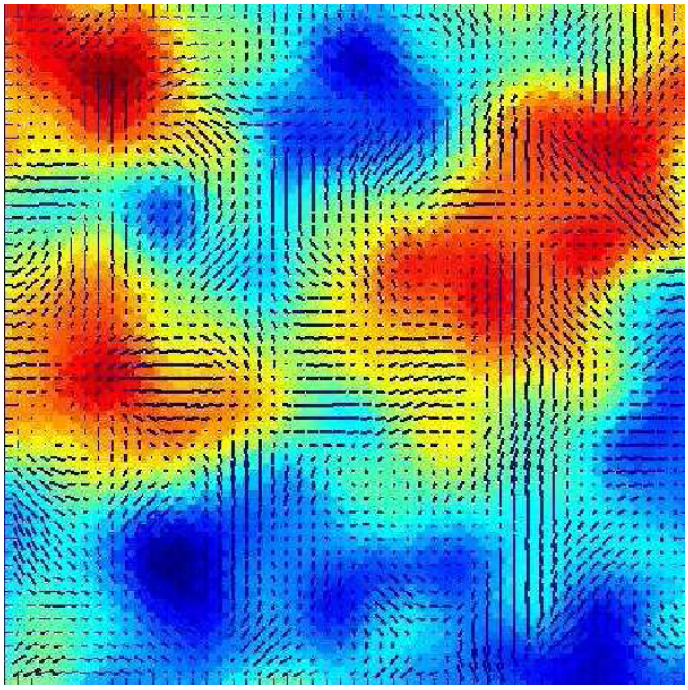

Figure 4.4: A simulated CMB temperature map and the corresponding polarized component represented by the polarization vector P, for a standard cosmological model where only scalar density perturbations are present. The field is $6^o \times 6^o$, the resolution is $10'$ FWHM.[159]

where the generalization of spherical harmonics for arbitrary spin has been used [124]. The statistical properties of the CMB anisotropies polarization are then characterized by six power spectra: C_l^T for the temperature, C_l^E for the E-type polarization, C_l^B for the B-type polarization, $C_l^{TE}, C_l^{TB}, C_l^{EB}$ for the cross correlations. Each of the power spectra is computed in the usual way from the spherical harmonic coefficients, as:

$$\left\langle a_{lm}^{X*} a_{l'm'}^{X'} \right\rangle = C_l^{XX'} \delta_{ll'} \delta_{mm'} \tag{4.9}$$

For the CMB, $C_l^{TB} = C_l^{EB} = 0$. Furthermore, since B relates to the component of the polarization field which possesses a handedness, one has $C_l^B = 0$ for scalar density perturbations. The detection of a non zero B component would then point to the existence of a tensor contribution to density perturbations. An example of theoretical power spectra is shown in Figure(4.5).

The relation between (E, B) and (Q, U) has a non-local nature. This can be easily

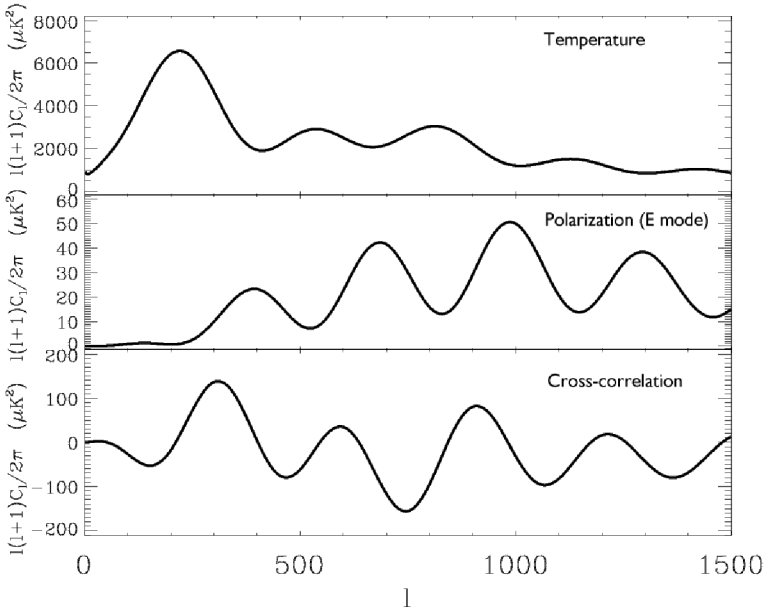

Figure 4.5: An example of the theoretical prediction for the power spectrum of CMB temperature fluctuations (upper panel), polarization E-mode (central panel), and cross-correlation between temperature and E-modes (bottom panel). It is quite noticeable the fact (described in the text) that peaks in E spectrum are out of phase with those in the T spectrum. Polarization also peaks on smaller angular scales and has a much lower intensity than temperature.[159]

seen in the limit of small angles, where it can be written as:

$$E(\theta) = -\int d^2\theta' \omega(\tilde{\theta}) Q_r(\theta'),$$

$$B(\theta) = -\int d^2\theta' \omega(\tilde{\theta}) U_r(\theta'), \tag{4.10}$$

where the 2D angle θ defines a direction of observation in the coordinate system perpendicular to z,

$$Q_r(\theta) = Q(\theta')\cos(2\tilde{\phi}) - U(\theta')\sin(2\tilde{\phi}),$$

$$U_r(\theta) = U(\theta')\cos(2\tilde{\phi}) + Q(\theta')\sin(2\tilde{\phi}), \tag{4.11}$$

and $\omega(\tilde{\theta})$ is a generic window function.

4.2.3 CMB polarization as a cosmological tool

The polarization power spectrum for the E mode shows the same kind of acoustic features that are now well known to exist in the temperature anisotropy spectrum. The peaks in polarization, however, are out of phase with those in the temperature: E mode polarization has maximum intensity where the temperature is at a minimum, and vice versa. This is due to the fact that polarization is generated by quadrupolar anisotropy at last scattering, and this is closely related to the velocity of the coupled photon-baryon fluid. The maximum compression or rarefaction (and minimum velocity) of the fluid corresponds to peak in the temperature anisotropy (and troughs in the polarization). For the same reason, the cross-correlation power spectrum between temperature and E polarization shows pronounced peaks corresponding to the interleaved sets of maxima and minima in the two separate components. A detection of such features in the polarization and cross-polarization power spectra is then crucial for two reasons: first, to give an independent confirmation of the fact that the temperature anisotropy peaks are a sign of genuine acoustic oscillation in the primeval plasma; second, to confirm the adiabatic nature of primordial perturbations (the only known way to produce acoustic oscillations) thus providing strong support to cosmic inflation.

A large amount of valuable cosmological information can be extracted from the observation of CMB polarization. Since it probes the epoch of decoupling, polarization allows one to perform detailed tests of the recombination physics. In particular, it is a well known fact that the universe underwent a phase of reionization at redshifts of at least $z \sim 5$, during the formation of early cosmic structure. The investigation of this so-called dark ages is an active subject of investigation [125]. The CMB temperature anisotropy signal gets damped when the photons are diffused by free electrons along the line of sight. The amount of damping would be a powerful probe of the optical depth to reionization. However this effect is masked by other physical mechanisms. For example, there is a strong degeneration with the spectral index of primordial perturbations. CMB polarization would prove very powerful in removing these degeneracies: if the optical depth is non zero, a recognizable polarization signature gets generated at large angular scales, allowing to investigate the detailed reionization history, discriminating models that have the same optical depth but a different evolution of the ionization fraction with redshift [126]. Not only the characterization of the detailed ionization history of the universe would have a strong scientific impact, but it would also greatly increase the accuracy of the determination of other cosmological parameters, such as the above mentioned spectral index

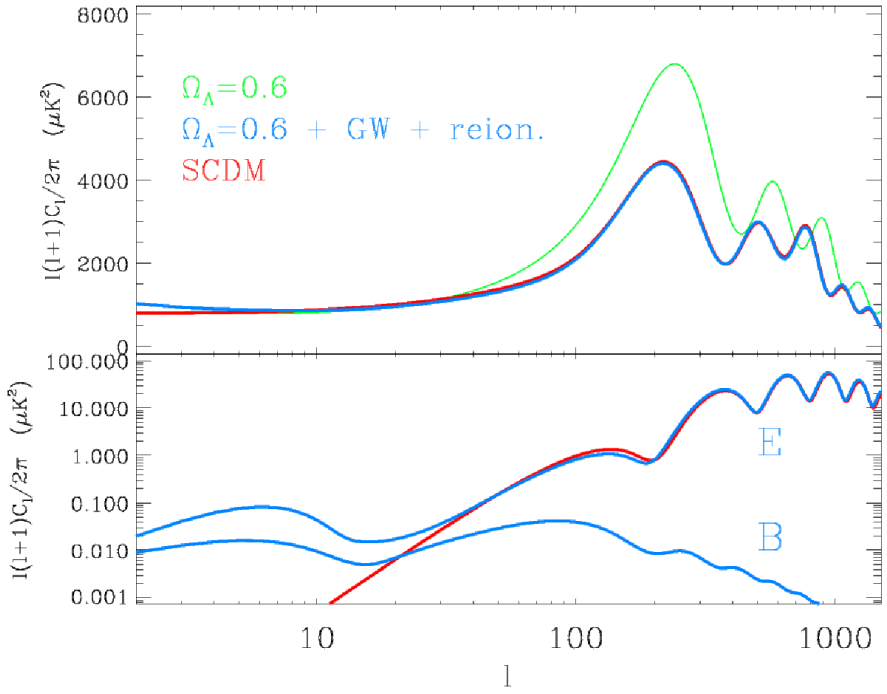

Figure 4.6: Top panel: Temperature power spectra for a standard CDM model (solid line), and the same CDM model with a fraction of the critical density coming from a cosmological constant (dotted line). If we add to the latter a contribution from tensor perturbations (gravitational waves background) and reionization (dashed line) we can make it indistinguishable from the standard CDM model. Bottom panel: The same models and their polarization power spectra. The CDM model can be identified by its polarized signal, because it does not generate a B-type component.[177]

of scalar primordial perturbations. This, in turn, would be extremely important when constraining models of inflation.

One crucial aspect of CMB polarization has to do with the properties of its B component. The consequences of detecting B polarization for theoretical models would be enormous. B modes, as mentioned above, can only be generated when a tensor component of primordial perturbations is present (namely, a background of primordial gravitational waves). This is precisely one of the prediction of inflationary scenarios. The ratio of scalar to tensor fluctuations r, related to the amplitude of B modes, is a direct signature of the inflation energy scale. On the other hand, observing the B component is the hardest challenge faced by experimentalists, since the signal is expected to be extremely faint, and possibly contaminated by diffuse galactic emission. Furthermore, the B spectrum

should peak at large angular scales (the most affected by cosmic variance) and can be contaminated by spurious leakage from E modes when the observed area does not cover the entire sky. The level of B signal also depends very strongly on the epoch and amount of reionization, so that the predictions of detectabilities are affected by the assumptions made on the ionization history of the universe. Finally, weak lensing from large scale structure in the local universe affects the distribution of CMB photons (resulting in a so-called cosmic shear). This can induce a curl component in the polarization signature, that can be wrongly interpreted as evidence for non zero B modes, or act as a background that would make the tensor primordial contribution impossible to detect [127]. Techniques to detect and remove the shear contribution have been developed and should prove effective when dealing with future data [128]. The shear contribution has also a scientific interest in itself, since it has been shown [79] that it can lead to a determination of the neutrino mass from measurements of CMB temperature and polarization alone.

4.2.4 Information carried by CMB polarization

The CMB temperature fluctuations are the imprint on the last scattering surface of density and metric perturbations. They are classified as scalar, vector and tensor depending on their transformation properties under rotations. Vector perturbations get damped by expansion and only the scalar and tensor ones survive. The scalar contributions comprise total density fluctuations, also called curvature or adiabatic perturbations, and isocurvature fluctuations where only the relative densities of the different components vary. Tensor fluctuations are expected from the primordial gravity waves predicted in the inflationary scenario. CMB polarization allows to separate them from scalar perturbations [129, 126].

E polarization: scalar fluctuations

Scalar perturbations only generate positive parity polarization patterns, and therefore can only produce E type CMB polarization fluctuations. In the absence of isocurvature perturbations, the TE spectrum is completely calculable from the EE spectrum. This property is extremely well verified by the TE spectrum observed by the WMAP collaboration (Fig. 4.8).

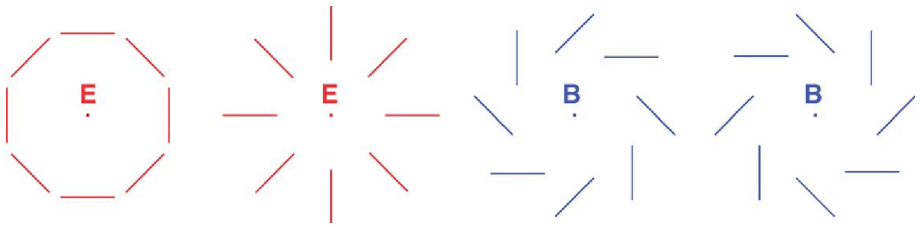

Figure 4.7: Typical E or B polarization patterns.[129]

B Polarization: tensor fluctuations

On the other hand, tensor fluctuation can produce both E and B polarization [131, 132]. Therefore the relative intensity of B polarization modes is a constraint on the ratio r of tensor to scalar fluctuations.

Link with the inflation paradigm

The inflation paradigm was introduced by Guth [44], Linde [45] and Albrecht and Steinhardt [46] to solve the horizon problem: the present observed Universe appears homogeneous on scales which have never been in causal contact, due to the finite light speed. In particular the CMB is homogeneous across the whole sky at the 10^{-5} level, although the horizon size at the time of decoupling is of order 1 degree on the sky sphere.

In inflationary models, the very early Universe undergoes a rapid expansion phase driven by the vacuum energy of some scalar field. This inflation must last long enough for the comoving size of the horizon before inflation to be larger than the present size of the horizon ($\simeq 1/H_0$). This implies an inflation factor of order e^{40} to e^{60}, depending on when inflation ends (after GUT symmetry breaking and before baryogenesis).

Although the horizon problem, the near flatness of our universe and the elimination of unwanted relics (GUT's monopoles, domain walls, . . .) were the original motivations to propose inflation, this scenario also naturally provides the seeds of the present large scale structures. These seeds are the microscopic quantum fluctuations of the inflation field, which are inflated to macroscopic adiabatic scalar perturbations during inflation. One of the generic predictions of inflation is the presence of acoustic peaks in the C_l spectrum which have now been observed beyond any doubt [133 - 135, 109]. The reason is that perturbations begin to oscillate when they enter the horizon and all perturbations

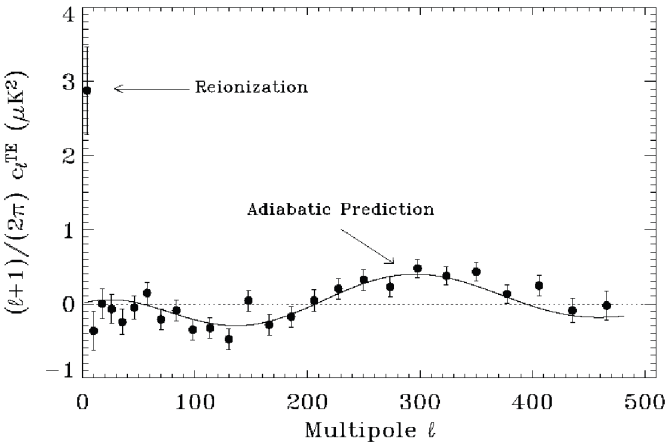

Figure 4.8: The TE spectrum as observed by WMAP. The solid line is computed from the best fit to the TT spectrum, without additional free parameter, assuming adiabatic perturbations.[130]

with the same size do so at the same time. The acoustic peaks arise from this coherent oscillation. The fact that the peaks in the TE spectrum observed by WMAP are out of phase with the temperature peaks is a further confirmation of the acoustic scenario because polarization originates in velocity gradients. The dip in the TE spectrum around $l \simeq 150$ indicates the presence of superhorizon size fluctuations at the time of decoupling, which is a strong indication in favor of inflation.

In much the same way, the space metric also undergoes quantum fluctuations which produce primordial gravity waves (tensor perturbations). The ratio between tensor and scalar perturbations, defined as $r = (C_l^T/C_l^S)_{l=2}$, is related to the energy scale of inflation $E_{inflation}$. For example, in the popular slow-roll approximation [136],

$$r = 0.1\Big(\frac{E_{inflation}}{2 \times 10^{16} GeV}\Big)^4 \tag{4.12}$$

Therefore, detection of B-mode polarization will allow to measure this energy scale, but the quick decrease of r with $E_{inflation}$ may make it difficult.

4.3 CMB polarization detection

It has been realized as early as 1968 [69] that, close to decoupling, Thomson scattering would induce a small degree of linear polarization on unpolarized but anisotropic CMB photons. However, the weakness of this contribution has prevented its detection until very recent times. Over four decades of experimental efforts have resulted in a quite lengthy series of upper limits (e.g. [29, 133, 137 - 144]). These limits speak of a steady increase towards the level of the polarization anisotropy, a quest well motivated by the understanding - that had become clear along road - of the wealth of cosmological information encoded in the polarization power spectra.

The long pioneering phase was ended by the DASI (Degree Angular Scale Interferometer) [145] detection of a TE and EE signal in 2002. DASI is a ground based interferometer located at the South Pole Amundsen-Scott research station. When configured as a polarimeter, it has sensitivity to all four Stokes parameter, and has been optimized to study CMB anisotropy in the range $140 \lesssim l \lesssim 900$ [15]. The first release has reported a detection of EE mode polarization with an rms amplitude of 0.8μK at 4.9σ and $a \sim 2\sigma$ detection of TE, values strengthened to 6.3σ (2.9σ) for $EE(TE)$ in the three years release [146].

DASI is a compact interferometric array optimized for the measurement of CMB temperature and polarization anisotropy. Because they directly sample Fourier components of the sky, interferometers are well suited to measurements of the CMB angular power spectrum. In addition, an interferometer gathers instantaneous two-dimensional information while inherently rejecting large-scale gradients in atmospheric emission. For observations of CMB polarization, interferometers offer several additional features. They can be constructed with small and stable instrumental polarization. Furthermore, linear combinations of the data can be used to construct quantities with essentially pure $E-$ and $B-$mode polarization response patterns on a variety of scales. This property of the data greatly facilitates the analysis and interpretation of the observed polarization in the context of cosmological models.

After the first detection of CMB polarization spectrum by the DASI on the intermediate band of angular scales ($l \sim 200 - 440$) in late 2002 [15], the field has rapidly grown, with measurements coming in from a host of ground-based and balloon-borne dedicated CMB polarization experiments. The full sky E-mode polarization maps and polarization spectra from WMAP were a new milestone in CMB research [130, 147]. Although the

CMB polarization is a clean probe of the early Universe that promises to complement the remarkable successes of CMB anisotropy measurements it is also a much subtler signal than the anisotropy signal. Measurements of polarization by ongoing experiments at sensitivities of μK (E-mode) have had to overcome numerous challenges in the past decade. The tens of nK level B-mode signal pose the ultimate experimental and analysis challenge to this area of observational cosmology. The most current CMB polarization measurement of C_l^{TT}, C_l^{TE} and C_l^{EE} and a non-detection of B-modes come from QUaD and BICEP. They also report interesting upper limits C_l^{TB} or C_l^{EB} , over and above observational artifacts [148]. A non-zero detection of C_l^{TB} or C_l^{EB} , over and above observational artifacts, could be tell-tale signatures of exotic parity violating physics [149, 150] and the CMB measurements put interesting limits on these possibilities.

PLANCK [151] considered the ultimate CMB temperature anisotropy mission, has polarization capabilities in all its coherent (LFI) detectors and in many bolometric (HFI) detectors. The uniqueness of Planck is in that it will produce Q and U maps over the full sky over a wide range of frequencies, with the combination of high sensitivity and tight control of systematics that is only achievable from space.

4.3.1 Current implications for cosmology

The present status of CMB polarization observations does not allow a determination of cosmological parameters at the same level of accuracy obtainable using temperature anisotropies. The most useful cosmological result established using CMB polarization data is, currently, one of consistency: the standard cosmological model (a universe with flat geometry, dominated by dark matter and dark energy of unknown nature, and consistent with the basic predictions of the inflationary scenario) predicts a level of CMB polarization that is not ruled out by observations, and actually seems to be of the right intensity to match the present data. Intriguingly, the peak and trough positions in the E polarization spectrum seems to fall in the right places to match the predictions of the adiabatic primordial perturbation scenario [152]. The level of B polarization is well within the upper limits derived from the observations. These results lend further support to the basic cosmological scenario - although they are undoubtedly in need of stronger confirmations.

Perhaps, the strongest cosmological constraints from CMB polarization are currently indirect ones. For example, when the WMAP EE data are taken into account, they help to exclude a significant set of values for the optical depth to reionization. Claims of

a very early reionization epoch from the first year release of WMAP data [153] were essentially driven by a large TE correlation detected at large angular scales: this has now dramatically changed, once better data from observations and new constraints on E modes were taken into account [154]. Better constraints on τ have, in turn, had a consequence for the determination of the primordial spectral index, since the degeneracy between τ and n_s got significantly reduced.

To summarize, the CMB polarization looks currently very promising as a tool to constrain cosmological models, but observations are not at the level of accuracy needed to push the envelope of parameter determination. Clearly, much better data are needed, particularly in the area of B modes, still almost unexplored.

4.3.2 Experimental concerns

Before CMB polarization measurements can be turned into a high precision cosmological tool, thorough understanding of many experiment related issues is required. In comparison with intensity anisotropy measurements, significant complications arise.

One obvious issue is detector sensitivity: detecting the CMB E mode polarization requires an instrumental sensitivity a couple of orders of magnitude higher than intensity, and even in the most favorable models the B mode signal is a further order of magnitude below E. However, very little room is left for improvement in single detector technology: bolometers used in modern CMB missions (such as BOOMERanG and Planck HFI) are already photon noise limited [155], while coherent detectors (e.g., HEMT based radiometers) are not expected to improve significantly in the near future[156]. The only possible way to increase sensitivity is thus by statistical redundancy, increasing the total integration time and/or the number of detectors that populate the focal plane. The former strategy clearly speaks in favor of ground based and space borne missions, although Ultra Long Duration Ballooning (ULDB) CMB aimed flights could be achieved in the near future. In any case, long term stability of highly sensitive instruments is a matter of concern. On the other hand, integration of many detectors on a single focal plane seems to be an unavoidable complication. Concerns here mainly relate to manufacturing costs, since it is unsuitable to mass produce highly sensitive CMB detectors, and, in the case of space borne experiments, power budget availability, since active cooling is likely to be required. In addition, it is unclear how high density focal plane will behave in terms of cross talk between detectors. The current trend is towards photolithographic arrays

of bolometers, although techniques are being devised that could make radiometer arrays perfectly feasible and competitive.

Detector sensitivity is not the only problem. Polarization measurements inherit and magnify all the contaminations by systematic effects that have plagued high precision temperature observation. In addition, being polarization a tensor quantity, its measurement strategies are usually more complicated than those adopted for intensity. Hence, a number of polarization specific systematic effects have been predicted - and encountered - that are likely to complicate or even hamper detection, regardless of statistical noise control. The long list includes optics induced polarization (most telescopes used for CMB are off-axis system due to the necessity of controlling sidelobes), band and gain mismatch between detectors, cross polarization (i.e. far from perfect isolation effects) and beam asymmetry, that induces leakage of I into Q and U. Furthermore, due to limiting scanning strategy constraints, polarization is usually estimated by joint analysis of several detectors, both in order to gain sensitivity and account for poor redundancy in detector orientation. This fact further complicates the analysis, as optical beam mismatches and detector cross talks become sources of concern. For instance, BOOMERanG 03 had to correct for noise correlated among different detectors [157], while WMAP has encountered problems related to gain variations [158]. The above complications also reflect onto data analysis techniques, which often must be redesigned to tackle polarization [159].

Our best window for observing the temperature anisotropies lies close to 70 GHz, where foreground emission seems to display a minimum. This has permitted accurate mapping of the CMB intensity pattern, without sacrificing much sky to foregrounds. However, when precision measurements are at the stake, cleaning or component separation techniques are needed [160, 161]. A fortiori, the same is deemed true for polarization measurements, although not much is known about polarized foreground emission. Archeops has measured polarized emission from dust at 353 GHz both in the Galactic plane [84] and at higher Galactic latitudes [106]. In the latter case, extrapolation of their findings suggest that polarized dust emission will be a major source of concern for measurements above 100 GHz [106]. WMAP found significant contamination from polarized foreground extended to large portions of the sky; the WMAP team analysis shows that a foreground model must be subtracted from the data to obtain meaningful detections of CMB polarization at low $(l < 10)$ multipoles and that the cleanest window for polarization measurements is located at about 60 GHz [162]. Under the hypothesis that all other statistical and systematic error sources will eventually be tamed, foreground con-

taminations are likely to dominate the uncertainties in future measurements of the CMB anisotropy pattern, just like what is happening today with intensity. It is also likely that component separation methods will play an important role in the analysis [163].

4.3.3 Exploiting the B modes: an experimental challenge

The current goal in CMB science is to measure the B modes and distillate cosmological information out of them. The two hot fronts of this research are the low $l(\sim 100)$ signal from primordial gravitational waves and the high l contribution from lensed E modes. It is likely that, if inflation is a reliable theory and if there are no unforeseen systematic complication, one or more sub orbital efforts will actually detect these modes. Another question, however, is whether such a detection will prove robust and accurate enough to derive firm consequences for Cosmology. It is a widely accepted argument that only a satellite mission can achieve the correct combination of full sky sampling, sensitivity, thermal stability and spectral coverage that will turn the detection into solid science. In this respect, the many suborbital efforts under development will act as pathfinders, returning invaluable testing of frontier technological devices.

Several post PLANCK orbital efforts are under study. NASA has solicited proposals for its "Beyond Einstein program in structure and evolution of the universe; in particular, the request is for a medium size mission code named Inflation Probe, to search for the gravitational wave signature in the CMB. The current Inflation Probe candidate is called CMBPOL [164]. If selected, this mission could be flown as early as 2018.

4.4 Summary

In this chapter we have presented a brief overview of the status and prospects of CMB polarization research. We discussed how Thomson scattering of anisotropic radiation at last scattering gives rise to linear polarization in the microwave background. The polarization signal depends more directly than the temperature signal on the fluctuations at the last scattering surface and thus encodes a wealth of cosmological information, some of which is complementary to the temperature anisotropies. In addition, large-angle polarization is generated by subsequent rescattering as the Universe reionizes, providing a unique probe of the thermal history of the Universe at the end of the dark ages (redshifts

$z \lesssim 50$) when the first stars and galaxies formed. The scientific potential of investigating polarization cannot be underestimated: we can obtain crucial information on such topics as the physics of reionization, the energy scale of inflation, we can get much better constraints on cosmological parameters that are currently affected by severe degeneracies and even measure accurately the mass of the neutrino. The flatness of the universe and the harmonic structure of the CMB spectrum are now well established. The first observations of CMB polarization by DASI and WMAP point in the direction of inflation. We have seen that CMB polarization observations have a high potential to assess the cosmological scenario and in particular have much to say about inflation. Moreover, it carries information on early star formation and high redshift matter distribution. CMB polarization, being very small and the polarized foregrounds poorly known, is extremely difficult to measure. The field is already in a phase of hectic activity, data of increasing quality are being released and many new missions devised.

Looking to the future, further potential returns from polarization observations include: improved limits on cosmological parameters, in particular the lifting of several degeneracies that involve the optical depth through reionization; a probe of the detailed ionization history beyond a single optical depth estimate; the clean signature of a stochastic background of gravitational waves generated during inflation; evidence for weak gravitational lensing through the distortion of the CMB polarization on small scales.

Chapter 5

Cosmological Parameter Estimation

5.1 Introduction

Cosmology has advanced from an era of largely qualitative questions (like geometry of the universe, dark energy etc.) to one wherein precise determinations of many of the Universe's properties are possible. We have cosmological models capable of explaining the detailed observations available and whose parameters may soon be pinned down at the 10% level, and in some cases the 1% level [165]. Nevertheless, quality cosmological data are an expensive resource, and it is imperative to make the best possible use of them. This implies use of the best available statistical tools in order to obtain accurate and robust conclusions.

The established leading cosmological model considered five material constituents: baryons (taken, imprecisely, to include electrons), photons, neutrinos, cold dark matter (CDM), and dark energy. The simplest model for dark energy, a cosmological constant Λ, is in excellent agreement with observations, and the model is thus known as the ΛCDM model. The most important constraints on this model come from the evolution of cosmic structures. These are seeded by small initial density perturbations, which in the standard cosmological model are taken as adiabatic, Gaussian, and nearly scale invariant, as predicted by the simplest models of cosmological inflation [136].

The ΛCDM model is supported and constrained by a series of cosmological observations. The most important of these are measurements of the CMB anisotropies, particularly those taken by WMAP. Typical analysis also incorporate other data, such as galaxy

clustering data, the luminosity distance-redshift relation of type Ia supernovae, and direct measures of the Hubble constant. The region of parameter space in which the ΛCDM model matches all these data is often referred to as the concordance model.

This model's simplest incarnation contains three assumptions: (a) The photon density is well measured by the CMB temperature, (b) neutrinos are nearly massless, and (c) the Universe is spatially flat. The model then features only four fundamental parameters: the Hubble parameter h, the densities of baryons Ω_b and CDM Ω_{CDM}, and the amplitude of primordial density perturbations A_S. In addition, a comparison with data usually includes extra phenomenological parameters, which can be computed from the above in principle but not in practice. For CMB studies, the optical depth τ , which measures the fraction of CMB photons scattering from ionized gas at low redshift, is needed, whereas use of galaxy clustering data may require inclusion of the galaxy bias parameter b, which relates galaxy clustering to dark matter clustering.

Beyond these basic parameters, cosmologists hope that future investigations will uncover new physical processes, permitting extra parameters to be incorporated and measured. In some cases, it is all but certain that the parameter is relevant and that observational sensitivity will soon become sufficient to reveal its physical effects. Examples of such parameters are neutrino masses and the cosmic helium fraction (although the latter is-again, in principle-computable from other parameters, independent verification of its value would be an important consistency check).

Much more numerous, however, are the parameters describing effects that may or may not be relevant to our Universe [166]. Are the primordial perturbations precisely scale invariant, or do they have a scale dependence quantified by the spectral index n? Do primordial gravitational waves exist, as predicted by inflation? Does the dark energy density evolve with time? Are there cosmic strings in the Universe? Are the initial perturbations really adiabatic and Gaussian? A fuller account of these parameters can be found in [167].

Creation of precision cosmological models is an ongoing process with two distinct goals. The first is to determine the set of parameters (i.e., physical processes) necessary to describe the available observations. The second is to determine the preferred values of these parameters. We can then pursue the ultimate aim of relating cosmological observations to underlying fundamental physics.

5.2 Statistical Tools

A given cosmological model is specified by a set of cosmological parameters:

$$\mathbf{P} = \{p_1, p_2, p_3, ...p_n\} \tag{5.1}$$

entering in the calculation of the theoretical power spectrum, $\bar{C}_l$. A CMB experiment measures the temperature fluctuation of the CMB in different directions on the sky. These data are used to build a minimum variance map of the CMB. From the map, maximum likelihood estimates of the power spectrum are extracted as a set of average band power measurements over an interval b in l:

$$C_b \equiv \sum_{l \in b} S_l C_l \tag{5.2}$$

where the shape function S_l is usually assumed to be $S_l \propto l(l+1)$.

The best estimate of the cosmological parameters from a set of measured band powers can be derived in a Bayesian sense by maximizing the likelihood function:

$$L(p) \propto P(C_b|p)P(p|prior) \tag{5.3}$$

Since CMB anisotropies and polarization measurements can be used to constrain cosmological models and their parameters, it is time to take a closer look on how to obtain the information we want from a set of data. Most of this information can only be obtained using a statistical analysis, which requires some set of tools, which we will review in this section.

5.2.1 Probabilities and likelihood

Let us start by the concept of probability distribution function $P(X)$. It measures a degree of possibility that a given random variable X takes a specific value x. This random variable can be the temperature power spectrum of the CMB at a given multipole l.

The p.d.f for every random variable must satisfy the axioms of probability:

- $P(x) \geq 0$. —-The probability is a non negative real number.
- $\int P(x)dx = 1$. —- The probability of all events occurring is equal to one.

- $P(a,b) = P(a)P(a|b)$. —-The probability of a and b to happen is the probability of a times the conditional probability of b given a. The reverse is also true.

The p.d.f allows to define some important quantities for the random variable X, such as the mean $\bar{X}$ and variance $Var(X)$:

$$\bar{X} = \int XP(X)dX \tag{5.4}$$

$$VarX = \int (X - \bar{X})^2 P(X)dX \tag{5.5}$$

The p.d.f can be generalized to describe the joint probability of n random variables. This can be written as $P(X_1, ..., X_n)$. An important quantity that measures if a set of n random variables are independent or not is the covariance matrix, defined as:

$$C_{i,j} = \int P(X_1, ..., X_n)(X_i - \bar{X}_i)(X_j - \bar{X}_j) \tag{5.6}$$

If $C_{i,j}$is a diagonal matrix, all random variables are independent, otherwise, they are said to be correlated. The most commonly used p.d.f in Cosmology and astrophysics is the Gaussian distribution, which is characterized by two parameters, the mean μ and variance σ^2:

$$P(X) = \frac{1}{\sqrt{2\pi}\sigma} exp\Big(- \frac{(X-\mu)^2}{2\sigma^2}\Big) \tag{5.7}$$

The importance of this distribution is related to the central limit theorem, which states that the sum of many independent and identically distributed random variables converges to a Gaussian distribution, independent of the p.d.f of the individual variables. This applies in cosmology to considering Gaussian distribution for the data, even if each data point is not drawn from a Gaussian distribution. Also, the fluctuations in the CMB and matter power spectrum are expected to be Gaussian.

Let us now address the subject of parameter estimation. Generally, we are interested in using a limited number of observations, which constitute a random sample, and use them to determine the properties of the underlying p.d.f, which in turn are related to a set of unknown parameters we want to measure. Consider then a set of n observations $y = \{y_1, y_2, ..., y_n\}$ of the random variable vector $Y = \{Y_1, Y_2, ..., Y_n\}$ and a set of p parameters used to model the distribution data $\theta = \{\theta_1, \theta_2, ..., \theta_p\}$.

One can define the likelihood for the observed data as the joint conditional probability density function for observing the data points y_i, given the values for the parameters

θ:

$$L(y|\theta) = \prod_{i=1}^{n} P(y_i|\theta) \tag{5.8}$$

Since the data points are observed and fixed, one can see the likelihood as a function of the parameters θ With this definition, we introduce the maximum likelihood estimator (MLE) for θ, which is simply the set of parameters $\hat{\theta}$ that maximizes the probability of the observed data. That is,$\hat{\theta}$ is the parameter vector that satisfies:

$$L(y|\hat{\theta}) = max|_{\theta\in\Omega}[L(y|\theta)] \tag{5.9}$$

Where Ω represents the space of all possible values of θ.

In many practical cases, we are considering that our data points arise from independent Gaussian distributions with mean value given by our model $y_i(\theta)$ and variance given by the square of measurement errors σ_i^2. In this case, maximizing the the likelihood is equivalent to minimizing the quantity:

$$\chi^2 = -2\ln L = \sum_{i=1}^{n} \Big(\frac{y_i - y_i(\theta)}{\sigma_i}\Big)^2 \tag{5.10}$$

If the data represents a sample from random variables which are not independent, but with a p.d.f that is described by a multivariate Gaussian, then the χ^2 takes the more general form:

$$\chi^2 = (y - y(\theta))^T C^{-1} (y - y(\theta)) \tag{5.11}$$

Where C^{-1} is inverted covariance matrix. The MLE can give the information of which is the parameters most probable to have generated the observed data. However, quantifying the error of this estimate is something more sensible, since it requires to deal with the exact definition of what probability means. To this subject, there are two fundamentally different points of view, which are the frequentist (classical) and Bayesian.

5.2.2 The frequentist approach

The classical way to define probability is through empirical repetition. If one experiment is performed N times and the event A occurs M times, then the probability for A to happen is

$$P(A) \equiv \lim_{n\to\infty} \frac{M}{N} \tag{5.12}$$

This definition for probability allows to introduce the concept of confidence intervals or exclusion regions when we are dealing with parameter estimation.

Consider then a random variable Y whose p.d.f depends on the parameter vector θ we wish to estimate. To simplify things, we take the example of the minimum-χ^2 estimator introduced above, with the data points arising from independent Gaussian distributions.If we perform the minimization we would obtain an estimate θ^*. Imagine that we could obtain a number m of realizations for our data. By repeating the process, one would get a distribution representing the p.d.f of our estimates $\{\theta_i^*, ..., \theta_m^*\}$. It can be shown that for the case of the χ^2 , its p.d.f is a chi-square distribution with $\nu = n - p$ degrees of freedom $-P_{\chi^2_\nu}$, where n is the number of data points and p is the number of parameters estimated.

Under these assumptions, the distribution $P_{\chi^2_\nu}$ provides a measure of the goodness of fit: if a given parameter set θ_0 is the correct one and in one realization, we have measured the minimum χ^2_0 exactly for θ_0. Then if the measurement would be repeated many times in different realizations, the probability to measure a minimum χ^2 equal or larger than the true value χ^2_0 is

$$P(\chi^2 > \chi^2_0) = \int_{\chi^2_0}^{\infty} P_{\chi^2_f}(x)dx \tag{5.13}$$

The frequentist interpretation for the above equation is that if some other parameters θ_1 have $\chi^2(\theta_1) = \chi^2_1 \gg \chi^2_0$, then the chance that θ_1 is the correct set and we are only seeing a realization far out in the tail of the distribution is very small. Generally, one can evaluate the probability 5.8 for one given estimate θ^*, which should be sufficiently high for the estimated model to be a good fit to the data. Very small probabilities would mean that either the model with those parameters can be rejected, or the measurement errors were underestimated or they are not Gaussian.

In this approach, a confidence interval at a $100\alpha\%$ level comprises parameters whose measured χ^2 is smaller than the value corresponding to the 1α quantile for the distribution $P_{\chi^2_f}$. The quantile q for a given p.d.f is defined as the value x so that

$$\int_x^{\infty} P(u)du = q \tag{5.14}$$

The frequentist meaning or the confidence interval is that if we could repeat the measurements a great number of times, then the above confidence interval would include the true value for the parameters $100\alpha\%$ of the time.

Although this approach is mathematically well defined and appealing in this sense, it can present some theoretical and practical drawbacks. One of the main criticism for the application of frequentist techniques in cosmology and astrophysics is that most of the times we just have one data realization for a given model we want to test. In this way, the notions of confidence intervals and parameter errors are weakened because they invoke hypothetical measurements that can not take place.

A more practical problem can arise when exploring the likelihood using typical griding methods. Imagine we use a very coarse grid with only 10 points per parameter. If we want to constrain a minimum of 6 parameters, it would require to determine 10^6 models. Even using parallelized codes such as CAMB to determine the CMB anisotropies and matter transfer function, the calculation of one model takes a typical 2 seconds. This implies about 23 days to perform our constrain. It may not seem a great amount of time, but consider now that adding one parameter to the model would make the calculation time increase by a factor 10 to 230 days. It is clearly not a good approach when we want to study models with a high number of parameters. However, more efficient minimization techniques can be used to avoid this problem and derive constraints within reasonable time [168].

5.2.3 The Bayesian approach

In the Bayesian approach, probabilities are not defined in terms of frequency of events, but rather in terms of our degree of belief that one hypothesis is true. In this sense, a probability equal to 1 or 0 means that we are absolutely certain that a given statement is true or false. A probability equal to 0.5 means that we are maximally uncertain whether the statement is true or false.

Some criticism can be raised against this approach, since the concept of certainty is somehow subjective. However, the Bayesian formalism allows to treat problems that are unscientific in the frequentist point of view. For example Bayesans can talk about the probability that there is life out side of our own solar system. In classical probability theory this kind of probability cannot be discussed, since there either is or is not, but there is nothing random in it. But if astronomers found evidence for an extra solar planet with very similar conditions as the Earth, one could say that the probability of finding life would increase given that new information. This is the main principle behind Bayesian inference or estimation, that we can actualize our probabilities as we collect new information.

Mathematically, the Bayesian approach for cosmological parameter estimation is based on the Bayes theorem, which is no more than the conditional probability axiom, defined as

$$P(\theta|d) = \frac{P(d|\theta)P(\theta)}{P(d)} = \frac{L(d|\theta)P(\theta)}{\int L(d|\theta)P(\theta)d(\theta)} \tag{5.15}$$

The Bayes theorem states that the posterior probability distribution for the parameters depends on the likelihood of the data given the parameters times the prior distribution of the parameters divided by the evidence for the data. Since we assume that a given set of data is observed, then the evidence can be regarded as a simple normalization constant independent of the parameters.

The prior distribution is a unique and important feature of the Bayesian approach, describing all the information one has on the parameters before measuring the data. This information is then updated together with the likelihood which contains all the information coming from the data. The posterior gives us the final distribution describing which of the parameters are more credible to be true. It is common to attribute flat priors to the parameters in question, meaning that over a certain range we consider to be adequate for each parameter, the probability distribution is constant. However, a flat prior on θ does not correspond to a flat prior on some other set θ' obtained after a non-linear transformation of θ. This constitutes a great conceptual problem with Bayesian analysis, since the final results can depend on the prior choice. However, in practical problems with good data quality, these changes are expected not be significant.

One of the great advantages of the Bayesian approach is that the posterior distribution and its interpretation give us a more intuitive and direct way to determine the most probable values for the parameters, confidence intervals, marginalization of parameters and other derived quantities. First let us assume that we are working with flat priors. In this case, the posterior distribution in our region of interest will be directly proportional to the likelihood. In this case, the preferred parameter set will be the one that maximizes the likelihood. In fact, Bayesian inference in this case will be equivalent to the MLE discussed above. There is however a conceptual difference, since in the Bayesian paradigm we are maximizing the joint probability P, while the MLE maximizes the conditional probability $L(d|\theta)$.

For the confidence intervals on our estimation, they come directly from the posterior (likelihood), and can be seen as regions where we have $\alpha\%$ of certainty that the true values will be in. This is radically different from the frequentist interpretation discussed above.

Formally, all parameter values contained in the region R centered at the best estimate θ^*, so that

$$\int_R P(\theta|d)d\theta = \alpha, \tag{5.16}$$

are said to be within the $\alpha\%$ confidence interval in the Bayesian framework. One can take different approaches to choose this region, such as centered on the mean of the distribution, centered on the maximum, etc. If one wants to report the results independently of the prior, one can use a likelihood ratio. In this case we compare the likelihood at a particular point in the parameter space with the value of the maximum likelihood. Then a given set of parameters is said to be acceptable if

$$-2\ln\Big(\frac{L(\theta)}{L_{max}}\Big) \leq \gamma \tag{5.17}$$

In the particular case where our data arises from independent Gaussian distributions and the model depends linearly on the parameters, the threshold value γ corresponds to the confidence limit for a χ^2 distribution with p degrees of freedom, where p is the number of parameters. In this case we have similar way to access confidence intervals as in the frequentist approach. However, since the frequentist χ^2 distribution as $f = n - p$ degrees of freedom, this implies that the Bayesian constraints are generally tighter than the frequentist ones.

In many practical cases, we are interested in the posterior distribution of just one or two parameters, so that we can visualize them. To do this we can marginalize over the other parameters, which is a very straightforward procedure in the Bayesian analysis. All we have to do is integrate the posterior distribution over the parameters we are not interested in, so that in the general case where we are interested in n of the total p parameters:

$$P(\theta_1, ..., \theta_n|d) = \int P(\theta|d)d\theta_{j+1}, ..., d\theta_p. \tag{5.18}$$

This procedure is also useful when we wish to get rid of nuisance parameters, such as calibration factors or unknown amplitudes. For some of these cases the above integration can be performed analytically, as long as the likelihoods are Gaussian and the prior on the nuisance parameter is flat. Following [169], we can write the marginalized posterior as:

$$P \propto L = \int P(\alpha)\exp\Big[-\frac{1}{2}(X+\alpha V)^T C^{-1}(X+\alpha V)d\alpha\Big], \tag{5.19}$$

where V and X are vectors, C is the data covariance matrix and α is our nuisance parameter. For the case of a flat prior, the above integral gives

$$-2\ln L = X^T\Big(C^{-1} - \frac{C^{-1}VV^TC^{-1}}{V^TC^{-1}V}\Big)X + \ln(V^TC^{-1}V) + const. \tag{5.20}$$

So, if V is a constant vector, one has $L \propto e^{-\chi^2_{eff}/2}$ where

$$\chi^2_{eff} = X^T\Big(C^{-1} - \frac{C^{-1}VV^TC^{-1}}{V^TC^{-1}V}\Big)X. \tag{5.21}$$

If V is a vector of equal constants the above result is independent of V and is equivalent to maximize the likelihood with respect to α.

As we have seen, the ability to integrate often complex and high dimensional functions is extremely important in Bayesian statistics, whether it is for marginalization proposes, expectation values, or confidence intervals. Often, an explicit analytical evaluation of these integrals (as in eq.5.19 and 5.20) is not possible and, normally, we would be forced to use numerical integration based on griding or analytical approximation techniques which would result in the same practical problem as the frequentist approaches, which is the great computational time required. However, Markov Chain Monte Carlo methods provide an alternative and more feasible approach to this problem, which is the principle reason why they have become a standard tool for large parameter space constrains, as is the case in cosmology.

5.2.4 Markov Chains Monte Carlo

MCMC methods can be seen as a way to sample directly from the posterior distribution, obtaining sample estimates of the quantities of interest, hence performing implicit integrations. The idea of MCMC sampling was first introduced by Metropolis et al.[170] and later generalized by Hastings [171] to treat many different statistical problems. The paper of [172] first introduced the advantages of applying MCMC in cosmological parameter estimation, particularly for CMB studies. May be the main advantage is the required MCMC computational time that scales linearly on the number of parameters, which allows to perform constrains in a reasonable amount of time.

The idea of MCMC is rather simple: to construct a sequence of points in parameter space - a chain - so that the density of points is proportional to the posterior distribution.To

do this, one can use a particular type of chain, called Markov chain, that can be simply defined as a sequence of random points where the probability of advancing to the $(i+1)$th point only depends on the value of the ith element. One can show that these type of chains converge to a stationary state where successive elements of the chain are samples from the target distribution, in our case, the posterior $P(\theta|d)$.

Metropolis-Hastings algorithm

The evolution of the chain is probabilistic in nature, and various different algorithms for this evolution are available, depending on the particular problem we want to solve. Some examples are the Metropolis-Hasting algorithm, Gibbs sampling or importance sampling. A popular choice for high dimensional problems is the Metropolis-Hastings algorithm. In this framework, the evolution of the chain in controlled by the kernel $T(\theta_n, \theta_{n+1})$ which determines the conditional probability for the chain to move from θ_n to θ_{n+1}. The transitional kernel must satisfy the detailed balance:

$$P(\theta_{n+1}|d)T(\theta_{n+1}, \theta_n) = P(\theta_n|d)T(\theta_n, \theta_{n+1}) \tag{5.22}$$

This guarantees that the P chain will be the equilibrium distribution for the Markov chain. The Metropolis-Hastings generates density using the technique of rejection sampling. This is done using a proposal density distribution $q(\theta_n, \theta_{n+1})$, but instead of rigorously accepting or rejecting a new candidate θ_{n+1}, it is accepted with a certain acceptance probability $\alpha(\theta_n, \theta_{n+1})$ chosen so that the kernel will follow the detailed balance above. This is done by setting:

$$T(\theta_n, \theta_{n+1}) = q(\theta_n, \theta_{n+1})\alpha(\theta_n, \theta_{n+1}) \tag{5.23}$$

$$\alpha(\theta_n, \theta_{n+1}) = min\Big\{\frac{P(\theta_{n+1}|d)q(\theta_{n+1}, \theta_n)}{P(\theta_n|d)q(\theta_n, \theta_{n+1})}\Big\} \tag{5.24}$$

By using this algorithm with enough iterations, after a burn-in period the chain will converge to a stationary state, sampling directly from the posterior distribution.

Convergence

An important aspect of the MCMC formalism is how to know if the chain is converged. First there is the burn-in period when the chain moves towards its equilibrium position. To remove this effect it suffice to discard the first elements of the chain. Typically the

burn period is no more than 1000 iterations, but for a more conservative approach to this problem, one can discard the first half of the chain and then test for convergence. To access if a Markov chain as properly converged, various methods have been proposed. Essentially, one can consider two different ways for testing convergence. Either run one long chain and test the statistical stability using some diagnostic quantity such as the variance of the quantiles for the chain distribution as proposed by Rafetery and Lewis [173] or run several multiple chains with dispersed starting values. In this way convergence is achieved when the chains have forgotten their initial values and the output of each chain is indistinguishable. This is the Gelman and Rubin test [174].

Proposal density

The optimal choice for the proposal density is the key factor for an efficient implementation of MCMC methods. One is interested that the proposed points will have a good acceptance ratio, so that the chain will converge rapidly, but also that they will present a good mixing, i.e., that the chain will cover most of high dimensional parameter space, accounting for the tails of the posterior distribution. A popular choice for the proposal density is a Gaussian with step size given by its rms along a given parameter direction. In order to improve the mixing, one can run a short chain to roughly sample the posterior distribution, then determine the covariance matrix of the parameters, and use it to construct a new parameter basis that reduces the parameter degeneracies. This will allow for much more effective exploration of the target distribution.

Results from the chain

Once the chain has converged, one can obtain estimates on the expectation value (mean) of any function of the parameters, via the Monte Carlo integration:

$$\bar{h}(\theta) \simeq \frac{1}{N} \sum_{n=1}^{N} h(\theta^{(n)}) \tag{5.25}$$

Remember that the chain is sampled from the posterior distribution, which causes the empirical mean of the chain elements to identify with the wanted expectation value. As for the marginal posterior on one or two parameters, we are interested in evaluating eq.(5.18), which in the MCMC formalism becomes trivial: again, since the elements of the Markov

chain are samples from the full posterior, their density reflects the value of this distribution. For example, if we want to marginalize in respect of θ_1, it is sufficient to divide the range of this parameter in a series of bins and count the number of samples falling within each bin, simply ignoring the values of the other parameters. For a 2-D marginalization, a similar analysis can also be applied.

COSMOMC

Over the past decade, MCMC methods have become the standard tool for cosmological constraints due to the conceptual and implementation advantages that have been resumed above. Besides these advantages, the popularity of MCMC in the cosmology community has widely increased after the release of the publicly available code COSMOMC [169]. This a Fortran 90 code that was build to incorporate the parallelized Bolzmann code CAMB for the calculation of CMB anisotropies. The code allows for integration of different parametrization by the user, a choosing from different data to perform constraints. The diagnostic analysis is indeed very user friendly, which explains its wide implementation.

5.3 Constraints on cosmological parameters and the theoretical models

A cosmological model with total density close to critical (and flat geometry), dominated by dark matter and dark energy of unknown nature, and consistent with the basic predictions of the inflationary scenario is a very good fit to a variety of cosmological probes: the anisotropy of the CMB, the large scale distribution of matter, the luminosity distance of high-redshift type Ia supernovae and so on. These high-quality data have established a new standard of precision in the determination of cosmological parameters.

5.3.1 The standard cosmological model

Cosmology has a standard model, which provides a well-established framework to understand the global properties of the physical universe. There is a strong interplay between fundamental physics and cosmology, since the early universe is a natural laboratory for

high energy physics.

The big bang model (or, more precisely, the Friedmann-Robertson-Walker model) provides a very successful description of the physical universe from very early times ($t \sim 10^{-2}s$) to the present. It can easily explain some key features of the observed universe, such as:

- the expansion law.
- the abundance of light elements.
- the existence of the cosmic microwave background.
- the age of the oldest objects observed.

Furthermore, it provides a framework where the gravitational instability scenario that explains the growth of cosmic structures can be easily accommodated.

An additional ingredient of the standard cosmological model, needed to extend the description of the universe back to very early times ($t \sim 10^{-43}$ s after the big bang) is a period of cosmological inflation, i.e. a very short time ($t \sim 10^{-35}s$) during which the universe expanded exponentially (changing its size of a factor $\sim 10^{30}$). The inflation mechanism has proved quite powerful as a refinement of the classic big bang model, and is now considered an important element of the standard cosmological model. Independently of the details of the specific model, the inflationary scenario makes a number of testable predictions:

- The universe must be very close to flat.
- Primordial density perturbations in the universe are Gaussian distributed, adiabatic and have a power-law power spectrum.
- A stochastic background of gravitational waves should be present in the universe.

Although no universally accepted and tested model for inflation currently exists, there are a number of viable candidates, all of which are based in one way or another on the dynamics of a weakly coupled, homogeneous scalar field ϕ [45, 46]. In its simplest form, the equation of motion of such a field is:

$$\ddot{\phi} + 3H\dot{\phi} + V'(\phi) = 0 \tag{5.26}$$

and its energy density and pressure are given by:

$$\rho_\phi = \frac{1}{2}\dot{\phi}^2 + V(\phi) \tag{5.27}$$

$$p_\phi = \frac{1}{2}\dot{\phi}^2 - V(\phi) \tag{5.28}$$

Here H is the expansion rate of the universe, and V is the scalar field potential. A common solution to the field equation of motion is based on the so-called slow-roll approximation, which assumes that the field acceleration $\ddot{\phi}$ is negligible, so that :

$$3H\dot{\phi} \simeq -V'(\phi) \tag{5.29}$$

The conditions for the slow-roll assumption to hold are given by

$$\varepsilon \equiv \frac{1}{16\pi G}\Big(\frac{V'}{V}\Big)^2 \ll 1; \tag{5.30}$$

$$|\eta| \equiv \frac{1}{8\pi G}\Big|\frac{V''}{V}\Big| \ll 1 \tag{5.31}$$

Where ε and η are called slow-roll parameters. Constraining the slow-roll parameters by measuring the exact shape of the power spectrum of primordial perturbations can rule out specific models of inflation.

One important feature of inflation is that it provides a mechanism to generate super-horizon primordial density perturbations in the early universe. Broadly speaking, the mechanism goes as follows: consider a generic quantum fluctuation $\delta\phi(\vec{x}, t)$ in the scalar field ϕ. The Fourier expansion coefficients of this fluctuation are $\delta\phi_k$. During inflation the wavelength of each Fourier component will rapidly grow much bigger than the causal horizon. When this happens, the corresponding fluctuation will freeze, since no causal mechanism will be able to influence its evolution. At later times, long after inflation ends, each wavelength will re-enter the horizon, and the associated component of the fluctuation will be seen as a density perturbation. Note that there is no way of producing such a mechanism in classical cosmology: in the standard big bang model, a certain comoving scale becomes smaller than the causal horizon at some given time, and remains inside the horizon ever after. In a similar way, inflation also produces a stochastic background of gravitational waves. Gravitational waves correspond to tensor perturbations in the space-time metric, while density perturbations are scalar. Density perturbations produced during

inflation are adiabatic , or isentropic: they are genuine curvature perturbations in the space time metric and leave the ratio of matter and radiation (or of any other two species) constant at any point in space. Furthermore, they are Gaussian distributed (or very close to Gaussian). The power spectrum of density perturbations produced by inflation in the slow-roll approximation is quite simple:

$$P_s(k) = A_s k^{n_s}; \quad P_t(k) = A_t k n_t \tag{5.32}$$

for scalar and tensor density perturbations respectively, with:

$$n_s = 1 - 4\varepsilon + 2\eta; \quad n_t = 2\varepsilon \tag{5.33}$$

Of course, since in the slow-roll regime η and ε must both be very small, inflationary models usually predict a scalar spectral index very close to 1, a property termed scale-invariance. Similarly, the power spectrum of tensor perturbations should be roughly constant, since $n_t \simeq 0$. The ratio of the amplitude of tensor and scalar perturbations must satisfy the so-called consistency relation $r \equiv A_t/A_s = 13.6\varepsilon$. Measuring the power spectrum of density perturbations is then a powerful tool to test the inflationary parameters.

5.3.2 The cosmological parameters

The evolution of the universe in the big bang model is essentially determined by its content. The density of each component i is measured by its value Ω_i in units of a critical value ($\rho_c = 3H^2/8\pi G$), so that $\rho_i \propto \Omega_i H^2$. The total density parameter in a multi-component universe is the sum of the density parameters of the single components:

$$\Omega = \sum_i \Omega_i \tag{5.34}$$

Assuming that each component has an equation of state of the form $p = w\rho$, with w independent of time, the Friedmann equation describing the evolution of the universe can be written as:

$$\left(\frac{\dot{a}}{a}\right)^2 = H_0^2 \Big[\sum_i \Omega_i a^{-3(1+w_i)} + (1-\Omega) a^{-2} \Big] \tag{5.35}$$

where a is the scale factor parameterizing the expansion, and the density parameters are evaluated at present time. One of the main tasks of observational cosmology is to obtain

accurate estimates of the parameters in the right hand side of the Friedmann equation: the Hubble constant H_0 and the contributions to Ω from the various components in the universe. In addition to this, one needs to get some estimate of the parameters defining the inflationary model, such as the amplitude and spectral index of the primordial power spectrum (for both scalar and tensor perturbations). Let us review the status of our knowledge on these parameters.

Hubble constant

The present expansion rate of the universe is measured by the Hubble constant, often parametrized in terms of the adimensional quantity h as $H_0 = 100h\ Kms^{-1}Mpc^{-1}$.The best value of the Hubble constant comes from the measurements of the Hubble Space Telescope Key Project [175], which calibrated the cosmic distance scale by observing Cepheids in nearby and distant galaxies. This resulted in a value $H_0 = 72 \pm 3$(statistical) ± 7(systematical) $km/s/Mpc$ [154]. The value derived from WMAP 3-year observations of CMB anisotropy under the assumption that the universe is flat is in remarkable agreement with this: $H_0 = 73.4^{+2.8}_{-3.8}\ km/s/Mpc$ [154]. The recently released WMAP 7-year data gives a value of $H_0 = 70.4^{+1.3}_{-1.4} km/s/Mpc$.[11]

The present age of the universe is directly related to the Hubble parameter by an integral over the redshift z, as $t_0 = \int_0^\infty dz/(1+z)H(z)$. A lower 2σ limit of 11.2 Gyr comes from observations of globular clusters in the Milky Way [176], while WMAP can only constrain the present age when a flat universe is assumed. Under this assumption, $t_0 = 13.75 \pm 0.11$ Gyr [11].

Total density

The total density of the universe Ω also specifies its spatial curvature: the space-time metric has flat spatial sections when $\Omega = 1$. The best way to determine Ω is through the position of acoustic features in the angular power spectrum of CMB temperature fluctuations. This provides a direct measurement of the angular size of sound horizon at recombination (~ 300000 years after the big bang), which is strongly dependent on Ω. Strong evidence that the universe is flat (as predicted by inflation) first came from balloon-borne experiments such as MAXIMA and Boomerang [177, 178]. WMAP confirmed this results to greater precision: deviations of Ω from unity are currently constrained to $0.015^{+0.020}_{-0.016}$ and

will improve by at least an order of magnitude by Planck data.

Radiation density

The radiation component of the universe (relativistic particles) has equation of state $p_R = \rho_R/3$. When the universe is radiation dominated, the scale factor evolves as $a \propto t^{1/2}$ .According to the standard cosmological model, today the radiation in the universe is made of the cosmic microwave background photons and 3 species of relic massless neutrinos. The present radiation density can be expressed in terms of the photon temperature T, as:

$$\rho_R = \frac{\pi^2}{30} g_* T^4 \tag{5.36}$$

where g_* counts the total number of effectively massless degrees of freedom. This can be computed, giving $g_* = 3.36$, while the cosmic microwave background average temperature is accurately measured to be $T = 2.725 \pm 0.001K$ [30]. Thus, today the radiation gives a totally negligible contribution to the critical density: $\Omega_R = 4.31 \times 10^{-5} h^{-2}$.

Matter density

The equation of state of matter, or non-relativistic particles, is $p_M = 0$, so that during matter domination the scale factor evolves as $a \propto t^{2/3}$. The most familiar contribution to matter in the universe comes from baryons (or nucleons). The abundance of light elements produced in the early universe is strongly dependent on the baryon-to-photon ratio, which is directly related to the present baryon density. Measurement of primordial abundances of D, He^3, He^4, Li^7 are a strong probe of the baryon density, and indicate that baryons contribute to roughly 5% of the critical density [179]. A consistent result is obtained from CMB anisotropy observations, which provide a tight constraint on the baryon density since the ratio of acoustic peak heights is strongly dependent on the baryon-to-photon ratio in the universe. If $\Omega \sim 1$, as predicted by inflation and now accurately confirmed by cosmological observations, most of the universe is not made of the same stuff we are made of.

There is strong observational evidence that a large contribution (about 30%) to the critical density comes from so-called dark matter. This constraint comes from a variety of large scale structure probes, such as the shape of matter power spectrum measured from galaxy redshift surveys such as SDSS or 2dF, the gas fraction in clusters of galaxies, the

study of peculiar velocity fields, and so on. Similar results come from the height of the third acoustic peak in the CMB power spectrum observed by WMAP, although better data would be needed to obtain a robust estimate. Theoretically, the most plausible candidate for dark matter is some heavy, weakly-interacting massive particle, left from the very early stages of the evolution of the universe. The standard picture for the production of such a relic is as follows. The candidate particle is assumed to be initially in thermal equilibrium with the primordial plasma, so that its abundance decreases as $exp(-M_X/T)$ where M_X is the particle mass and T is the photon temperature. When the interaction rate of the particle, Γ, becomes smaller than the expansion rate of the universe, H, the particle decouples from the thermal plasma and its abundance becomes constant (a moment known as freeze-out). Then, a cosmologically relevant relic abundance can be achieved provided the particle has a large enough mass, and a small enough interaction rate. There are many candidates for dark matter (for example, super symmetric partners): unfortunately, since it interacts so weakly, direct detection of dark matter proves challenging. Some light on the nature of dark matter can be shed by accurate measurements of its present density by cosmological observations.

Dark energy

In its most general form, Einstein equation includes a so-called cosmological term Λ in addition to the familiar stress-energy tensor:

$$R_{\mu\nu} - \frac{1}{2} g_{\mu\nu} R = 8\pi G T_{\mu\nu} + \Lambda g_{\mu\nu} \tag{5.37}$$

Adding a cosmological constant term is completely equivalent to introducing a new contribution to the stress-energy tensor from a component with:

$$\rho_V = \Lambda / 8\pi G; \quad p_V = -\Lambda / 8\pi G \tag{5.38}$$

It can be shown that this is exactly the kind of contribution resulting from zero-point fluctuations of quantum fields, or vacuum energy. The equation of state of vacuum energy is $p_V = -\rho_V$, and the universe expands exponentially when it is vacuum dominated: $a \propto exp[(\Lambda/3)^{1/2} t]$.

The evidence in favour of a non-null cosmological constant has been mounting over the past few years. First, measurement of the luminosity distance of high-redshift type

Ia supernovae (a particularly good kind of standard candles) can only be explained by a recent accelerated expansion of the universe, a behaviour that cannot be obtained within a Friedmann model containing only matter. Moreover, as we just mentioned, the universe seems to be very close to flat (i.e. it has a total density equal to the critical value) but there is not enough matter (either baryonic or non baryonic) to explain the observed flatness. The observed accelerated expansion and the need for a substantial contribution to the cosmic budget, in addition to other clues, such as the need to reconcile the age of the universe to that of the oldest globular clusters, point toward the existence of a cosmologically significant amount of vacuum energy: $\Omega_\Lambda \sim 0.7$.

Unfortunately, the introduction of this seemingly harmless contribution to the energy density of the universe has disturbing implications. First of all, any estimate of plausible values for the vacuum energy density from fundamental physics exceeds the critical density ρ_C by at least 40 (and often as much as 120) orders of magnitude, while observational cosmology sets the total energy density of the universe at roughly the critical value, $\Omega \sim 1$. One might hope that some mechanism is leading to an exact cancellation of the contributions to the vacuum energy, so that it is exactly $\rho_V = 0$: however, such a mechanism is currently unknown. The situation is even more puzzling, since (as we just mentioned) recent observations of distant type Ia supernovae [180, 181] have shown that we live in a universe that has just entered a vacuum dominated epoch, starting a phase of accelerated expansion. This means that the cosmological constant term is still very small compared to theoretical estimates, but it is large enough $(\rho_V/\rho_C \sim 0.7)$ to be cosmologically relevant in the present universe. There seems to be a serious fine-tuning problem: if Λ is non-zero, then why is it so small? Furthermore, given the observed value of Λ, vacuum-energy was never important in the past evolution of the universe, but it is starting to be the dominant contribution at present time. We then seem to live in a very special moment in the universe: an annoying coincidence indeed.

The vacuum energy problem may in fact be the biggest mystery of modern physics [182]. A possible way to alleviate it, and one that has interesting and testable implications for cosmology, is to consider a generalization of the cosmological constant term, that has been termed dark energy. As shown when discussing inflation, a scalar field ϕ with effective potential $V(\phi)$ has an equation of state with $w = (\dot{\phi}^2/2 - V)/(\dot{\phi}^2/2 + V)$. Any value of w such that $1 + 3w < 0$ results in an accelerated expansion, so it is dynamically equivalent to a cosmological constant. The interesting feature of these models is that they admit tracking solutions, in which the dark energy can reach the present value

starting from a very different set of initial conditions. This mitigates the fine tuning and coincidence problems but, of course, leaves open the questions about the nature of the field ϕ. Cosmological constraints to w can be able to discriminate among dark energy models by saying something about the scalar field potential V. The phenomenology of dark energy can in principle be described in terms of a small number of parameters. In addition to the equation of state w (which in general is a function of cosmic time) an important quantity is the sound speed $c_s^2 \delta p / \delta \rho$, which is crucial to describe the clustering behaviour of dark energy, if any. The sound speed needs not be the usual adiabatic one, but can be modified to account for entropy fluctuations, thus encompassing a broad set of dark energy candidates. Other explanations of the puzzle could lie in the gravity sector, involving some modifications of the left-hand side of Einstein's equation (e.g. the existence of non-minimal couplings, or higher dimensional theories, or the feedback from inhomogeneities). T. Padmanabhan [183] gives an excellent review on dark energy from the point of view of both cosmology and fundamental physics.

But how to constrain the properties of dark energy? The crucial observable is the evolution of the Hubble parameter, giving a record of the expansion history of the universe. This can be probed in several ways: through the measurement of the luminosity distance of high redshift supernovae, through the determination of the angular diameter distance from the CMB angular power spectrum or from baryonic acoustic features in galaxy redshift surveys, through the age of the universe, and so on. These observations are all related to the background cosmology, but clustering can play an important role in discriminating dark energy candidates. In fact, theoretical prediction can be grossly misestimated when the behaviour of dark energy perturbations is not properly taken into account. The main observables that can be used to track the effects of clustering are the evolution of the number of sources in the comoving volume, as estimated for example from galaxy cluster counts obtained using the Sunyaev-Zel'dovich effect, or the measurement of shear convergence from weak lensing.

A very promising tool is the cross-correlation of CMB temperature anisotropy maps to tracers of the local distribution of dark matter, such as the projected galaxy distribution. This allows to extract the signal from the integrated Sachs-Wolfe (ISW) effect [32], which is due to the evolution of gravitational potential along the line of sight. The ISW is strongly affected by dark energy and is a powerful way of discriminating theoretical models. It is hard to detect the ISW in CMB maps because of the unavoidable cosmic variance which is dominant on large angular scales, exactly where the ISW signal is ex-

pected to peak. However, the cross-correlation of CMB maps and large scale structure probes can enhance the detection power and lead to significant constraints. The first detection of the ISW [184, 64] was obtained by combining the WMAP 1st year CMB data with the hard X-ray background observed by the High Energy Astronomy Observatory-1 satellite (HEAO- 1 [185]) and with the radio galaxies of the NRAO VLA Sky Survey (NVSS [186]). The positive correlation with NVSS was later confirmed by other authors, including the WMAP team [187]. Other large scale structure tracers that led to similar positive results were the APM galaxy survey [188], the Sloan Digital Sky Survey (SDSS [189]) and the near infrared 2 Micron All Sky Survey eXtended Source Catalog (2MASS XSC) [190-196]. All of these results collected additional evidence of the existence of a dark energy component (or something with the same gravitational behaviour) which is currently dominating the cosmic expansion. However, much work remains to be done to extract further information on the detailed nature of dark energy: at the moment, there are no strong indications that w is different from the cosmological constant value -1 or that it significantly evolved over time. Better data are needed, especially from future and ongoing redshift surveys.

Inflationary parameters

The recent 3-year WMAP data significantly constrained the space of inflationary parameters. The Harrison-Zeldovich primordial spectrum, with $n_s = 1$ and a null ratio of tensor to scalar perturbation ($r = 0$), seems to be disfavoured by the data, although it is still within the 95% confidence level [197]. The WMAP results seem also to show a preference for a $m^2\phi^2$ potential over a $\lambda\phi^4$. A significant deviation from a unit spectral index is also found when a combination of data from the Lyman-α forest, galaxy clusters, supernovae and CMB is considered [198]. The WMAP upper limits on tensor perturbations are $r < 0.55$ at 2σ, while this gets tighter ($r < 0.28$) when SDSS data are included in the analysis. However, this bounds get looser when the scalar spectral index is allowed to vary with k, as predicted by some inflationary models. With its extended lever arm in multipole space, Planck will be able to significantly strengthen the constraints on inflation.

Reionization

The hydrogen in the universe is completely reionized at redshift at least as high as 5. The exploration of the so called dark ages, i.e. the time before the formation of the first

structures in the universe is an active subject of investigation. The CMB temperature anisotropy signal gets damped when the photons are diffused by free electrons along the line of sight. The amount of damping is a powerful probe of the optical depth to reionization. Furthermore, CMB polarization is generated when the photons last scatter on the free electrons: if the optical depth is non zero, a recognizable polarization signature gets generated at large angular scales, allowing to investigate the detailed reionization history, discriminating models that have the same optical depth but a different evolution of the ionization fraction with redshift. It is not possible to get into this kind of details with present data, but shedding some light on the dark ages should be well within the capabilities of Planck. WMAP data currently constrain the optical depth at a value of roughly $\tau \sim 0.1$, consistent with complete reionization at $z \sim 10$.

5.4 Summary

In this chapter, We discussed the statistical methods presently used in cosmological data analysis. CMB anisotropy data could put powerful constraints on theories of the evolution of our Universe. The extraction of information from cosmic microwave background (CMB) anisotropies is a classic problem of model testing and parameter estimation, the goals being to constrain the parameters of an assumed model. Using the observations of the large number of CMB experiments, many studies have put constraints on cosmological parameters assuming different frameworks. Assuming for example inflationary paradigm, one can compute the confidence intervals on the different components of the energy densities, or the age of the Universe, inferred by the current set of CMB observations. The aim is to present some of the available methods to derive the cosmological parameters with their confidence intervals from the CMB data, as well as some practical issues to investigate large number of parameters. The computational demands of Bayesian inference with large numbers of parameters are best met with MCMC methods. These methods have demonstrated their importance in numerous applications. As cosmological models grow in complexity it will become necessary to use techniques such as those discussed here in order to handle marginalization of parameters. Markov chain Monte Carlo methods provide a means of handling large parameter numbers, and maintain a rigorous approach to Bayesian inference. The capacity of different observational data in constraining cosmological models based on the standard CDM and dark energy paradigm (i.e. models where the energy content of the universe is largely dominated by two unknown components, the

non-baryonic cold dark matter and a mysterious dark energy component that drives an accelerated expansion of the universe in low to intermediate redshifts) is well studied.

Cosmology has developed into a fully mature science. The parameters of the big bang model are now known with great accuracy, and the constraints are expected to get tighter in the future. Inflation has not been falsified, and its main predictions are strikingly consistent with observations. The results obtained using completely different cosmological probes are in remarkable agreement among themselves, as well as with theoretical predictions. Nonetheless, many fundamental questions are still open. The pace of experimental and theoretical progress, however, does not seem to be close to a halt.

Chapter 6

Conclusions and Future Outlook

The aim of this dissertation is to study CMB temperature and polarization anisotropies to constrain the cosmological parameters and the theoretical models. The cosmic microwave background, since its discovery, has been one of the most informative observable of the Universe. As discussed in chapter 2, it has first permitted to rule out alternate cosmological scenarios, confirming the success of the hot Big-Bang model. The standard hot Big-Bang scenario, which was originally supported by three fundamental observations (Hubble expansion, abundance of light elements, and CMB radiation), has been tested and confirmed by a wealth of new precise observations, such as the cosmic microwave background anisotropies, Type-Ia supernovae, and the large scale clustering of galaxies. The observational data provide strong support for a Universe which is spatially flat and accelerating at the present day, consisting of approximately 73% dark energy, 23% cold dark matter, and 4% baryons, which leads to the concordance model ΛCDM. Testing this concordance model and exploring unknown physics beyond this model (for example, the nature of dark energy) have become important tasks for cosmologists. It has unveiled the first seeds of structures which give rise eventually to the present large scale structures. Even, more, it serves as a strong testground for the consistency of the cosmological model permitting also, thanks to a number of very successful experiments, to measure with accuracy the cosmological parameters describing our Universe as a whole.

Results from BOOMERANG, MAXIMA-1, ARCHEOPS, CBI, DASI and WMAP were so important that they have taken the field into the era of precision cosmology. These studies have produced impressive constraints on many fundamental cosmic parameters and have led to a very definite picture of the structure and evolution of the Universe. The

microwave background has the ultimate potential to determine fundamental cosmological parameters describing the universe with percent-level precision.

As described in Chapter 3, beyond the basic hot Big Bang picture and the precise values of parameters, the CMB has taught us that:

- The Universe recombined at $z \sim 1100$ and started to become ionized again at z$\sim$10. The study of the reionization process is a crucial test of the correctness of our knowledge of the processes of the formation of structure in the Universe.
- Gravitational instability is sufficient to grow all of the observed large structures in the Universe.
- Topological defects were not important for structure formation.
- There are synchronized super-Hubble modes generated in the early Universe.
- The initial perturbations were adiabatic in nature.
- The perturbations had close to Gaussian (i.e., maximally random) initial conditions.

The measurement of CMB polarization, discussed in chapter 4, is one of the best tests for constraining inflationary scenarios, and permit to constrain physics at energies well above the reach of human-made accelerators. There is an open question regarding primordial gravitational waves. Polarization measurements of the CMB can serve as a detector of stochastic background of the primordial gravitational waves. The pattern of polarization directions in the sky will be different if a stochastic primordial gravitational radiation exists. In this case the so-called pseudoscalar or magnetic part of the polarization would not be equal to zero. It should be emphasized that the inflation model predicts the existence of such radiation. These measurements, then, with better precision than those of DASI and WMAP, will open a window on the early Universe. These investigations are especially important because there is a huge project, the Laser Interferometer Space Antenna (LISA), which may allow direct detection of a continuous spectrum of primordial gravitational radiation. Comparison of the PLANCK and LISA results, obtained by these absolutely different methods of observation, is extremely important.

The statistical tools described in chapter 5 can be used to estimate the cosmological parameters and help in pinpointing a consistent model of the universe. CMB fluctuations are the most accurate and theoretically the best understood dataset and hence

ideally suited to determine the parameters of the background cosmology and the initial fluctuations. The cosmological information is encoded in about a dozen cosmological parameters, each of which describes a basic property of the universe. Because of the technological advancements, the accuracy with which these cosmological parameters are estimated is improving. Planck is expected to improve it further which will put more rigorous constraints on theoretical models.

Although so much has been learnt from Cosmic Microwave Background Cosmology, the study of CMB physics is not coming to an end. There are still many unsolved problems in cosmology, and another generation of satellite experiments, as well as ground based and balloon-borne experiments, is needed. The deeper science penetrates and the more mysteries it solves, the more problems it discovers, each more daunting and less predictable than the last. Among the fundamental problems which arose after the recent success of cosmology, we mention the following.
(a) What is the nature and origin of dark energy? How did it evolve?
(b) Why does $\Omega_\Lambda \simeq 0.73$ in the current state of the Universe?
(c) What is the nature of dark matter?
(d) Why does $\Omega_{dm} \simeq 0.3$? What theory could provide this value?

These problems present a tremendous challenge. There are also problems and uncertainties directly related to the interpretation of recent observational data. Recent experiments focused much attention on the separation of the primordial cosmological signal from noise and the foreground and on the statistical properties of the signal. The assumption that the statistical properties of the primordial CMB signal are Gaussian is the crucial requirement for deriving cosmological parameters from temperature and polarization power spectra.

Fortunately, we live at a time when results from complimentary experiments will soon be available. The Planck satellite, launched by the European Space Agency, will release the first full-sky CMB map in January 2013. Since Planck has 9 frequency bands, extending over a wide frequency range than WMAP's 5 bands, it provides much more information on Galactic foregrounds. One should therefore be able to reconstruct the CMB reliably to lower Galactic latitude, therefore obtain a more stable reconstruction of the all sky CMB.

So far, people have been searching for the statistical anisotropic power spectrum in the WMAP temperature maps [199]. The WMAP polarization maps cannot be used

to test departures from statistical isotropy because they have very large noise and beam asymmetries. As Planck will release high precision polarization maps, a direct extension of the work from Chapter 4 would be to investigate the anisotropic power spectrum in the polarization map, and provide complimentary checks of the temperature analysis, particularly if the temperature data suggest a nonzero result.

It should be mentioned that the possible existence of a primordial magnetic field can also be tested using CMB observations [200]. Another fundamental problem of modern cosmology is the possibility of other types of primordial perturbations in the early Universe, different from the adiabatic ones (for example, isocurvature perturbations).

We should remember that the impressive constraints on many fundamental cosmic parameters, produced by WMAP and other projects, reside within the framework of a definite cosmological model. If we take into account the possibility of a wider class of cosmological models, it may be that the actual uncertainty is much greater. We will have to wait for forthcoming observations to reduce the current uncertainties.

After the beginning of the era of precision cosmology, the number of questions affecting the basic fundamentals of cosmology increased significantly. Both cosmological and physical communities are now working on future projects such as PLANCK, ALMA, LISA, etc. Beyond doubt, these are the most exciting times to work in cosmology and we hope to have answers to some of the most baffling questions about of universe in a decade or so.

Prospective Problems for Ph.D

With rapid improvement in measurements, the ability to estimate the parameters of cosmological models beyond the simplest version is progressively limited by the efficacy of the estimation method employed. The increased dimensionality of parameter space as one attempt to refine our understanding of the cosmological model make computational costs of the current methods prohibitive.

Our prime objective in future is to develop and implement working codes and be ready to mine the Planck surveyor data due to be released in 2013. The ability to explore larger dimensional parameter space of cosmology would allow us to address questions beyond the standard model analysis. These issues include:

- To study the deviations from Gaussian distribution of primordial fluctuation in specific classes of models of inflation.
- To explore and identify features in primordial power spectrum combining the temperature and polarization data from Planck.
- To measure the statistical isotropy of the CMB maps and estimate deviations.
- To study the origin and nature of the dark matter and dark energy.
- To determine the neutrino mass, He fraction, constrain variations in the fundamental constants such as fine structure constant.

Besides, we expect some surprises from the ongoing and future CMB missions which may pave way for some further investigations. We hope to carry out this work in collaboration with Professor Tarun Souradeep (IUCAA) who is an established scientist in the international CMB community.

Bibliography

[1] G. F. Smoot et al, 1992, *ApJ*, **396**, 1

[2] E. Komatsu et al, 2009, *ApJS*, **180**, 330

[3] B. Gold et al, 2009, *ApJS*, **180**, 265

[4] G. Hinshaw et al, 2007, *ApJS*, **170**, 288

[5] D. Spergel et al. 2007, *ApJS*, **170**, 377

[6] C. L. Bennett et al, 2003, *ApJS*, **148**, 1

[7] C. R. Lawrence, D. Scott and M. White, 1999, *PASP*, **111**, 525

[8] M.Tegmark et al., 2006, *phRvD*,**74**,123507

[9] S. Coles et al., 2005,*MNRAS*, **362**, 505

[10] S. Ho et al., 2008, *PhRvD*, **78**, 043519

[11] N. Jarosik et al, 2011,*ApJS*, **192**, 14

[12] E. Komatsu et al, 2011, *ApJS*, **192**, 18

[13] B. Gold et al, 2011, *ApJS*, **192**, 15

[14] C. L. Bennett et al, 2011, *ApJS*, **192**, 17

[15] J. M. Kovac et al, 2002, *Nature*, **420**, 772

[16] C. W. Odell et al, 2003, *PhRvD*, **68**, 042002

[17] A. C. S. Readhead, et al., 2004, *Science*, **306**, 836

[18] D. Barkats, et al., 2005, *ApJS*, **159**, 1

[19] T. E. Montroy, et al., 2006, *ApJ*, **647**, 813

[20] P. Ade, et al., 2008, *ApJ*, **674**, 22

[21] A. R. Levy, et al., 2008, *ApJS*, **177**, 419

[22] H. C. Chiang, et al., 2010, *ApJ*, **711**, 1123

[23] G. Hinshaw, et al., 2009, *ApJS*, **180**, 225

[24] D. Bessada, and O. D. Miranda, 2009, *J. Cosmology and Astro-Particle Physics*, **8**, 33

[25] D. Bessada, and O. D. Miranda, 2009, *Classical and Quantum Gravity*, **26**, 045005

[26] Linde, A. D., 1983, *Phys Lett B.*, **129**, 177

[27] Linde, A. D., 1991, *Particle physics and inflationary cosmology*, Hardwood Academic Publishers.

[28] Gamow, G., 1948, *Phys. Rev.*, **74**, 505

[29] Penzias, A. A., & Wilson, R. W.,1965, *ApJ*,**142**, 419

[30] D. J. Fixsen et al. 1996, *ApJ*, **473**, 576

[31] G. F. Smoot et al., 1977, *Phys. Rev. Lett.*, **39**, 898

[32] R. K. Sachs & A. M. Wolfe, 1967, *ApJ* **147**, 73

[33] Silk J., 1968. *ApJ*, **151**, 459.

[34] Sunyaev R. A., Zeldovich Y. B., 1970. *Astrophys. Space Sci.*, **7**, 3.

[35] Souradeep, T., Sahni, V., 1992, *Mod. Phys. Lett. A*, **7**, 3541

[36] R. Saha, P. Jain & T. Souradeep, 2006, *Astrophys. J. Lett.*, **645**, L89

[37] B. E. Corey, D. T. Wilkinson, 1976, *Bull. Am. Astron.Soc.*, **8**, 351

[38] Gawiser, E. & Silk, J., 2000, preprint, astro-ph/0002044v1

[39] Padmanabhan, T., 1993, *Structure Formation in the Universe* (Cambridge University Press; Cambridge, UK)

[40] Peebles, P. J. E., 1993, *Principles of Physical Cosmology* (Princeton University Press; Princeton, NJ)

[41] Shu, F. H., 1991, *The Physics of Astrophysics, Volume I: Radiation* (University Science Books; Mill Valley, CA)

[42] Hu, W., 1995, PhD thesis, U. C. Berkeley, astro-ph/9508126

[43] Tolman, R. C., 1934, *Relativity, Thermodynamics, and Cosmology* (Clarendon Press; Oxford, UK)

[44] Guth, A., 1981, *Phys. Rev. D*, **23**, 347

[45] Linde, A. D., 1982, *Phy. Lett.*, **B108**, 389

[46] Albrecht, A. & Steinhardt, P. J., 1982, *Phys. Rev. Lett.*, **48**, 1220

[47] Mather, J. C. et al., 1994, *ApJ.*, **420**, 439

[48] White, M., Scott, D., & Silk, J., 1994, *Ann. Rev. Astron. Astrophys.*, **32**, 319

[49] Puget, J. L. et al., 1996, *Astron. Astrophys.*, **308**,L5

[50] Burigana, C. & Popa, L., 1998,*Astron. Astrophys*., **334**, 420

[51] Fixsen, D. J., Dwek, E., Mather, J. C., Bennett, C. L., & Shafer, R. A., 1998, *ApJ*, **508**, 123

[52] Schlegel, D. J., Finkbeiner, D. P., & Davis, M., 1998, *ApJ*, **500**, 525

[53] Dwek, E. et al.,1998, *ApJ*,**508**, 106

[54] Kolb, E. W. & Turner, M. S., 1990, *The Early Universe* (Addison-Wesley Publishing; Company Reading, MA)

[55] Refregier, A., Spergel, D. N., & Herbig, T., 1998, preprint, astro-ph/9806349

[56] Yamada, M., Sugiyama, N., & Silk, J., 1999,*ApJ* , **522**, 66

[57] D. Scott and G. F. Smoot, 2008, *Physics Letters*, **B667**, 1

[58] Bond, J. R., Efstathiou, G., and Silk, J., 1980, *Physical Review Letters*, **45**, 1980

[59] Doroshkevich, A. G., Zeldovich, Y. B., Syunyaev, R. A., and Khlopov, M. Y., 1980, *Pisma Astronomicheskii Zhurnal*, **6457**.

[60] Ryden, B. S., 2002, *Introduction to Cosmology*, (Addison Wesley)

[61] Dodelson, S., 2002, *Modern Cosmology*, (Academic Press; Amsterdam)

[62] Aghanim, N., Majumdar, S., & Silk, J., 2008, *RPPh*, **71**, 066902

[63] Diego, J. M., Hansen, S. H., & Silk, J., 2003, *MNRAS*, **338**, 796

[64] Boughn, S. P., & Crittenden, R. G., 2005, *NewAR*, **49**, 75

[65] Fosalba, P., & Gaztanaga, E., 2004, *MNRAS*, **350**, L37

[66] Afshordi, N., Lin, Y. T., & Sanderson, A. J. R., 2005, *ApJ*, **629**, 1

[67] Padmanabhan, N., Hirata, C. M., Seljak, U., Schlegel, D. J., Brinkmann, J., & Schneider, D. P., 2005b, *PhRvD*, **72**, 043525

[68] Giannantonio, T., Scranton, R., Crittenden, R. G. Nicol, R. C., Boughn, S. P., Myers, A. D., & Richards, G. T., 2008, *PhRvD*, **77**, 123520

[69] Rees, M. J., & Scaima, D. W., 1968, *Nature*, **517**, 611

[70] Birkinshaw, M., & Gull, S. F., 1983, *Nature*, **302**, 315

[71] Seljak, U., 1996a, *ApJ*, **460**, 549

[72] Hu, W., 2000, *ApJ*, **529**, 12

[73] Cooray, A., 2002a, *PhRvD*, **65**, 3518

[74] Blanchard, A., & Schneider, J., 1987, *A&A*, **184**, 1

[75] Bernardeau, F., 1997, *A&A*, **324**, 15

[76] Zaldarriaga, M., 2000, *PhRvD*, **62**, 063510

[77] Cooray, A., 2002c, *PhRvD*, **65**, 3512

[78] Kesden, M., Cooray, A., & Kamionkowski, M., 2003, *PhRvD*, **67**, 123507

[79] Kaplinghat, M., Knox, L., & Song, Y. S., 2003, *PRL*, **89**, 011303

[80] Smith, K. M., Zahn, O., & Dore, O., 2007, *PhRvD*, **76**, 043510

[81] Das, S., & Spergel, D. N., 2008, *PhRvD*, **79**, 043509

[82] Gunn, J. E., & Peterson, B. A., 1965, *ApJ*, **142**, 1633

[83] Barkana, R. & Loeb, A. 2007, *Reports on Progress in Physics*, **70**, 627

[84] Ostriker, J. P., & Vishniac, E. T., 1986, *ApJ*, **306**, L51

[85] Dodelson, S., & Jubas, J. M., 1995, *ApJ*, **439**, 503

[86] Scannapieco, E., 2000, *ApJ*, **540**, 20

[87] Zhang, P., Pen, U., & Trac, H., 2004, *MNRAS*, **347**, 1224

[88] Sunyaev, R. A., & Zel'dovich, Ya. B., 1980, *MNRAS*, **190**, 413

[89] Rephaeli, Y., 1995, *ARA&A*, **33**, 541

[90] Bhattacharya, S., & Kosowsky, A., 2008, *PhRvD*, **77**, 3004

[91] Sunyaev, R. A., & Zel'dovich, Ya. B., 1972, *Comments Astrophys. Space Phys.*,**4**, 173

[92] Carlstrom, J., E., Holder, G., P., & Reese, E. D., 2002, *ARA&A*, **40**, 643

[93] Kogut, A., Banday, A. J., Bennett, C. L., Gorski, K. M., Hinshaw, G., Smoot, G. F., & Wright, E. L., 1996b, *Astrophys. J., Lett.*, **464**, L29

[94] Ferreira, P. G. & Magueijo, J., 1997, *PhRvD*, **55**, 3358

[95] Ferreira, P. G., Magueijo, J., & Silk, J., 1997, *PhRvD*, **56**, 4592

[96] Gaztanaga, E., Fosalba, P., & Elizalde, E., 1998, *Mon. Not. R. Astron. Soc.*, **295**, L35

[97] Ferreira, P. G., Magueijo, J., & Gorski, K. M., 1998, *Astrophys. J., Lett.*, **503**, L1

[98] Pando, J., Valls-Gabaud, D., & Fang, L. Z., 1998, *Phys. Rev. Lett.*, **81**, 4568

[99] Bromley, B. C. & Tegmark, M., 1999, *Astrophys. J., Lett.*, **524**, L79

[100] Bouchet, F. R. and Gispert, R., 1999, *New Astron.*, **4** , 443

[101] de Zotti, G. et al., 1999, *AIP Conf. Proc.*, **476** ,204

[102] Watson, R. A. et al., 2005, *Astrophys. J. Lett.*, **624**, L89

[103] Giardino, G. et al., 2002, *Astron. Astrophys.*, **387**, 82

[104] Barnes, C. et al., 2003, *ApJ Suppl.*,**148**, 51

[105] Benoit, A. et al., 2004, *Astron. Astrophys.*, **424**, 571

[106] Ponthieu, N., Macias-Perez, J-F., Tristram, M. et al., 2005, *Astron. Astrophys.* **444**, 327

[107] Boughn, S. P., Cheng, E. S., Cottingham, D. A., and Fixsen, D. J., 1992, *ApJ* **391L**, 49B

[108] Ganga, K., Cheng, E., Meyer, S., and Page, L., 1993, *ApJ* **410L**, 57

[109] Benoit, A. et al., 2003, *Astron. Astrophys.* **399**, L19

[110] Finkbeiner, D. P. et al., 1999, *ApJ*, **524**, 867

[111] Hinderks, J., 2005, PhD Thesis Stanford University

[112] Allen, T. J., Grinstein, B., and Wise, M. B., 1987, *Physics Letters B*, **197**, 66

[113] Falk, T., Rangarajan, R., and Srednicki, M., 1993, *ApJ*, **403**, L1-L3.

[114] Gangui, A., Lucchin, F., Matarrese, S., and Mollerach, S., 1994, *ApJ*, **430**, 447

[115] Hu, W., 2001, *PhRvD*, **64**(8), 083005-+.

[116] Winitzki, S., and Kosowsky, A., 1998, *New Astronomy*, **3** 75.

[117] Kogut, A., Banday, A. J., Bennett, C. L., Gorski, K. M., Hinshaw, G., Smoot, G. F., and Wright, E. I., 1996, *ApJ*, **464**, L5+.

[118] Aghanim, N., and Forni, O., 1999, *A&A*, **347**, 409

[119] Komatsu, E., 2003, *New Astronomy Review*, **47**, 797

[120] Cabella, P., & Kamionkowski, M., [astro-ph/0403392] (2004)

[121] Kosowsky, A., 1998, *Annals Phys.*, **246** 49

[122] Hu, W., & White, M., 1997, *New Astron.*, **2**, 323

[123] Chandrasekhar, S., 1960, *Radiative Transfer*, (Dover, New York)

[124] Varshalovich, D.A., Moskalev, A.N. and Khersonskii, V.K., 1988, *Quantum Theory of Angular Momentum*, (World Scientific, Singapore)

[125] T. Roy Choudhury & A. Ferrara, (2006), this volume, astro-ph/0603149

[126] W. Hu & G. P. Holder, 2003, *PhRvD*, **68**, 023001

[127] Knox, L., & Song, Y. S.,2002, *Phys. Rev. Lett.* **89**, 011303

[128] Seljak, U., & Zaldarriaga, M.,1999 *Phys. Rev. Lett.* **82**, 2636

[129] M. Zaldarriaga, *The Polarization of the Cosmic Microwave Background, Vol 2*: Measuring and Modeling the Universe of Carnegie Observatories Astrophysics Series, Cambridge University Press, 2003, astro-ph/0305272.

[130] A. Kogut, et al., 2003, *Astrophys. J.* (Supp.), **148**.

[131] U. Seljak, M. Zaldarriaga, 1997, *Phys. Rev. Lett.* **78**, 2054.

[132] M. Kamionkowski, A. Kosowsky, 1998 ,*PhRvD*, **57**, 685.

[133] C.B. Netterfield, M.J. Devlin, N. Jarolik, L. Page, E.J. Wollack, 1997, *ApJ* **474** (1), 47.

[134] S. Hanany, et al., 2000, *Astrophys.J. Lett.* **545**, L5.

[135] P. de Bernardis, et al.,2002, *Nature* **404**, 955.

[136] A.R. Liddle, D.H. Lyth, *Cosmological Inflation and Large-Scale Structure*, Cambridge University Press, 2000.

[137] Nanos G. P., Jr., 1979, *ApJ*, **232**, 341

[138] Caderni N., Fabbri R., Melchiorri B., Melchiorri F., Natale V., 1978, *PhRvD*, **17**, 1901

[139] Lubin, P. M., & Smoot, G. F., 1981, *ApJ*, **245**, 1

[140] Lubin, P., Melese, P., & Smoot, G., 1983, *ApJ*, **273**, L51

[141] Sironi, G., Boella, G., Bonelli, G., Brunetti, L., Cavaliere, F., Gervasi,M.,Giardino, G., & Passerini, A., 1998, *New Astronomy*, **3**, 1

[142] Partridge R. B., Nowakowski J., Martin H. M., 1988, *Nature*, **331**, 146

[143] de Oliveira-Costa, A., Tegmark, M., Odell, C., Keating, B., Timbie,P., Efstathiou, G., & Smoot, G., 2003, *PRD*, **68**, 083003

[144] Wollack, E. J., Jarosik, N. C., Netterfield, C. B., Page, L. A., & Wilkinson,D., 1993, *ApJ*, **419**, L49

[145] Leitch, E. M., et al., 2002, *Nature*, **420**, 763

[146] Leitch, E. M., Kovac, J. M., Halverson, N. W., Carlstrom, J. E., Pryke,C., & Smith, M. W. E., 2005, *ApJ*, **624**, 10

[147] T. Souradeep, 2011, *Bull. Astr. Soc. India*, **39**, 1

[148] Wu E.Y.S., et al., 2009, *Phys.Rev.Lett.*, **102**, 161302

[149] Lue A., Wang L., Kamionkowski M., 1999, *Phys. Rev. Lett.*, **83**, 1506

[150] Maity D., Majumdar P., Sengupta S., 2004, *JCAP*, **0406**, 005

[151] The Scientific Programme of Planck, The Planck collaboration [arXiv:astro-ph/0604069]. Also see http://www.rssd.esa.int/Planck

[152] MacTavish, C. et al., (2005) astro-ph/0507503

[153] Spergel, D.N. et al., 2003, *Astrophys.J.Suppl.*, **148**, 175

[154] Spergel, D.N. et al., (2006) astro-ph/0603449

[155] Jones, W. C., Bhatia, R., Bock, J. J., & Lange, A. E., 2003, *SPIE*, **4855**, 227

[156] Bersanelli, M., Maino, D., & Mennella, A., 2004, *AIP Conf. Proc. 703*, **703**, 385

[157] Masi, S., et al., 2005, submitted to *A&A* [astro-ph/0507509]

[158] Jarosik, N., et al. 2006, Submitted to ApJ, arXiv:astro-ph/0603452

[159] de Gasperis, G., Balbi, A., Cabella, P., Natoli, P., & Vittorio, N., 2005, *A&A*, **436**, 1159

[160] Tegmark, M., de Oliveira-Costa, A., & Hamilton, A. J., 2003, *PhRvD*, **68**, 123523

[161] Baccigalupi, C., 2003, *New Astronomy Review*, **47**, 1127

[162] Page, L., et al., 2006, submitted to ApJ [astro-ph/0603450]

[163] Delabrouille, J., Kaplan, J., Piat, M., & Rosset, C., 2004, *Comptes Rendus Physique*, **4925**, 2003

[164] Bock J., et al., 2006, *astro*, arXiv:astro-ph/0604101 (final report of the US CMB Task Force)

[165] Dunkley J., et al., 2009, *Astrophys. J. Supp.*, **180**, 306

[166] Liddle AR., 2004, *MNRAS*, **351**, L49

[167] Lahav O., Liddle AR., 2008, *Phys. Lett.*, **B667**, 232.

[168] Yeche, Ch., Ealet, A., Refregier, A. et al., 2005, *A&A*, **448**, 831

[169] Lewis, A. & Bridle, S., *PhRvD*, **66**, 10

[170] N. Metropolis, A.W. Rosenbluth, M.N. Rosenbluth, et al., 1953, *Journal of Chemical Physics*, **21**, 1087

[171] Hastings,W.K., 1970, *Biometrika*, **57**,97

[172] Christensen, N., Meyer, R., 2000, eprint arXiv:astro-ph/0006401

[173] Raftery, A. E., Lewis, S. M., in eds Bernardo, J. M., Berger, J. O., Dawid, A.,Smith, A., *Baysean Statistics* **4**, 763, Oxford University Press.

[174] Gelman, A & Rubin, D.B., 1992, *Statistical Science*, **7**, 457

[175] W. L. Freedman et al., 2001, *ApJ*, **553**, 47

[176] L. M. Krauss & B. Chaboyer, 2003, *Science*, **299**, 65

[177] A. Balbi et al., 2000, *ApJ*, **545**, L1

[178] P. de Bernardis et al., 2000, *Nature*, **404**, 955

[179] B. Fields & S. Sarkar, 2006, astro-ph/0601514

[180] S. Perlmutter et al., 1999, *ApJ*, **517**, 565

[181] A. G. Riess et al., 2001, *ApJ*, **560**, 49

[182] S. E Rugh & H. Zinkernagel, 2002, *Studies in History and Philosophy of Modern Physics*, **33**, 663

[183] T. Padmanabhan, 2003, *Phys. Rept.*, **380**, 235

[184] S. P. Boughn & R. G. Crittenden, 2004, *Nature*, **427**, 45

[185] E. Boldt, 1987, *Phys. Rep.*, **146**, 215

[186] J. J. Condon et al., 1998, *AJ*, **115**, 1693

[187] M. R. Nolta et al., 2004, *ApJ*, **608**, 10

[188] S. J. Maddox et al., 1990, *MNRAS*, **242**, 43

[189] D. York et al., 2000, *AJ*, **120**, 1579

[190] T. H. Jarrett et al., 2000, *ApJ*, **119**, 2498

[191] P. Fosalba & E. Gaztanaga, 2004, *MNRAS*, **350**, L37

[192] R. Scranton et al., 2003, arXiv:astro-ph/0307335

[193] N. Afshordi, Y.-S. Loh, & M. A. Strauss, 2004, *PhRvD*, **69**, 083524

[194] N. Padmanabhan et al., 2005, *PhRvD*, **72**, 043525

[195] A. Cabre et al., 2006, arXiv:astro-ph/0603690

[196] P. Vielva, E. Martnez-Gonzlez, & M. Tucci, 2006, *MNRAS*, **365**, 891

[197] W. H. Kinney, E. W. Kolb, A. Melchiorri, A. Riotto, 2006, astro-ph/0605338

[198] U. Seljak, A. Slosar & P. McDonald, 2006, astro-ph/060433

[199] N. E. Groeneboom and H. K. Eriksen, 2009, *ApJ*, **690**, 1807

[200] Naselsky, P. D., Chiang, L.-Y., Olesen, P. and Verkhodanov, O.V., 2004, *ApJ*, **615**, 45.